Dark Matter Models in Non-Supersymmetric SO(10) Unification Models

A THESIS
SUBMITTED TO THE FACULTY OF THE GRADUATE SCHOOL
OF THE UNIVERSITY OF MINNESOTA
BY

Jiaming Zheng

IN PARTIAL FULFILLMENT OF THE REQUIREMENTS
FOR THE DEGREE OF
Ph.D.

Keith Olive

June, 2017

Acknowledgements

A lot of people have helped me a lot during my graduate study. Here I would like to thank my advisor, Keith Olive, for guiding me into research and for all the helpful advice and conversation on both academy and the real life. I would also express my thank to all the collaborators on the topic of this thesis, including Natsumi Nagata, who taught me of useful technical detail on calculation related to unification theory, and Yann Mambrini and Jeremie Quevillon who are great persons to work with.

I am also grateful to Arkady Vainshtein and Marco Peloso, who gave wonderful lectures on field theory and inspired me a lot in my early stage of the graduate study, to John Ellis who helped with my application to a postdoc position, and to Evan Skillman and Yuichi Kubota for their service in my defense committee.

I also want to thank Yusuf Buyukdag and Daniel Schubring for organizing the HEP theory study group which is a great place to learn something out of my field of study. I also benefit a lot from discussion with Andrew Miller, Caner Unal, and Jason Evans.

Finally, I would like to thank Yang Tang, Junfeng Wu, Morten Christensen, Michael Schuett, Peter Orth, Xin Li, Xiaoyu Wang, Chun Chen, and many others who contributed to my good time in graduate school.

Dedication

To my parents Yantao Mo, Hechang Zheng, my advisor Keith Olive and my fiancee Kaixi Feng.

Abstract

This thesis studies systematically non-supersymmetric models that contain dark matter candidates. The stability of the dark matter is guaranteed by a remnant $\mathbb{Z}_2$ symmetry embedded naturally in SO(10). We build models base on various dark matter production mechanism, including the non-equilibrium thermal dark matter scenario, the weakly interactive massive particle scenario, and the asymmetric dark matter scenario. Although we start from very general assumptions on the choice of dark matter representation and the symmetry breaking pattern, the number of viable models is severely restricted by the requirement of gauge coupling unification. These models are then checked against several phenomenological constraints, such as the light neutrino masses, direct detection bounds on dark matter candidates and the proton decay lifetime. Finally, we demonstrate that the vacuum stability problem of the Standard Model can be evaded by one of our scalar dark matter models.

Contents

List of Tables

List of Figures

Chapter 1

Introduction

The known interactions of the elementary particles are well described by gravity and the Standard Model(SM) of the particle physics. The latter describes the strong force, weak force and electromagnetic force in the framework of $\mathrm{SU}(3)_C \otimes \mathrm{SU}(2)_L \otimes \mathrm{U}(1)_Y$ gauge interactions with spontaneous symmetry breaking. The last piece of the SM, the Higgs boson has been discovered with a mass of $m_h \simeq 125$ GeV [4]. So far, particle colliders have observed all elementary particles, and verified that the interactions between them are consistent with the SM with a high precision.

Yet, the SM has its limit and does not describe everything in the universe. To list a few, the SM cannot explain how the neutrinos obtain their masses and oscillate between different flavor states; there is more matter than anti-matter in the universe and the CP violation phase in the SM alone is not enough to explain all of it; dark energy and dark matter(DM) contributes about 70% and 27% of the total energy of the observable universe and they are not within the content of the SM. On the theoretical side, the three gauge groups of the SM are completely independent of each other. In principle, the U(1) hypercharge can be anything, yet in reality, the hypercharge of quarks and leptons are integer multiples of 1/6. This quantized structure suggests that $\mathrm{U}(1)_\mathrm{Y}$ is a subgroup of a larger simple group whose weights are always rational numbers.

The questions listed above motivates various extensions of the SM. In particular, the gauge coupling unification theories(GUT) are a class of models that try to embed the SM gauge group $G_{\mathrm{SM}} = \mathrm{SU}(3)_C \otimes \mathrm{SU}(2)_L \otimes \mathrm{U}(1)_Y$ into a larger simple gauge group, so that the three gauge couplings have a common origin. This unified gauge group is

broken spontaneously at a very high energy scale so that the gauge bosons and Higgs particles relevant to the broken symmetry are extremely heavy and remain undetectable in current experiments.

The first attempt for unification is the SU(5) unification theory [2] since SU(5) is the only rank-four simple group that contains $G_{\rm SM}$ as a subgroup. In minimal SU(5) GUT the unified SU(5) is broken directly to the SM gauge group $G_{\rm SM}$ at the grand unification scale $M_{\rm GUT}$, usually of order $10^{15} \sim 10^{16}$ GeV. All the new particles that are not contained in the SM lie at or above the GUT scale. Thus the Renormalisation Group Equations(RGEs) that govern the running of the gauge couplings to the GUT is only dependent on the content of the SM. This attempt fails to obtain the correct gauge couplings at the weak scale obtained by experiments. In Fig. 1.1 the gauge couplings are run to the GUT scale starting from their initial values at the weak scale. $g_1 = \sqrt{5/3}g'$ as defined by the embedding of $\mathrm{U}(1)_Y$ in SU(5), and $\alpha_i = \frac{g_i^2}{4\pi}$. In a successful unification theory, these couplings should converge to a point at a high energy scale, and it is not the case in the figure. Improving the precision of the running by using two-loop RGEs does not solve this problem.

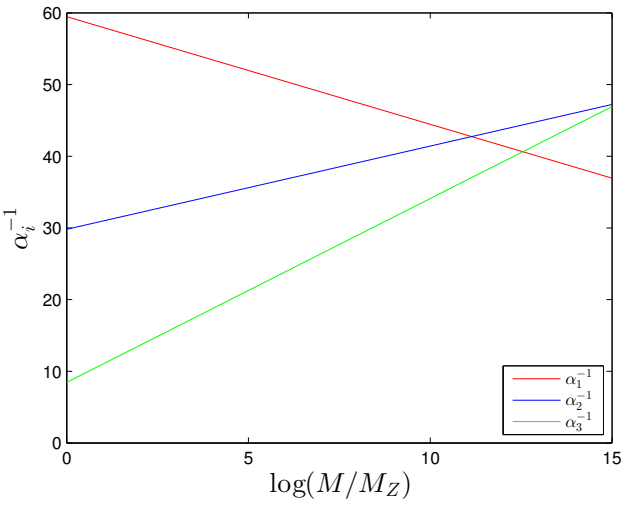

Figure 1.1: *Running of the gauge couplings induced by SM particles.* $g_1 = \sqrt{5/3}g'$ *by the embedding of U(1)$_Y$ in SU(5).*

The supersymmetric version of SU(5) unification theory introduces superpartners of SM particles around the weak scale and surprisingly unifies the running of the coupling at a scale of $\sim 10^{16}$ GeV [3]. Moreover, it also contains a candidate for the dark matter particle if a discrete symmetry is enforced by hand to render the candidate stable. With other attractive features, such as being free of quadratic divergence in the theory, the stability of vacuum and the radiative breaking of electroweak symmetry, the Minimal Supersymmetric extension of the Standard Model(MSSM) is one of the most studied extensions of the SM.

On the other hand, the framework of non-supersymmetric SO(10) unification theory can also achieve gauge coupling unification by introducing an intermediate energy scale $M_{\rm int}$ between $M_{\rm GUT}$ and the weak scale M_Z. The running of the gauge couplings is modified above $M_{\rm int}$ because of the new particles lie around $M_{\rm int}$ enforced by the intermediate gauge symmetry. It is thus possible to obtain unification of couplings with a new degree of freedom in energy scale. Besides unification, SO(10) theories has other interesting features. For example, it predicts the existence of right-handed neutrinos that are in the same fundamental representations as other SM fermions of the same generation; the breaking of intermediate symmetry can induce the seesaw mechanism that generates small neutrino masses. Moreover, since the rank of SO(10) is larger than $G_{\rm SM}$, the discrete symmetry that stabilizes the dark matter candidate can be obtained as the remnant of the extra U(1) symmetry.

The purpose of this thesis is to study systematically the possibility of adding a dark matter candidate to non-supersymmetric SO(10) unification theory. In this thesis, the dark matter is assumed to be a stable elementary particle that does not participate electromagnetic interaction. Minimal non-supersymmetric SO(10) unification model does not contain a dark matter candidate so we need to introduce a new dark matter multiplet. Such multiplet influences the running of couplings and changes the scales significantly in most of the models we consider, and thus the requirement of gauge coupling unification and proton decay experiments can place strong constraints on model building. We will consider several different dark matter scenarios, including the Non-equilibrium Thermal Dark Matter(NETDM), the Weakly Interactive Massive Particle(WIMP) scenario and the Asymmetric Dark Matter(ADM) scenario. We will also investigate the stability of the vacuum and the possibility of breaking electroweak

symmetry radiatively with one of our WIMP DM models.

The outline of the rest of this thesis is the following:

- Chapter 2 gives a brief description of a minimal non-supersymmetric SO(10) unification model. This model serves as the base of model-building in the rest of the thesis.

- Chapter 3 provides a list of representations that contain candidates of dark matter particles. The dark matter candidates in Chapter 4, 5 and 6 are chosen from this list. We also discuss how to split components into different energy scales by fine-tuning the couplings between the DM representation and the Higgs representations.

- Chapter 4, 5 and 6 discuss NETDM, WIMP, and ADM, respectively. In these chapters, we select DM representations from the list provided in Chapter 3 and add them to the minimal model described in Chapter 2. We then discuss the constraints on this model imposed by gauge coupling unification and by various phenomenological observations, such as neutrino masses, the proton decay lifetime, DM direct detection experiments, etc.

- Chapter 7 investigates the stability of vacuum and the possibility of radiative symmetry breaking in the context of a scalar WIMP model obtained in Chapter 5. And then we give a brief summary and outlook in Conclusion.

  This thesis is a combination of several recent works of the author in Ref. [1].

Chapter 2

SO(10) gauge unification theory without dark matter

In this chapter, we introduce the "minimal" non-supersymmetric SO(10) model without getting into details of group theory. This model will act as the starting point of the model building in the later chapters that includes various kinds of dark matter. This model is minimal in the sense that it only contains the minimal numbers of particles for the embedding of the standard model and the need of symmetry breaking. In Sec. 2.1 we discuss how SO(10) can be broken spontaneously to $G_{\rm SM}$; Sec. 2.2 describes the particle content of SO(10) unification theory and how these particles distribute over different energy scales; Finally in Sec. 2.3, we calculate the running of couplings and energy scales by assuming gauge coupling unification at a high scale.

2.1 Breaking train of SO(10)

SO(10) is a rank-five group while the Standard Model gauge group, $G_{\rm SM} = {\rm SU}(3)_C \otimes {\rm SU}(2)_L \otimes {\rm U}(1)_Y$ is rank-four. This implies that the breaking of SO(10) to $G_{\rm SM}$ can take place in multiple steps. As we will see later, this feature is essential for achieving gauge coupling unification without supersymmetry [5–7]. In this work, we assume a two-step symmetry breaking train from SO(10) to the SM: the SO(10) gauge group is first spontaneously broken to an intermediate subgroup $G_{\rm int}$ at the GUT scale $M_{\rm GUT}$,

and subsequently broken to the SM gauge group $G_{\rm SM}$ at an intermediate scale $M_{\rm int}$:

$$\mathrm{SO}(10) \xrightarrow{R_1} G_{\rm int} \xrightarrow{R_2} G_{\rm SM} \otimes \mathbb{Z}_N \ , \tag{2.1}$$

with $G_{\rm SM} \equiv \mathrm{SU}(3)_C \otimes \mathrm{SU}(2)_L \otimes \mathrm{U}(1)_Y$. The Higgs multiplets which break SO(10) and $G_{\rm int}$ are called R_1 and R_2, respectively. In addition, we require that there is a remnant discrete symmetry $\mathbb{Z}_2$ that is capable of rendering a charge-neutral field to be stable and hence account for the DM in the Universe [8, 9]. Such mechanism will be discussed in more detail in Sec. 3.1. Overall, there are three energy scales that are important in this thesis: the GUT scale $M_{\rm GUT}$, the intermediate scale $M_{\rm int}$ and the weak scale M_Z.

In Table 2.1, we summarize the rank-five subgroups of SO(10) and the Higgs multiplets R_1 whose Vacuum Expectation Values(VEVs) break SO(10) into the subgroups.[1] Here the SO(10) representations are labeled by their dimensions. We only consider the representations whose dimensions are less than or equal to 210. Here, D denotes the so-called D-parity or the left-right symmetry [10], that is, the symmetry with respect to the exchange of $\mathrm{SU}(2)_L \leftrightarrow \mathrm{SU}(2)_R$. In cases where the D-parity is not broken by R_1, it is subsequently broken by R_2 at the scale of $M_{\rm int}$. Note that the VEVs of the R_1 Higgs fields will be taken to be even under the $\mathbb{Z}_2$ symmetry. Thus, there is no danger for this $\mathbb{Z}_2$ symmetry to be spontaneously broken by the R_1 Higgs fields.

In the rest of the thesis we only consider subgroups without an explicit SU(5) factor. Since the DM is necessarily a color singlet, the running of the strong gauge coupling is unaltered by the presence of a new DM particle below the intermediate scale. Thus even though the addition of a DM multiplet yields unification of the gauge couplings, the unification scale $M_{\rm int}$ is always less than 10^{14} GeV as the contribution to the $\mathrm{U}(1)_Y$ beta function is always positive. If we now associate $M_{\rm int}$ with SU(5), this low partial unification is heavily disfavored on the basis of proton lifetime constraints. Flipped SU(5) usually has a high intermediate scale and a high GUT scale close to the Planck scale. In this case higher dimension operators suppressed by Planck scale become important, and one may also need to rely on a double seesaw for the explanation of neutrino masses. These bring extra complication into our model and we do not consider these possibilities here. Other intermediate gauge groups in the table are subgroups of

[1] See Ref. [28] for detailed table of branching rules of SO(10) to its various subgroups.

Table 2.1: *Candidates for the intermediate gauge group G_{int}.*

$G_{\rm int}$	R_1
$\mathrm{SU}(4)_C \otimes \mathrm{SU}(2)_L \otimes \mathrm{SU}(2)_R$	**210**
$\mathrm{SU}(4)_C \otimes \mathrm{SU}(2)_L \otimes \mathrm{SU}(2)_R \otimes D$	**54**
$\mathrm{SU}(4)_C \otimes \mathrm{SU}(2)_L \otimes \mathrm{U}(1)_R$	**45**
$\mathrm{SU}(3)_C \otimes \mathrm{SU}(2)_L \otimes \mathrm{SU}(2)_R \otimes \mathrm{U}(1)_{B-L}$	**45**
$\mathrm{SU}(3)_C \otimes \mathrm{SU}(2)_L \otimes \mathrm{SU}(2)_R \otimes \mathrm{U}(1)_{B-L} \otimes D$	**210**
$\mathrm{SU}(3)_C \otimes \mathrm{SU}(2)_L \otimes \mathrm{U}(1)_R \otimes \mathrm{U}(1)_{B-L}$	**45**, **210**
$\mathrm{SU}(5) \otimes \mathrm{U}(1)$	**45**, **210**
Flipped $\mathrm{SU}(5) \otimes \mathrm{U}(1)$	**45**, **210**

$\mathrm{SU}(4)_C \otimes \mathrm{SU}(2)_L \otimes \mathrm{SU}(2)_R \otimes D$, and $\mathrm{U}(1)_{B-L}$ is a subgroup of $\mathrm{SU}(4)_C$. The relationship among hypercharge Y, the $\mathrm{U}(1)_{B-L}$ charge $B-L$, and the third component of the $\mathrm{SU}(2)_R$ generators T_R^3 is very useful for determining the quantum numbers of DM candidates:

$$Y = \frac{B-L}{2} + T_R^3 \,. \tag{2.2}$$

The convention we are using for hypercharge is such that electric charge is given by $Q = T_L^3 + Y$, with T_L^3 denoting the third component of the $\mathrm{SU}(2)_L$ generators.

To break $G_{\rm int}$ to $G_{\rm SM}$, a VEV needs to be developed in a component of R_2 that is singlet under $G_{\rm SM}$ but charged under the rest of $G_{\rm int}$. If we restrict ourselves to SO(10) representation with dimension not larger than **210**, the only possible choices are 16_C and 126_C, where the subscript C stands for complex representations. Among the two choices, only 126_C leaves a remnant $\mathbb{Z}_2$ symmetry that is required for stabilizing the dark matter. Thus for the rest of the thesis, 126_C is always responsible for breaking the intermediate gauge symmetry $G_{\rm int}$.

2.2 Particle content and mass hierarchy

In SO(10) GUTs, the SM fermions as well as three right-handed neutrinos are embedded into three copies of the **16** spinor representations, while the SM Higgs boson is usually included in a **10** representation. The components of an SO(10) representation generally

have masses of different energy scales. To determine the mass hierarchy of componets in an SO(10) representation, we work with the so-called extended survival hypothesis [11,12]; that is, at each scale, we assume that a minimal set of Higgs multiplets necessary to realize the symmetry breaking exists in low-energy region. The rest of the SO(10) representation lies at the highest possible scale that is consistent with the symmetry groups at each scale. The motivation of this assumption is to minimize the fine-tuning condition needed for the low energy spectrum.

Within this assumption the whole R_1 representation lies at $M_{\rm GUT}$. For R_2, only the component that developes a VEV and its companions under $G_{\rm int}$ transformation lie at $M_{\rm int}$ for the purpose of intermediate scale symmetry breaking. The rest of R_2 stay at $M_{\rm GUT}$. The masses of the gauge bosons are determined by the Higgs mechanism: the mass scale of the gauge boson is the mass scale where the related symmetry is broken. Above the intermediate scale, the presence of the additional Higgs multiplet and intermediate gauge bosons change the gauge coupling running from that in the SM. This makes it possible to realize gauge coupling unification in this scenario.

Since intermediate gauge groups we consider is related to the Pati-Salam gauge group [13], it is useful to decompose the SO(10) multiplets into multiplets of the $\mathrm{SU}(4)_C \otimes \mathrm{SU}(2)_L \otimes \mathrm{SU}(2)_R$ gauge group. The **16** spinor representation in SO(10) is decomposed into a $(\mathbf{4},\mathbf{2},\mathbf{1})$ and $(\overline{\mathbf{4}},\mathbf{1},\mathbf{2})$ of $\mathrm{SU}(4)_C \otimes \mathrm{SU}(2)_L \otimes \mathrm{SU}(2)_R$. We denote them by Ψ_L and Ψ^c_R, respectively, in which the SM fermions are embedded as follows:

$$\Psi_L = \begin{pmatrix} u^1_L & u^2_L & u^3_L & \nu_L \\ d^1_L & d^2_L & d^3_L & e_L \end{pmatrix} , \qquad \Psi^c_R = \begin{pmatrix} d^c_{R1} & d^c_{R2} & d^c_{R3} & e^c_R \\ -u^c_{R1} & -u^c_{R2} & -u^c_{R3} & -\nu^c_R \end{pmatrix} , \tag{2.3}$$

where the indices represent the $\mathrm{SU}(3)_C$ color and c indicates charge conjugation. The SM Higgs field is, on the other hand, embedded in the $(\mathbf{1},\mathbf{2},\overline{\mathbf{2}})$ component of the ten-dimensional representation. As discussed in Ref. [14], to obtain the viable Yukawa sector,[2] we need to consider a complex scalar $\mathbf{10}_C$ for the representation, not a real one. Thus, $(\mathbf{1},\mathbf{2},\overline{\mathbf{2}})$ is also a complex scalar multiplet and includes two Higgs doublets. In the following calculation, we regard one of these doublets as the SM Higgs boson, and the other has a mass around the intermediate scale. Other components in the $\mathbf{10}_C$ can only lie at the GUT scale because they induce proton decay. The $\mathrm{SU}(4)_C \otimes \mathrm{SU}(2)_L \otimes \mathrm{SU}(2)_R$

[2] For a general discussion on the Yukawa sector in SO(10) GUTs, see Refs. [14, 15].

gauge group is broken by the VEV of the $(\mathbf{10}, \mathbf{1}, \mathbf{3})$ component in the $\mathbf{126}_C$. In the presence of the left-right symmetry, we also have a $(\overline{\mathbf{10}}, \mathbf{3}, \mathbf{1})$ above the intermediate scale. We assume that the $(\overline{\mathbf{10}}, \mathbf{3}, \mathbf{1})$ field does not acquire a VEV, with which the constraint coming from the ρ-parameter is avoided. [3] From these charge assignments, one can readily obtain the quantum numbers for the corresponding fields in the other intermediate gauge groups, since they are subgroups of the $\mathrm{SU}(4)_C \otimes \mathrm{SU}(2)_L \otimes \mathrm{SU}(2)_R$.

2.3 Gauge coupling unification

With this field content, we study whether the gauge coupling unification is actually achieved or not for the first six intermediate gauge groups listed in Table 2.1. We perform the analysis by using the two-loop RGEs, which are given in Appendix B. We will work in the $\overline{\mathrm{DR}}$ scheme [16], as there is no constant term in the intermediate and GUT scale matching conditions. The input parameters that we use to obtain the the weak scale couplings in our analysis are listed in Table A.1 in Appendix A. By solving the RGEs and assuming gauge coupling unification, we determine the intermediate scale $M_{\rm int}$, the GUT scale $M_{\rm GUT}$, and the unified gauge coupling constant $g_{\rm GUT}$. If we fail to find the appropriate values for these quantities, we will conclude that gauge coupling unification is not realized in this case. To determine their central values as well as the uncertainty coming from the input parameters, we form a χ^2 statistics as

$$\chi^2 = \sum_{a=1}^{3} \frac{(g_a^2 - g_{a,\rm exp}^2)^2}{\sigma^2(g_{a,\rm exp}^2)} \ , \tag{2.4}$$

where g_a are the gauge couplings at the electroweak scale obtained by solving the RGEs on the above assumption, $g_{a,\rm exp}$ are the experimental values of the corresponding gauge couplings with $\sigma(g_{a,\rm exp}^2)$ denoting their uncertainty. The central values of $M_{\rm int}$, $M_{\rm GUT}$, and $g_{\rm GUT}$ are corresponding to a point at which χ^2 is minimized.[4]

By using the method discussed above, we carry out the analysis and summarize the results in Table 2.2. Here, we show $\log_{10}(M_{\rm int})$, $\log_{10}(M_{\rm GUT})$, and $g_{\rm GUT}$. For

[3] The ρ-parameter is defined as the ratio between the strength of the neutral and the charged current. $\rho = 1$ at tree level of the SM, and deviates from this value if the Higgs VEV contains any component that is not part of a doublet.

[4] We also use the χ^2 statistics to determine the value of the input Yukawa coupling in a similar manner, though it scarcely affects the uncertainty estimation of $M_{\rm int}$, $M_{\rm GUT}$, and $g_{\rm GUT}$.

Table 2.2: $\log_{10}(M_{int})$, $\log_{10}(M_{GUT})$, *and* g_{GUT}. *For each* G_{int}, *the upper shaded (lower) row shows the 2-loop (1-loop) result.* M_{int} *and* M_{GUT} *are given in GeV. The blank entries indicate that gauge coupling unification is not achieved.*

$G_{\rm int}$	$\log_{10}(M_{\rm int})$	$\log_{10}(M_{\rm GUT})$	$g_{\rm GUT}$
$\mathrm{SU}(4)_C \otimes \mathrm{SU}(2)_L \otimes \mathrm{SU}(2)_R$	11.17(1)	15.929(4)	0.52738(4)
	11.740(8)	16.07(2)	0.5241(1)
$\mathrm{SU}(4)_C \otimes \mathrm{SU}(2)_L \otimes \mathrm{SU}(2)_R \otimes D$	13.664(3)	14.95(1)	0.5559(1)
	13.708(7)	15.23(3)	0.5520(1)
$\mathrm{SU}(4)_C \otimes \mathrm{SU}(2)_L \otimes \mathrm{U}(1)_R$	11.35(2)	14.42(1)	0.5359(1)
	11.23(1)	14.638(8)	0.53227(7)
$\mathrm{SU}(3)_C \otimes \mathrm{SU}(2)_L \otimes \mathrm{SU}(2)_R \otimes \mathrm{U}(1)_{B-L}$	9.46(2)	16.20(2)	0.52612(8)
	8.993(3)	16.68(4)	0.52124(3)
$\mathrm{SU}(3)_C \otimes \mathrm{SU}(2)_L \otimes \mathrm{SU}(2)_R \otimes \mathrm{U}(1)_{B-L} \otimes D$	10.51(1)	15.38(2)	0.53880(3)
	10.090(9)	15.77(1)	0.53478(6)
$\mathrm{SU}(3)_C \otimes \mathrm{SU}(2)_L \otimes \mathrm{U}(1)_R \otimes \mathrm{U}(1)_{B-L}$			

each intermediate gauge group, the upper shaded (lower) row shows the 2-loop (1-loop) result. $M_{\rm int}$ and $M_{\rm GUT}$ are given in GeV. The blank entries indicate that gauge coupling unification is not achieved. The uncertainties of the last digits of the numbers resulting from the input parameters are also shown in the parentheses. Threshold corrections at $M_{\rm int}$ and $M_{\rm GUT}$ [17] due to the non-degeneracy of the particles that have masses of the order of these scales contribute to the uncertainties that are generally larger than the ones from the input error.[5] For a recent discussion of threshold corrections, see Ref. [18]. In addition, we neglect the contribution of Yukawa couplings above the intermediate scale, which causes additional error. These are expected to give $\mathcal{O}(1)\%$ uncertainty to the resulting scales and coupling.

From Table 2.2, it is found that gauge coupling unification is not achieved in the

[5] Note that the intermediate scale in the left-right symmetric theories does not depend on physics beyond $M_{\rm int}$, as discussed in Appendix D.

case of $G_{\rm int} = {\rm SU}(3)_C \otimes {\rm SU}(2)_L \otimes {\rm U}(1)_R \otimes {\rm U}(1)_{B-L}$. Moreover, we find that relatively low GUT scales are predicted for $G_{\rm int} = {\rm SU}(4)_C \otimes {\rm SU}(2)_L \otimes {\rm SU}(2)_R \otimes D$ and ${\rm SU}(4)_C \otimes {\rm SU}(2)_L \otimes {\rm U}(1)_R$, and thus the proton decay constraints may be severe in these cases, as discussed in Sec. 4.4.2. Furthermore, except for $G_{\rm int} = {\rm SU}(4)_C \otimes {\rm SU}(2)_L \otimes {\rm SU}(2)_R \otimes D$, we obtain low intermediate scales, with which it may be difficult to account for the neutrino masses, as explained in Sec. 4.4.1. As we will see in Chapter 4, this situation can be improved in the NETDM models.

Chapter 3

Dark matter candidates

In this chapter, we will give a list of SO(10) representations that can contain a dark matter candidate. We only require the dark matter candidate to be stable and neutral under the strong interaction and the electromagnetic interaction. Further constraints on the dark matter will be placed in Chapter 4, 5, 6, where we discuss different dark matter scenarios. Again, we only consider SO(10) representations with dimension not larger than 210.

3.1 Extra U(1) and dark matter stability

For a wide class of DM models, the dark matter particle candidate is stable or have a sufficiently long lifetime compared to the age of the Universe. This stability is usually protected by a discrete symmetry of the model. For example, the R-parity in MSSM [19], the Kaluza-Klein parity in universal extra dimensional models [20] and T-parity in the Littlest Higgs model [21] yield stable particles, which can also be promising DM candidates. The origin of such symmetry is often imposed by hand. Thus it would be interesting if a theory can generate this discrete symmetry naturally.

In fact, GUTs can provide such a framework. Suppose that the rank of a GUT gauge group is larger than four. In this case, the GUT symmetry contains extra symmetries beyond the SM gauge symmetry. These extra symmetries should be spontaneously broken at a high-energy scale by a vacuum expectation value (VEV) of a Higgs field. Then, if we choose the proper representation for the Higgs field, there remain discrete

symmetries, which can be used for DM stabilization [8, 9, 22–26]. The discrete charge of each representation is uniquely determined, and thus we can systematically identify possible DM candidates for each symmetry.

This mechanism can be summarized briefly as the following: suppose there is an extra U(1) gauge symmetry in addition to the SM gauge group. We define the normalization of the U(1) coupling such that all of the fields ϕ_i in a given model have integer charges Q_i with the minimum non-zero value of $|Q_i|$ equal to +1. Now, let us suppose that a Higgs field ϕ_H has a non-zero charge Q_H. Then, if $Q_H = 0$ (mod. N) with $N \geq 2$, the U(1) symmetry is broken to a $\mathbb{Z}_N$ symmetry after the Higgs field obtains a vacuum expectation value (VEV). One can easily show this by noting that both the Lagrangian and the VEV $\langle\phi_H\rangle$ are invariant under the following transformations:

$$\phi_i \to \exp\left(\frac{i2\pi Q_i}{N}\right)\phi_i \ , \qquad \langle\phi_H\rangle \to \exp\left(\frac{i2\pi Q_H}{N}\right)\langle\phi_H\rangle = \langle\phi_H\rangle \ . \tag{3.1}$$

Thus the stability of DM can be guaranteed by the remnant $\mathbb{Z}_N$ symmetry originating from the extra U(1) gauge symmetry if the U(1) charge of the DM is chosen correctly.

SO(10) has one more rank compared to the SM gauge group and the mechanism described above can be applied directly to the extra U(1) factor in SO(10). For the intermediate scale gauge groups we consider in Table 2.2, we can focus on the breaking of

$$\mathrm{U}(1)_{B-L} \times \mathrm{U}(1)_R \to \mathrm{U}(1)_Y \ . \tag{3.2}$$

If this breaking is caused by a Higgs field with even B − L, the low energy theory will be invariant under the matter parity $P_M = (-1)^{3(B-L)}$. For representations of $\dim(R) \leq 210$, only **16** and **126** contain SM singlets that are charged under $\mathrm{U}(1)_{B-L} \times \mathrm{U}(1)_R$. The $|B-L|$ number of the singlets are one and two respectively. Thus **126** is the only choice of the Higgs multiplet that breaks $G_{\rm int}$ to $G_{\rm SM}$ and a discrete symmetry. Finally, it is worth noting that all the components of a SO(10) representation has the same matter parity, thus the heavier components of the dark matter representation will decay to the dark matter particle and SM particles. [1]

[1] For a group theoretical treatment of general Higgs representation that give rise to a discrete symmetry in addition to $G_{\rm SM}$, see [27]

3.2 Dark matter representations

In the last section, we showed that a $\mathbb{Z}_2$ symmetry can be preserved at the low energy with a suitable choice of representation R_2. This symmetry is equivalent to the matter parity $P_M = (-1)^{3(B-L)}$, and we can combine it with rotational symmetry to get the $\mathcal{R}$-parity usually imposed by hand on supersymmetric dark matter models:

$$\mathcal{R} \equiv (-1)^{3(B-L)+2s} \,, \tag{3.3}$$

where s is the spin of the particle. The standard model fermions belong to **16** representations and have $P_M = -1$; the SM Higgs doublet belongs to **10**, the SM gauge bosons belong to **45** and thus the SM bosons have $P_M = +1$; Thus the SM particles has $\mathcal{R} = +1$, and the $B - L$ quantum number of the dark matter particle needs to be odd(even) for scalar(fermion) candidate.

Following the branching rules given in Ref. [28], in Table 3.1, we list $\mathrm{SU}(2)_L \otimes \mathrm{U}(1)_Y$ multiplets in various SO(10) representations that contain an electrically neutral color singlet. A similar list of candidates can be found in earlier work [9]. The table is classified by $B - L$ so one can check the matter parity of the candidates easily; $B - L = 0,\ 2$ candidates are fermionic while $B-L = 1$ candidates are scalar, labeled by an "F" or "S" at the beginning of each row, respectively. A fermionic DM candidate should belong to a **10**, **45**, **54**, **120**, **126**, **210** or **210′** representation, while scalar DM is belongs to a **16** or **144** representation [26,27,29]. The subscript of the model names denotes the $\mathrm{SU}(2)_L$ representation, while the superscript shows hypercharge. A hat is used for $B - L = 2$ candidates.

Different type of dark matter models can be constructed according to the $\mathrm{SU}(2)_L \otimes \mathrm{U}(1)_Y$ assignment of the DM multiplet and the possible interactions between SM particles and the DM candidate. For example, the fermionic candidates $\mathtt{F}^0_\mathbf{1}$ and $\widehat{\mathtt{F}}^0_\mathbf{1}$ are SM singlets and can only interact with SM particles through exchange of intermediate scale virtual particles. The interaction rate is suppressed by the intermediate scale and thus these fermionic candidates will never reach equilibrium with the thermal bath of SM particles. This fits in the frame work of Non-Equilibrium Thermal Dark Matter(NETDM) Scenario, where the dark matter particles are produced continuously out-of-equilibrium after the reheating process. We will consider this class of model in detail in Chapter 4.

Table 3.1: *List of $SU(2)_L \otimes U(1)_Y$ multiplets in SO(10) representations that contain an electric neutral color singlet.*

Model	$B-L$	$\mathrm{SU}(2)_L$	Y	SO(10) representations
$\mathtt{F}_{\mathbf{1}}^{0}$	0	**1**	0	**45**, **54**, **210**
$\mathtt{F}_{\mathbf{2}}^{1/2}$		**2**	1/2	**10**, **120**, **126**, **210′**
$\mathtt{F}_{\mathbf{3}}^{0}$		**3**	0	**45**, **54**, **210**
$\mathtt{F}_{\mathbf{3}}^{1}$		**3**	1	**54**
$\mathtt{F}_{\mathbf{4}}^{1/2}$		**4**	1/2	**210′**
$\mathtt{F}_{\mathbf{4}}^{3/2}$		**4**	3/2	**210′**
$\mathtt{S}_{\mathbf{1}}^{0}$	1	**1**	0	**16**, **144**
$\mathtt{S}_{\mathbf{2}}^{1/2}$		**2**	1/2	**16**, **144**
$\mathtt{S}_{\mathbf{3}}^{0}$		**3**	0	**144**
$\mathtt{S}_{\mathbf{3}}^{1}$		**3**	1	**144**
$\widehat{\mathtt{F}}_{\mathbf{1}}^{0}$	2	**1**	0	**126**
$\widehat{\mathtt{F}}_{\mathbf{2}}^{1/2}$		**2**	1/2	**210**
$\widehat{\mathtt{F}}_{\mathbf{3}}^{1}$		**3**	1	**126**

Other candidates are either scalar singlet that can interact with the SM Higgs doublet through a quartic coupling, or are charged under the electroweak interaction so that they can interact with SM particles through exchange of W or$Z$ boson. Such candidates can interact with SM particles efficiently and fit in the Weakly Interactive Massive Particle(WIMP) DM scenario, which requires DM to be in thermal equilibrium with the SM particles before its abundance freezes out. Such possibility will be discussed in Chapter 5.

Finally, it is also possible that the $\mathcal{R}$-parity odd particles develope a matter-antimatter asymmetry in its number density in the early universe. This can be relavent to baryogenesis and is usually called the Asymmetric Dark Matter(ADM) scenario. This scenario is generally relevant to complex representations that can distinguishes matter and antimatter, such as **16**, **144** and **126**. We will show some realistic models in the context of SO(10) unification theory in Chapter 6.

3.3 Mass hierarchy of dark matter representation

The mass hierarchy of components of a dark matter representation follows a similar assumption as the "extended survival hypothesis" of Higgs reporesentation discussed in Sec. 2.2. That is, at each mass scale, there is a minimal number components necessary to achieve the observed dark matter abundance $\Omega_{\rm CDM}h^2 \approx 0.12$. [45]. For example, consider the doublet WIMP DM candidate $\mathtt{S}_{\mathbf{2}}^{1/2}$ in a complex scalar **16**, in an SO(10) unification with intermediate symmetry $\mathrm{SU}(4)_C \otimes \mathrm{SU}(2)_L \otimes \mathrm{SU}(2)_R$. The dark matter particle and its $\mathrm{SU}(2)_L$ companion should have mass of ~ 1 TeV to achieve the correct relic densityc ite, and according to the hypothesis, only these two complex degrees of freedom among the **16** lie at TeV scale. The branching rule of $\mathrm{SO}(10) supset \mathrm{SU}(4)_C \otimes \mathrm{SU}(2)_L \otimes \mathrm{SU}(2)_R$ gives

$$\mathbf{16} \to (\mathbf{4},\mathbf{1},\mathbf{2}) \oplus (\overline{\mathbf{4}},\mathbf{2},\mathbf{1}) \tag{3.4}$$

The DM doublet belongs to $(\mathbf{4},\mathbf{2},\mathbf{1})$, so to complete the $G_{\rm int}$ representation, the other 6 complex degrees of freedom should lies at the intermediate scale. The rest of the **16** les at the GUT scale, which is the highest scale of the model.

One of the motivation for this mass distribution is to minimize the fine-tuning condition needed to realized the mass spectrum. Moreover, a charged particle in the DM reporesentation can have a cosmological lifetime if its mass is nearly degenerate with the DM particle. For an example, consider a NETDM model with $G_{\rm int} = \mathrm{SU}(4)_C \otimes \mathrm{SU}(2)_L \otimes \mathrm{SU}(2)_R$ and a majorana **45** as the DM representation. The DM candidate can be chosen as the SM singlet of a right-handed triplet $(\psi^0, \psi^\pm)$. Now suppose the triplet have degenerate mass M around the TeV scale at tree level. $\psi^\pm$ are electrically charged and they will be in thermal equilibrium. The mass difference ΔM between the charged and neutral components induced by the radiative corrections can be estimated as

$$\Delta M \simeq \frac{\alpha_1}{4\pi} M \ln\left(\frac{M_{\rm int}}{M}\right) \sim 0.01 \times M \ , \tag{3.5}$$

where α_1 is the U(1) gauge fine-structure constant. The charged components $\psi^\pm$ can decay into the neutral DM ψ^0 only through the exchange of a virtual intermediate-scale gauge boson W_R, which decays into a pair of SM fermions subsequently. We estimate

the decay width as

$$\Gamma(\psi^+ \to \psi^0 f \bar{f}') \sim \frac{\alpha_R^2}{\pi} \frac{(\Delta M)^5}{M_{W_R}^4} \ , \tag{3.6}$$

where $\alpha_R = g_R^2/4\pi$ and g_R and M_{W_R} are the coupling and the mass of the intermediate gauge boson W_R, respectively. Then, for example, when the DM mass is $\mathcal{O}(1)$ TeV and the intermediate scale is $\mathcal{O}(10^{13})$ GeV, the lifetime of ψ^+ is much longer than the age of the Universe, and thus cosmologically stable. The abundance of such a stable charged particle is stringently constrained by the null results of the searching for heavy hydrogen in sea water [30]. The DM multiplets in other cases may also be accompanied by stable colored particles, whose abundance is severely restricted as well. If the intermediate scale is relatively low, the charged/colored particle can have a shorter lifetime. Even in this case, their thermal relic abundance should be extremely small in order not to spoil the success in the Big-Bang Nucleosynthesis (BBN). Quite generally, a degenerate mass spectrum leads to disastrous consequences. This is another motivation to split the DM representation into different mass scales.

The most straight forward way to split the masses of components in a DM representation is to make use of the VEVs that drive the spontaneous symmetry breaking chain, because the couplings of a VEV to different quadratic operators are in general different by the Clebsch-Gordon coefficients. For a scalar DM representation $R_{\rm DM}$, the Lagrangian that is relevant to the mass term can be written as

$$\begin{aligned} -\mathcal{L}_{\rm int} = {} & M^2 |R_{\rm DM}|^2 + \kappa_1 R_{\rm DM}^* R_{\rm DM} R_1 + \{\kappa_2 R_{\rm DM} R_{\rm DM} R_2^* + \text{h.c.}\} \\ & + \lambda_1^{\mathbf{1}} |R_{\rm DM}|^2 |R_1|^2 + \lambda_2^{\mathbf{1}} |R_{\rm DM}|^2 |R_2|^2 + \left\{\lambda_{12}^{\mathbf{126}} \left(R_{\rm DM} R_{\rm DM}\right)_{\mathbf{126}} \left(R_1 R_2^*\right)_{\overline{\mathbf{126}}} + \text{h.c.}\right\} \\ & + \sum_{R'} \lambda_1^{R'} \left(R_{\rm DM}^* R_{\rm DM}\right)_{R'} \left(R_1^* R_1\right)_{R'} + \sum_{R''} \lambda_2^{R''} \left(R_{\rm DM}^* R_{\rm DM}\right)_{R''} \left(R_2^* R_2\right)_{R''} \ , \end{aligned} \tag{3.7}$$

where the subscripts after the parentheses denote the SO(10) representation formed by the product in them. The last line is summed over all possible represenations R', R'' that can be obtained from $R_1^* R_1$ and $R_2^* R_2$ respectively. M, κ_1, and κ_2 are dimensionful parameters, which we assume to be $\mathcal{O}(M_{\rm GUT})$. The terms with the coefficients $\lambda_1^{\mathbf{1}}$ and $\lambda_2^{\mathbf{1}}$ are irrelevant to the generation of the mass splitting in the DM multiplet, as they only give a common mass to all of the components in the multiplet. It is also worth noting that terms including κ_2 and $\lambda_{12}^{\mathbf{126}}$ break the particle number which can be assigned to

the complex scalar $R_{\rm DM}$. Hence, these effects can split $R_{\rm DM}$ into two real scalars with different masses. We use these interactions to avoid the direct detection bound in the case of the complex hypercharged WIMP DM, which we discuss in Sec. 5.3.3

After R_1 gets a VEV, the terms with κ_1 and $\lambda_1^{R'}$ generate mass terms for the components in $R_{\rm DM}$ with different mass values, since the R_1 VEV couples to them with different Clebsch-Gordan coefficients. Thus, by fine tuning the coefficients M, κ_1 and $\lambda_1^{R'}$, one can arrange that the DM multiplet obtains a mass of $\mathcal{O}(M_{\rm int})$, with other multiplets remaining around $\mathcal{O}(M_{\rm GUT})$.

The next step is to separate the $\mathrm{SU}(2)_L$ multiplet $\mathtt{S}^{\mathtt{Y}}_{\mathbf{n}}$ from the intermediate gauge group multiplet. This can be accomplished by appropriately tuning the coefficients of κ_2, $\lambda_{12}^{\mathbf{126}}$ and $\lambda_2^{R''}$ so that the generated mass terms cancel out the intermediate scale mass obtained previously, leaving only the electroweak multiplet of DM candidate at TeV scale. After this step, we obtain a mass spectrum in which only the DM candidate lies around the TeV scale, while its partner fields with respect to the intermediate gauge symmetry are at $M_{\rm int}$. The rest of the components of $R_{\rm DM}$ have masses of $\mathcal{O}(M_{\rm GUT})$.

For the case of fermionic dark matter candidates, the renormalisable operators that give rise to the mass term of the dark matter has the form of

$$\begin{aligned} -\mathcal{L}_{\rm DM} &= M\overline{R}_{\rm DM}R_{\rm DM} - R_1\overline{R}_{\rm DM}R_{\rm DM} - R_2\overline{R}_{\rm DM}R_{\rm DM} \\ &\to (M - c_1 v_{\rm GUT} - c_2 v_{\rm int})\,\overline{\chi}\chi\ . \end{aligned} \tag{3.8}$$

The VEVs of the components of R_1 and R_2 that break SO(10) and $G_{\rm int}$ are denoted by $v_{\rm GUT} \sim M_{\rm GUT}$ and $v_{\rm int} \sim M_{\rm int}$, respectively; χ denotes the DM field and $M \sim M_{\rm GUT}$ is a universal mass. c_1 and c_2 are the Clebsch-Gordan coefficients that vary for different $R_{\rm DM}$ components. Thus, by fine-tuning M such that $M - c_1 v_{\rm GUT} - c_2 v_{\rm int} \sim 1$ TeV, we can set the DM triplet to be at TeV scale while leaving other contents in $R_{\rm DM}$ either around $M_{\rm int}$ or $M_{\rm GUT}$. Finally, it is worth noting that for fermionic $R_{\rm DM}$ listed in Table 3.1, it is impossible to form a singlet out of $R_{\rm DM}R_{\rm DM}\mathbf{126}_H$ or $R^*_{\rm DM}R_{\rm DM}\mathbf{126}_H$. Thus $c_2 = 0$ if $R_2 = \mathbf{126}$, and the whole $G_{\rm int}$ multiplet have a common mass. To split the mass of the dark matter candidate from other components, it is necessary to add extra components to R_2 so that $R_2 = \mathbf{126} \oplus R_2'$. R_2' is chosen from $\mathbf{45}$, $\mathbf{54}$ or $\mathbf{210}$ according to Table 2.1, and developes a VEV of $\langle R_2' \rangle \sim M_{\rm int}$ that breaks $G_{\rm int}$ partly. If $\langle R_2' \rangle$ can couple to the dark matter candidate through a Yukawa-like interaction $R^*_{\rm DM}R_{\rm DM}R_2'$,

the symmetry of the DM multiplet is broken at tree level and thus the mass of the DM candidate can be seperated from the rest of the multiplet by fine-tuning.

Chapter 4

Non-Thermal Equilirium Dark Matter

In this chapter, we consider candidates of Non-Equilibrium Thermal Dark Matter(NETDM) in an SO(10) unification theory. Candidates of NETDM should be a SM singlet so they can only interact extremely weakly with the SM thermal bath in the early universe. The production interaction of the NETDM will never be in equilibrium, and unlike the WIMP scenario, the relic density of NETDM is sensitive to the reheating temperature at which the production process begins.

4.1 Candidates of NETDM

The NETDM mechanism in an SO(10) unification model was first proposed in [7] where the DM particle is a SM singlet but charged under$G_{\rm int}$ so it can only be produced in the early Universe via the exchange of the heavy intermediate-scale particles. Therefore, the production rate is extremely small and their self-annihilation can be neglected. In addition, the produced DM cannot be in the thermal bath since they have no renormalizable interactions with the SM particles. These two features characterize the NETDM mechanism; the DM is produced by SM particles in the thermal bath via the intermediate boson exchange, while they do not annihilate with each other nor attain thermal equilibrium.

The out-of-equilibrium requirement disfavors scalar DM candidates since a scalar, ϕ,

Table 4.1: *Candidates for the NETDM.*

$G_{\rm int}$	$R_{\rm DM}$	SO(10)
$\mathrm{SU}(4)_C \otimes \mathrm{SU}(2)_L \otimes \mathrm{SU}(2)_R$	$(\mathbf{1}, \mathbf{1}, \mathbf{3})$	**45**
	$(\mathbf{15}, \mathbf{1}, \mathbf{1})$	**45**, **210**
	$(\mathbf{10}, \mathbf{1}, \mathbf{3})$	**126**
	$(\mathbf{15}, \mathbf{1}, \mathbf{3})$	**210**
$\mathrm{SU}(4)_C \otimes \mathrm{SU}(2)_L \otimes \mathrm{U}(1)_R$	$(\mathbf{15}, \mathbf{1}, 0)$	**45**, **210**
	$(\mathbf{10}, \mathbf{1}, 1)$	**126**
$\mathrm{SU}(3)_C \otimes \mathrm{SU}(2)_L \otimes \mathrm{SU}(2)_R \otimes \mathrm{U}(1)_{B-L}$	$(\mathbf{1}, \mathbf{1}, \mathbf{3}, 0)$	**45**, **210**
	$(\mathbf{1}, \mathbf{1}, \mathbf{3}, -2)$	**126**
$\mathrm{SU}(3)_C \otimes \mathrm{SU}(2)_L \otimes \mathrm{U}(1)_R \otimes \mathrm{U}(1)_{B-L}$	$(\mathbf{1}, \mathbf{1}, 1, -2)$	**126**

can always have a quartic coupling with the SM Higgs field H — $\lambda_{\phi H}|\phi|^2|H|^2$. Unless $|\lambda_{\phi H}|$ is extremely small for some reason, this coupling keeps scalar DM in thermal equilibrium even when the temperature of the Universe becomes much lower than the reheating temperature. Therefore, we focus on fermionic DM candidates $\mathtt{F}^0_{\mathbf{1}}$ and $\widehat{\mathtt{F}}^0_{\mathbf{1}}$ in Table 3.1: they should be contained in either a **45**, **54**, **126**, or **210** representation.

We follow the discussion in Section 3.3 to determine the mass scale of compoents in the dark matter representation. In Table 4.1, we summarize possible candidates for representation $R_{\rm DM}$ for each intermediate gauge group that contains the DM candidate. We assume the dark matter particle has a mass of TeV scale, and other components of $R_{\rm DM}$ lie around $M_{\rm int}$. The rest of the SO(10) representation have GUT scale masses. With this spectrum of DM representation in mind, we are now able to evaluate the running of the gauge coupling constants and the scales.

4.2 NETDM and gauge coupling unification

In this section we look for the NETDM models in which gauge coupling unification is realized with an appropriate intermediate unification scale. Here, we require $10^{15} \lesssim M_{\rm GUT} \lesssim 10^{18}$ GeV; if $M_{\rm GUT} < 10^{15}$ GeV, then proton decays are too rapid to be

consistent with proton decay experiments, while if $M_{\rm GUT} > 10^{18}$ GeV, then gravitational effects cannot be neglected anymore and a calculation based on quantum field theories may be invalid around the GUT scale. To search for promising candidates, we assume the following conditions. Firstly, a model should contain a NETDM candidate shown in Table 4.1, where only a singlet component has a mass much below the intermediate scale. This component does not affect the running of the gauge couplings. Secondly, the rest of the components in $R_{\rm DM}$ are assumed to be around $M_{\rm int}$ due to the mass splitting mechanism with an additional Higgs multiplet, discussed in Sec. 3.3. At this point, we only assume that there exists an extra Higgs multiplet from either the **45**, **54** or **210** whose mass is around the intermediate scale. Whether the VEV of the extra Higgs actually gives rise to the mass splitting or not will be discussed in the subsequent section. Thirdly, we require that only the SM fields, the intermediate gauge bosons, $R_{\rm DM}$, and R_2 are present below the GUT scale. For example, if we consider the (**1**, **1**, **3**) DM of the **45** given in the first column in Table 4.1, then we suppose that all of the components of the **45** except $R_{\rm DM} = (\mathbf{1}, \mathbf{1}, \mathbf{3})$ should have masses around the GUT scale. This condition is corresponding to the requirement of the minimal fine-tunings in the scalar potential to realize an adequate mass spectrum.

With the conditions, we then search for possible candidates by using the one-loop analytic formula given in Appendix D. In Table 4.2, we summarize the field contents that satisfy the above requirements, as well as the values of $\log_{10}(M_{\rm int})$, $\log_{10}(M_{\rm GUT})$, and $g_{\rm GUT}$, with $M_{\rm int}$ and $M_{\rm GUT}$ in GeV. All of the values are evaluated at one-loop level. Here the subscript R, C, W, or D of each multiplet indicates that it is a real scalar, a complex scalar, a Weyl fermion, or a Dirac fermion, respectively. As for the intermediate Higgs fields, R_2, listed in Table 4.2, $(\mathbf{10}, \mathbf{1}, \mathbf{3})_C$ and $(\mathbf{1}, \mathbf{1}, \mathbf{3}, -2)_C$ are from the **126** Higgs field, while all other representations included in R_2 are extra Higgs fields introduced to resolve the degeneracy problem. For the additional Higgs fields, we only show the real scalar cases for brevity. Indeed, we can also consider complex scalars for the Higgs fields and find that gauge coupling unification is also realized in these cases, where both the intermediate and GUT scales are only slightly modified.

Table 4.2: *Models that realize the gauge coupling unification. M_{int} and M_{GUT} are given in GeV. All of the values listed here are evaluated at one-loop level.*

$\mathrm{SU}(4)_C \otimes \mathrm{SU}(2)_L \otimes \mathrm{SU}(2)_R$				
R_{DM}	R_2	$\log_{10}(M_{\mathrm{int}})$	$\log_{10}(M_{\mathrm{GUT}})$	g_{GUT}
$(\mathbf{1},\mathbf{1},\mathbf{3})_W$	$(\mathbf{10},\mathbf{1},\mathbf{3})_C$ $(\mathbf{1},\mathbf{1},\mathbf{3})_R$	10.8	15.9	0.53
$(\mathbf{1},\mathbf{1},\mathbf{3})_D$	$(\mathbf{10},\mathbf{1},\mathbf{3})_C$ $(\mathbf{1},\mathbf{1},\mathbf{3})_R$	9.8	15.7	0.53
$\mathrm{SU}(4)_C \otimes \mathrm{SU}(2)_L \otimes \mathrm{SU}(2)_R \otimes D$				
R_{DM}	R_2	$\log_{10}(M_{\mathrm{int}})$	$\log_{10}(M_{\mathrm{GUT}})$	g_{GUT}
$(\mathbf{15},\mathbf{1},\mathbf{1})_W$	$(\mathbf{10},\mathbf{1},\mathbf{3})_C$ $(\overline{\mathbf{10}},\mathbf{3},\mathbf{1})_C$ $(\mathbf{15},\mathbf{1},\mathbf{1})_R$	13.7	16.2	0.56
$(\mathbf{15},\mathbf{1},\mathbf{1})_W$	$(\mathbf{10},\mathbf{1},\mathbf{3})_C$ $(\overline{\mathbf{10}},\mathbf{3},\mathbf{1})_C$ $(\mathbf{15},\mathbf{1},\mathbf{3})_R$ $(\mathbf{15},\mathbf{3},\mathbf{1})_R$	14.2	15.5	0.56
$(\mathbf{15},\mathbf{1},\mathbf{1})_D$	$(\mathbf{10},\mathbf{1},\mathbf{3})_C$ $(\overline{\mathbf{10}},\mathbf{3},\mathbf{1})_C$ $(\mathbf{15},\mathbf{1},\mathbf{3})_R$ $(\mathbf{15},\mathbf{3},\mathbf{1})_R$	14.4	16.3	0.58
$\mathrm{SU}(3)_C \otimes \mathrm{SU}(2)_L \otimes \mathrm{SU}(2)_R \otimes \mathrm{U}(1)_{B-L}$				
R_{DM}	R_2	$\log_{10}(M_{\mathrm{int}})$	$\log_{10}(M_{\mathrm{GUT}})$	g_{GUT}
$(\mathbf{1},\mathbf{1},\mathbf{3},0)_W$	$(\mathbf{1},\mathbf{1},\mathbf{3},-2)_C$ $(\mathbf{1},\mathbf{1},\mathbf{3},0)_R$	6.1	16.6	0.52

4.3 Models

In the previous section, we have reduced the possible candidates to those presented in Table 4.2. In this section, we study if any of those models are viable, *i.e.*, we check if they actually offer appropriate mass spectrum to realize the NETDM scenario, with the charged/colored components in R_{DM} acquiring masses of $\mathcal{O}(M_{\mathrm{int}})$.

First, let us consider the $(\mathbf{1},\mathbf{1},\mathbf{3})_{W/D}$ DM representation in the $\mathrm{SU}(4)_C \otimes \mathrm{SU}(2)_L \otimes \mathrm{SU}(2)_R$ gauge theory. To split the masses in the $(\mathbf{1},\mathbf{1},\mathbf{3})$ multiplet ψ^r, we need to couple

the DM with the $(\mathbf{1},\mathbf{1},\mathbf{3})_R$ Higgs ϕ^r, with r denoting the $\mathrm{SU}(2)_R$ index. Since the fields transform as triplets under the $\mathrm{SU}(2)_R$ transformations, to construct an invariant term from the fields, the indices should be contracted anti-symmetrically, *i.e.*, the coupling should have a form like

$$\epsilon_{pqr}(\overline{\psi})^p\psi^q\phi^r \ . \tag{4.1}$$

Then, if ψ^r is a Majorana fermion, the above term always vanishes. Thus, ψ^r should be a Dirac fermion, that is, $(\mathbf{1},\mathbf{1},\mathbf{3})_D$ is the unique candidate for NETDM in this case.

Next, we study the terms in the SO(10) Lagrangian relevant to the masses of the fields much lighter than the GUT scale. In SO(10), $(\mathbf{1},\mathbf{1},\mathbf{3})_D$, $(\mathbf{1},\mathbf{1},\mathbf{3})_R$, and $(\mathbf{10},\mathbf{1},\mathbf{3})_C$ are included in the $\mathbf{45}_D$, $\mathbf{45}_R$, and $\mathbf{126}_C$, respectively. The SO(10) gauge group is spontaneously broken by the $\mathbf{210}_R$ Higgs field (R_1) into the $\mathrm{SU}(4)_C\otimes\mathrm{SU}(2)_L\otimes\mathrm{SU}(2)_R$ intermediate gauge group. As is usually done in the intermediate scale scenario, we fine-tune the Higgs potential so that the $(\mathbf{1},\mathbf{1},\mathbf{3})_R$ and $(\mathbf{10},\mathbf{1},\mathbf{3})_C$ Higgs fields have masses around the intermediate scale. This can be always performed by using the couplings of the $\mathbf{45}_R$ and $\mathbf{126}_C$ fields with the $\mathbf{210}_R$ Higgs field, which acquires a VEV of the order of the GUT scale. Similarly, we give desirable masses to the fields in $(\mathbf{1},\mathbf{1},\mathbf{3})_D$ by carefully choosing the couplings of the $\mathbf{45}_D$ fermion with the $\mathbf{45}_R$ and $\mathbf{126}_C$ Higgs fields. Here, the relevant interactions are

$$\mathcal{L}_{\rm int} = -M_{45_D}\overline{\mathbf{45}_D}\mathbf{45}_D - iy_{45}\overline{\mathbf{45}_D}\mathbf{45}_D\mathbf{45}_R - y_{210}\overline{\mathbf{45}_D}\mathbf{45}_D\mathbf{210}_R \ . \tag{4.2}$$

Notice that $\mathbf{45}_D$ does not couple to the $\mathbf{126}_C$ field, as already mentioned in Sec. 3.3. After the $R_1 = \mathbf{210}_R$ Higgs field gets a VEV $\langle\mathbf{210}_R\rangle = v_{210}$, the interactions in Eq. (4.2) lead to the following terms:[1]

$$\mathcal{L}_{\rm int} \to -M_{\rm DM}(\overline{\psi})^r\psi^r - iy_{45}\epsilon_{rst}(\overline{\psi})^r\psi^s\phi^t \ , \tag{4.3}$$

with $M_{\rm DM} = M_{45_D} + y_{210}v_{210}/\sqrt{6}$. Here, ψ^r and ϕ^r denote the $(\mathbf{1},\mathbf{1},\mathbf{3})_D$ and $(\mathbf{1},\mathbf{1},\mathbf{3})_R$ components in $\mathbf{45}_D$ and $\mathbf{45}_R$, respectively. We find that although M_{45_D} and v_{210} are expected to be $\mathcal{O}(M_{\rm GUT})$, we can let $M_{\rm DM}$ be much lighter than the GUT scale by carefully choosing the above parameters so that they cancel each other. In addition, it turns out that the mass term of the $(\mathbf{1},\mathbf{3},\mathbf{1})_D$ component in $\mathbf{45}_D$ is given by M_{45_D} −

[1] For the computation of the Clebsch-Gordan coefficients, we have used the results given in Ref. [53].

$y_{210}v_{210}/\sqrt{6}$. Thus, even if we fine-tune M_{45_D} and y_{210} to realize $M_{\rm DM} \ll M_{\rm GUT}$, the mass of $(\mathbf{1},\mathbf{3},\mathbf{1})_D$ is still around the GUT scale. This observation reflects the violation of the D-parity in this model. At this point, all of the components in ψ^r have identical masses (the "degeneracy problem"). Once the neutral component of ϕ^r acquires a VEV $\langle\phi^3\rangle = v_{45}$, which is assumed to be $\mathcal{O}(M_{\rm int})$, the second term in Eq. (4.3) gives rise to additional mass terms for ψ^r. These are

$$\mathcal{L}_{\rm int} \to -M_{\rm DM}\overline{\psi^0}\psi^0 - M_+\overline{\psi^+}\psi^+ - M_-\overline{\psi^-}\psi^- \ , \tag{4.4}$$

where $M_\pm = M_{\rm DM} \mp y_{45}v_{45}$, and ψ^0 and $\psi^\pm$ are the neutral and charged components, respectively.[2] The above expression shows that the VEV of the $\mathbf{45}_R$ Higgs field indeed solves the degeneracy problem; if $M_{\rm DM} \ll M_{\rm int}$ and $y_{45}v_{45} = \mathcal{O}(M_{\rm int})$, then the charged components acquire masses of $\mathcal{O}(M_{\rm int})$, while the neutral component has a mass much lighter than $M_{\rm int}$. Thus, we obtain the mass spectrum we have assumed in the previous section.

In the next example, we consider the DM representation $R_{\rm DM} = (\mathbf{15},\mathbf{1},\mathbf{1})_W$ with $R_2 = (\mathbf{10},\mathbf{1},\mathbf{3})_C \oplus (\overline{\mathbf{10}},\mathbf{3},\mathbf{1})_C \oplus (\mathbf{15},\mathbf{1},\mathbf{1})_R$ in the left-right symmetric $\mathrm{SU}(4)_C \otimes \mathrm{SU}(2)_L \otimes \mathrm{SU}(2)_R$ gauge theory. In this case, $R_1 = \mathbf{54}_R$. We assume that the $(\mathbf{15},\mathbf{1},\mathbf{1})_W$ is a part of the $\mathbf{45}_W$, while both $(\mathbf{10},\mathbf{1},\mathbf{3})_C$ and $(\overline{\mathbf{10}},\mathbf{3},\mathbf{1})_C$ are part of the $\mathbf{126}_C$. The couplings of the DM with the Higgs fields, as well as its mass term, are then given by

$$\mathcal{L}_{\rm int} = -\frac{M_{45_W}}{2}\mathbf{45}_W\mathbf{45}_W - \frac{y_{54}}{2}\mathbf{45}_W\mathbf{45}_W\mathbf{54}_R - \frac{y_{210}}{2}\mathbf{45}_W\mathbf{45}_W\mathbf{210}_R + \text{h.c.} \ , \tag{4.5}$$

Here, $(\mathbf{15},\mathbf{1},\mathbf{1})_R$ is included in the $\mathbf{210}_R$ field; we cannot use a $\mathbf{45}_R$ in this case since the Weyl fermion $\mathbf{45}_W$ has no coupling to the $\mathbf{45}_R$.[3] As before, below the GUT scale, the VEV of $\mathbf{54}_R$, v_{54}, gives a common mass M to the $(\mathbf{15},\mathbf{1},\mathbf{1})_W$ multiplet with $M = M_{45_W} - y_{54}v_{54}/\sqrt{15}$. We can take $M = \mathcal{O}(M_{\rm int})$ by fine-tuning M_{45_W} and $y_{54}v_{54}$. The above Lagrangian then reduces to

$$\mathcal{L}_{\rm int} \to -\frac{M}{2}\psi^A\psi^A + \frac{2y_{210}}{\sqrt{3}}\mathrm{Tr}(\psi\phi\psi) + \text{h.c.} \ , \tag{4.6}$$

where ψ^A and ϕ^A denote the $(\mathbf{15},\mathbf{1},\mathbf{1})_W$ and $(\mathbf{15},\mathbf{1},\mathbf{1})_R$ fields, respectively, with $\psi \equiv \psi^A T^A$ and $\phi \equiv \phi^A T^A$; $A, B, C = 1, \ldots 15$ are the SU(4) adjoint indices and T^A are the

[2] Note that since ψ^r are Dirac fermions, $(\psi^0)^{\mathcal{C}} \neq \psi^0$ and $(\psi^\pm)^{\mathcal{C}} \neq \psi^\mp$

[3] It is also possible to embed $(\mathbf{15},\mathbf{1},\mathbf{1})_W$ into $\mathbf{210}_W$ and $(\mathbf{15},\mathbf{1},\mathbf{1})_R$ into $\mathbf{45}_R$. The phenomenology in this case is the same as that discussed in text.

SU(4) generators. The mass degeneracy in this case is resolved by the VEV of the $\mathbf{210}_R$ field,

$$\langle\phi\rangle = \frac{v_{210}}{2\sqrt{6}}\ \mathrm{diag}(1,1,1,-3), \tag{4.7}$$

with which Eq. (4.6) leads to

$$\mathcal{L}_{\rm int} \to -\frac{M_{\rm DM}}{2}\psi^0\psi^0 - \frac{M_{\tilde{g}}}{2}\widetilde{g}^A\widetilde{g}^A - M_\xi\overline{\xi}_a\xi^a + \text{h.c.}\ , \tag{4.8}$$

where ψ^0, $\widetilde{g}^A$, ξ^a, and $\overline{\xi}_a$ are the color singlet, octet, triplet, and anti-triplet components in $(\mathbf{15},\mathbf{1},\mathbf{1})_W$, respectively, with a denoting the color index, and

$$M_{\rm DM} = M + \frac{\sqrt{2}}{3}y_{210}v_{210}\ , \tag{4.9}$$

$$M_{\tilde{g}} = M - \frac{1}{3\sqrt{2}}y_{210}v_{210}\ , \tag{4.10}$$

$$M_\xi = M + \frac{1}{3\sqrt{2}}y_{210}v_{210}\ . \tag{4.11}$$

Therefore, by carefully adjusting $y_{210}v_{210}$, we can make the DM ψ^0 much lighter than $M_{\rm int}$ while keeping the other components around the intermediate scale.

There are two more possible representations for $R_{\mathrm{D}M}$ for the left-right symmetric $\mathrm{SU}(4)_C \otimes \mathrm{SU}(2)_L \otimes \mathrm{SU}(2)_R$ intermediate gauge group given in Table 4.2, namely $(\mathbf{15},\mathbf{1},\mathbf{1})_{W/D}$. In this case, however, one can readily conclude that the degeneracy problem cannot be solved by the $(\mathbf{15},\mathbf{1},\mathbf{3})_R$ and $(\mathbf{15},\mathbf{3},\mathbf{1})_R$ Higgs fields. This is because the Yukawa couplings between the DM and these Higgs fields are forbidden by the intermediate gauge symmetry. As a consequence, we can safely neglect these possibilities.

Finally, we discuss the model presented in the last column in Table 4.2. We again find that the $(\mathbf{1},\mathbf{1},\mathbf{3},0)_R$ Higgs field does not yield a mass difference among the components in the $(\mathbf{1},\mathbf{1},\mathbf{3},0)_W$ DM multiplet, since the operator in Eq. (4.1) vanishes when the DM is a Weyl fermion. Thus, we do not consider this model in the following discussion.

As a result, we obtain two distinct models for NETDM within SO(10). We summarize these two models in Table 4.3. We call them Model I and II in what follows. Here, $M_{\rm int}$ and $M_{\rm GUT}$ are given in GeV, and all of the values are evaluated with two-loop RGEs and differ somewhat from the 1-loop values given in Table 4.2. The errors shown in the parentheses arise from uncertainties in the input parameters. In addition, we

again expect threshold corrections at $M_{\rm int}$ and $M_{\rm GUT}$. Furthermore, we neglect the contribution of Yukawa couplings to the RGEs above the intermediate scale, and this also will contribute to the theoretical error. We estimate that these two sources cause $\mathcal{O}(1)\%$ uncertainties in the values displayed in Table 4.3. From these results, we find that the presence of the DM component as well as the extra Higgs bosons can significantly alter the intermediate and GUT scales,[4] because of their effects on the gauge coupling running. To illustrate this more clearly, in Fig. 4.1 we show running of gauge couplings in each theory. The left and right panels of Fig. 4.1 correspond to Model I and II, respectively. In each figure, solid (dashed) lines show the case with (without) DM and additional Higgs bosons. The blue, green, and red lines represent the running of the U(1), SU(2) and SU(3) gauge couplings, respectively, where the U(1) fine structure constant α_1 is defined by

$$\frac{1}{\alpha_1} \equiv \frac{3}{5}\frac{1}{\alpha_{2R}} + \frac{2}{5}\frac{1}{\alpha_4} \ , \tag{4.12}$$

while the $\mathrm{SU}(3)_C$ coupling α_3 is defined by $\alpha_3 \equiv \alpha_4$ above the intermediate scale. These figures clearly show the effects of the extra particles on the gauge coupling running. In particular, the GUT scale in Model II is now well above 10^{15} GeV, which allows this model to evade the proton decay constraints, as will be seen in the subsequent section.

Table 4.3: *NETDM models. M_{int} and M_{GUT} are given in GeV. All of the values are evaluated with the two-loop RGEs.*

	Model I	Model II
$G_{\rm int}$	$\mathrm{SU}(4)_C \otimes \mathrm{SU}(2)_L \otimes \mathrm{SU}(2)_R$	$\mathrm{SU}(4)_C \otimes \mathrm{SU}(2)_L \otimes \mathrm{SU}(2)_R \otimes D$
$R_{\rm DM}$	$(\mathbf{1},\mathbf{1},\mathbf{3})_D$ in $\mathbf{45}_D$	$(\mathbf{15},\mathbf{1},\mathbf{1})_W$ in $\mathbf{45}_W$
R_1	$\mathbf{210}_R$	$\mathbf{54}_R$
R_2	$(\mathbf{10},\mathbf{1},\mathbf{3})_C \oplus (\mathbf{1},\mathbf{1},\mathbf{3})_R$	$(\mathbf{10},\mathbf{1},\mathbf{3})_C \oplus (\mathbf{10},\mathbf{3},\mathbf{1})_C \oplus (\mathbf{15},\mathbf{1},\mathbf{1})_R$
$\log_{10}(M_{\rm int})$	8.08(1)	13.664(5)
$\log_{10}(M_{\rm GUT})$	15.645(7)	15.87(2)
$g_{\rm GUT}$	0.53055(3)	0.5675(2)

[4] However, their existence hardly changes the intermediate scale in Model II, which is clarified in Appendix D.

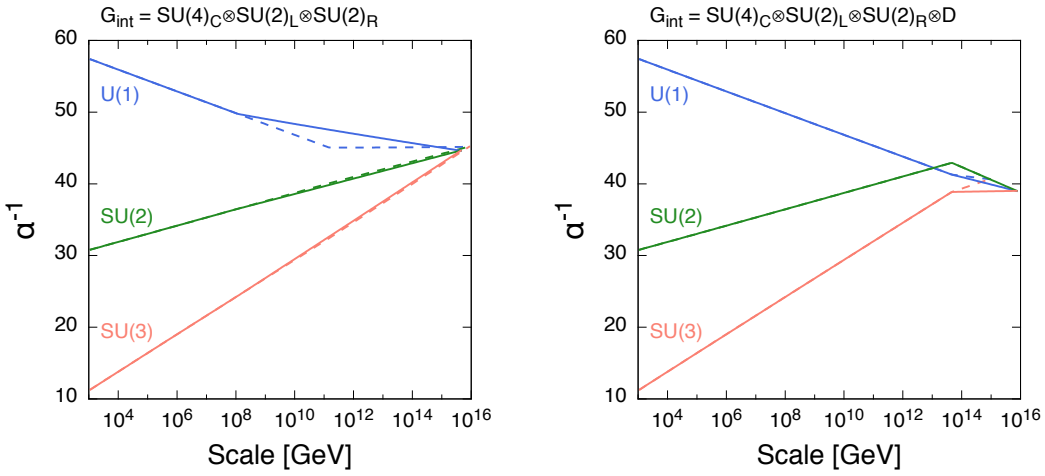

(a) Model I (b) Model II

Figure 4.1: *Running of gauge couplings. Solid (dashed) lines show the case with (without) DM and additional Higgs bosons. Blue, green, and red lines represent the running of the U(1), SU(2) and SU(3) gauge couplings, respectively.*

4.4 Phenomenological aspects

Now that we have obtained the NETDM models, we can study their phenomenological aspects and possible implications in future experiments. In Sec. 4.4.1, we first consider whether these models can give appropriate masses for light neutrinos. Next, in Sec. 4.4.2, we evaluate proton lifetimes in each model and discuss the testability in future proton decay experiments. Finally, we compute the abundance of DM produced by the NETDM mechanism in Sec. 4.4.3, and predict the reheating temperature after inflation.

4.4.1 Neutrino mass

In SO(10) GUTs, the Majorana mass terms of the right-handed neutrinos are induced after the $B-L$ symmetry is broken. These mass terms are generated from the Yukawa couplings of the **16** spinors with the $\mathbf{126}_C$ Higgs field. If the Yukawa couplings are $\mathcal{O}(1)$, then the Majorana mass terms are $\mathcal{O}(M_{\rm int})$. On the other hand, in these models, the Dirac masses of neutrinos are equal to the up-type quark masses, m_u, at the unification

scale. Therefore, via the seesaw mechanism [54], light neutrino masses are given by

$$m_\nu \simeq \frac{m_u^2}{M_{\rm int}} \ . \tag{4.13}$$

In Model II, $M_{\rm int} = \mathcal{O}(10^{13})$ GeV indeed gives proper values for neutrino masses.[5] However, in Model I, a low intermediate scale of $\mathcal{O}(10^8)$ GeV yields neutrino masses which are too heavy using the standard seesaw expression (4.13). Thus, Model I is disfavored on the basis of small neutrino masses.

The defect in Model I may be evaded if the $(\mathbf{15}, \mathbf{2}, \mathbf{2})$ component in $\mathbf{126}_C$ has a sizable mixing with the $(\mathbf{1}, \mathbf{2}, \overline{\mathbf{2}})$ Higgs boson and acquires a VEV of the order of the electroweak scale. In this case, the neutrino Yukawa couplings can differ from those of the up-quark, and thus the relation (4.13) does not hold any more. For sizable mixing to occur, the $(\mathbf{15}, \mathbf{2}, \mathbf{2})$ field should lie around the intermediate scale. One might think that the presence of additional fields below the GUT scale would modify the running of the gauge couplings and spoil the above discussion based on gauge coupling unification. However, it turns out that both the intermediate and GUT scales are hardly affected by the existence of this field, though the unified gauge coupling constant becomes slightly larger. This is because its contribution to the one-loop beta function coefficients is $\Delta b_4 = 16/3$ and $\Delta b_{2L} = \Delta b_{2R} = 5$, and thus their difference is very tiny (see the discussion given in Appendix D). Therefore, we can take the $(\mathbf{15}, \mathbf{2}, \mathbf{2})$ to be at the intermediate scale with little change in the values of $M_{\rm int}$ and $M_{\rm GUT}$. The presence of the $(\mathbf{15}, \mathbf{2}, \mathbf{2})$ is also desirable to account for the down-type quark and charged lepton Yukawa couplings [14, 50]. In addition, the higher-dimensional operators induced above the GUT scale may also affect the Yukawa couplings. Constructing a realistic Yukawa sector in these models is saved for future work.

4.4.2 Proton decay

Proton decay is a smoking gun signature of GUTs, and thus a powerful tool for testing them. In non-SUSY GUTs, $p \to e^+\pi^0$ is the dominant decay mode, which is caused

[5] Note that in a left-right symmetric model such as Model II there is in general also a type-II seesaw contribution to m_ν from the VEV of the $\mathrm{SU}(2)_L$ triplet in the $\mathbf{126}_C$. However, we know from constraints on the ρ-parameter that the VEV must be quite small and definitely much smaller than the VEV of the $\mathrm{SU}(2)_R$ triplet. For example, if the mixing between the $\mathrm{SU}(2)_L$ and $\mathrm{SU}(2)_R$ triplets with the Higgs doublets is small, it is safe to assume that the $\mathrm{SU}(2)_L$ triplet VEV is small and thus the type-II seesaw contribution is subdominant [55].

by the exchange of GUT-scale gauge bosons. This could be compared with the case of the SUSY GUTs; in SUSY GUTs, the color-triplet Higgs exchange usually yields the dominant contribution to proton decay, which gives rise to the $p \to K^+\bar{\nu}$ decay mode [56].

Since the $p \to e^+\pi^0$ decay mode is induced by gauge interactions, we can make a robust prediction for the partial decay lifetime of this mode. Details of the calculation are given in Appendix E. By using the results given there, we evaluate the partial decay lifetime of the $p \to e^+\pi^0$ mode in each theory, and plot it as a function of $M_X/M_{\rm GUT}$ (M_X denotes the mass of the GUT-scale gauge boson) in Fig. 4.2. Here, the blue and red solid lines represent Models I and II, while the blue and red dashed lines represent the models without the DM and extra Higgs multiplets as given in Table 2.2, namely $G_{\rm int} = {\rm SU}(4)_C \otimes {\rm SU}(2)_L \otimes {\rm SU}(2)_R$ and $G_{\rm int} = {\rm SU}(4)_C \otimes {\rm SU}(2)_L \otimes {\rm SU}(2)_R \otimes D$, respectively. The shaded area shows the region which is excluded by the current experimental bound, $\tau(p \to e^+\pi^0) > 1.4 \times 10^{34}$ years [57, 58]. We have varied the heavy gauge boson mass between $M_{\rm GUT}/2 \leq M_X \leq 2M_{\rm GUT}$, which reflects our ignorance of the GUT scale mass spectrum. From this figure, we see that the existence of DM and Higgs multiplets produces a large effect on the proton decay lifetime. In particular, in the case of ${\rm SU}(4)_C \otimes {\rm SU}(2)_L \otimes {\rm SU}(2)_R \otimes D$, the predicted lifetime is so small that the present bound has already excluded the possibility. This conclusion can be evaded, however, once the DM and R_2 Higgs multiplets are included in the theory as they raise the value of $M_{\rm GUT}$. Moreover, Model I is now being constrained by the proton decay experiments. In this case, the inclusion of the DM and Higgs multiplets decreases $M_{\rm GUT}$. Future proton decay experiments, such as the Hyper-Kamiokande experiment [59], may offer much improved sensitivities (by about an order of magnitude), with which we can probe a wide range of parameter space in both models.

4.4.3 Non-equilibrium thermal dark matter

Finally, we evaluate the relic abundance of DM produced by the NETDM mechanism [7] in Models I and II. In both of these models, the DM ψ^0 is produced in the early Universe via the exchange of the intermediate-scale particles. Therefore, the production rate is extremely small and their self-annihilation can be neglected. In addition, the produced DM cannot be in the thermal bath since they have no renormalizable interactions with

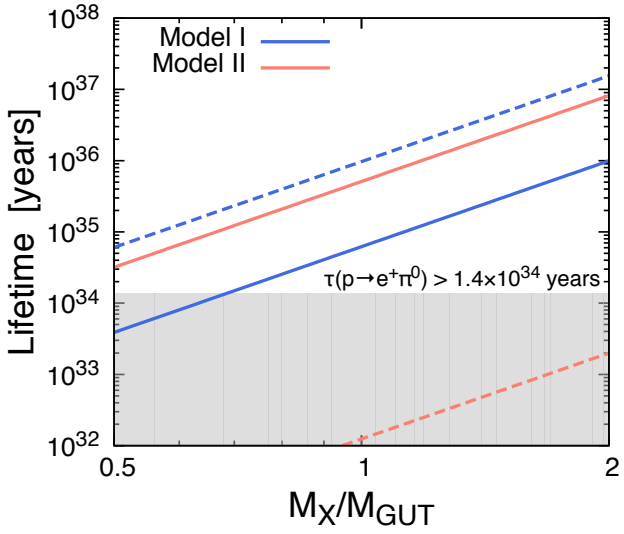

Figure 4.2: *Proton lifetimes as functions of M_X/M_{GUT}. Blue solid and red solid lines represent Model I and Model II, respectively. Blue dashed and red dashed lines represent the cases for $G_{int} = SU(4)_C \otimes SU(2)_L \otimes SU(2)_R$ and $G_{int} = SU(4)_C \otimes SU(2)_L \otimes SU(2)_R \otimes D$ when the DM and extra Higgs multiplets are not included. The shaded area shows the region which is excluded by the current experimental bound, $\tau(p \to e^+\pi^0) > 1.4 \times 10^{34}$ years [57, 58].*

the SM particles. These two features characterize the NETDM mechanism; the DM is produced by SM particles in the thermal bath via the intermediate boson exchange, while they do not annihilate with each other nor attain thermal equilibrium. In what follows, we estimate the density of the DM produced via this mechanism and determine the reheating temperature which realizes the observed DM density.

The Boltzmann equation for the DM ψ^0 is given by

$$\frac{dY_{\rm DM}}{dx} = \sqrt{\frac{\pi}{45}} \frac{g_{*s}}{\sqrt{g_{*\rho}}} M_{\rm DM} M_{\rm Pl} \frac{\langle \sigma v \rangle}{x^2} Y_{\rm eq}^2 \ , \tag{4.14}$$

with $Y_{\rm DM} \equiv n_{\rm DM}/s$ and $Y_{\rm eq} \equiv n_{\rm eq}/s$ where $n_{\rm DM}$ is the DM number density, $n_{\rm eq}$ is the equilibrium number density of each individual initial state SM particle, and s is the entropy of the Universe; $x \equiv M_{\rm DM}/T$ with T being the temperature of the Universe;

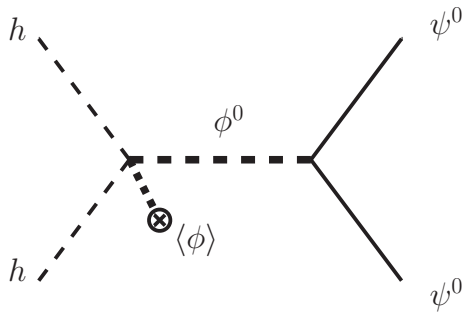

Figure 4.3: *Diagram responsible for the DM production in Model II.*

g_{*s} and $g_{*\rho}$ are the effective degrees of freedom for the entropy and energy density in the thermal bath, respectively; $M_{\rm Pl} \equiv 1/\sqrt{G_N} = 1.22 \times 10^{19}$ GeV is the Planck mass; $\langle\sigma v\rangle$ is the thermally averaged total annihilation cross section of the initial SM particles, f, into the DM pair. When we derive Eq. (4.14), we neglect the DM self-annihilation contribution as discussed above. From now on, we assume $g_{*s} = g_{*\rho} \equiv g_*$ for brevity.

We evaluate the thermal averaged cross section $\langle\sigma v\rangle$ multiplied by the equilibrium number density squared $n_{\rm eq}^2$ as

$$\langle\sigma v\rangle n_{\rm eq}^2 \simeq \frac{T}{512\pi^5}\int_{4M_{\rm DM}^2}^{\infty} d\hat{s}\sqrt{\hat{s}-4M_{\rm DM}^2}K_1(\sqrt{\hat{s}}/T)\sum|\mathcal{M}|^2 \ , \tag{4.15}$$

where $\sqrt{\hat{s}}$ denotes the center-of-mass energy, and $K_n(x)$ is the modified Bessel function of the second kind. Here, we have used the approximation $m_f \ll \sqrt{\hat{s}}$ with m_f the masses of the SM particles since the particle production predominantly occurs at high temperature, and neglected the angular dependence of $\mathcal{M}$ for simplicity. In addition, we have assumed the initial particles follow a Maxwell-Boltzmann distribution, and ignored statistical mechanical factors which may result from the Fermi-Dirac or Bose-Einstein distribution. $\sum|\mathcal{M}|^2$ indicates the sum of the squared-amplitude over all possible incoming SM particles, as well as the spin of the final state.

Next, we evaluate the amplitude $\mathcal{M}$ in each model. First, we consider the case of Model II. In this case, the dominant contribution comes from the tree-level Higgs-boson annihilation process displayed in Fig. 4.3. Here, ψ^0, h, and ϕ^0 denote the DM, the SM Higgs boson, and the singlet component of the $(\mathbf{15},\mathbf{1},\mathbf{1})_R$, respectively, and the VEV

$\langle\phi\rangle$ is given in Eq. (4.7). From the dimensional analysis, we estimate the contribution as

$$\sum |\mathcal{M}|^2 \simeq c\ \frac{\hat{s} - 4M_{\rm DM}^2}{M_{\rm int}^2}\ , \tag{4.16}$$

where c is a numerical factor which includes the unknown couplings appearing in the diagram. By substituting Eqs. (4.15) and (4.16) into Eq. (4.14), we have

$$\frac{dY_{\rm DM}}{dx} \simeq \frac{c}{1024\pi^7}\left(\frac{45}{\pi g_*}\right)^{\frac{3}{2}} \frac{M_{\rm Pl}M_{\rm DM}}{M_{\rm int}^2}\frac{1}{x^2}\int_{2x}^{\infty} t(t^2-4x^2)^{\frac{3}{2}}K_1(t)dt\ . \tag{4.17}$$

When $M_{\rm DM} \ll T_{\rm RH}$ with $T_{\rm RH}$ being the reheating temperature, the above equation is easily integrated to give

$$Y_{\rm DM}^{(0)} \simeq \frac{c}{64\pi^7}\left(\frac{45}{\pi g_*}\right)^{\frac{3}{2}} \frac{M_{\rm Pl}T_{\rm RH}}{M_{\rm int}^2}\ , \tag{4.18}$$

where the superscript "(0)" implies the present-day value. On the other hand, the current value of $Y_{\rm DM}^{(0)}$ is given by

$$Y_{\rm DM}^{(0)} = \frac{\Omega_{\rm DM}\rho_{\rm crit}^{(0)}}{M_{\rm DM}s^{(0)}}\ , \tag{4.19}$$

where $\Omega_{\rm DM}$ is the DM density parameter and $\rho_{\rm crit}^{(0)}$ is the critical density of the Universe. In the following calculation, we use $\Omega_{\rm DM}h^2 = 0.12$, $\rho_{\rm crit}^{(0)} = 1.05\times10^{-5}h^2$ GeV $\cdot$ cm^{-3}, and $s^{(0)} = 2.89\times10^3$ cm^{-3}, with h the Hubble parameter. As a result, we obtain

$$T_{\rm RH} \simeq 2.7\times10^4\ {\rm GeV}\times\left(\frac{\Omega_{\rm DM}h^2}{0.12}\right)\left(\frac{g_*^{\frac{3}{2}}c^{-1}}{10^4}\right)\left(\frac{M_{\rm DM}}{100\ {\rm GeV}}\right)^{-1}\ , \tag{4.20}$$

where we have set the value of $M_{\rm int} = 10^{13.66}$ GeV from the result in Table 4.3. This approximate formula is valid when $M_{\rm DM} \ll T_{\rm RH}$. Here, $g_*^{\frac{3}{2}}c^{-1}$ is an unknown factor and thus causes an uncertainty in the computation. For instance, if $g_* = \mathcal{O}(100)$ and the quartic coupling of h and ϕ is ~ 0.3, then $g_*^{\frac{3}{2}}c^{-1} = \mathcal{O}(10^4)$. Note that the perturbativity of the quartic coupling ensures that this factor cannot become too small. On the other hand, it also has an upper bound; if c is extremely small, then the one-loop gauge-boson exchange contribution dominates over the tree-level. Taking this consideration into account, we vary the value of $g_*^{\frac{3}{2}}c^{-1}$ by a factor of ten to estimate the uncertainty in the analysis given below.

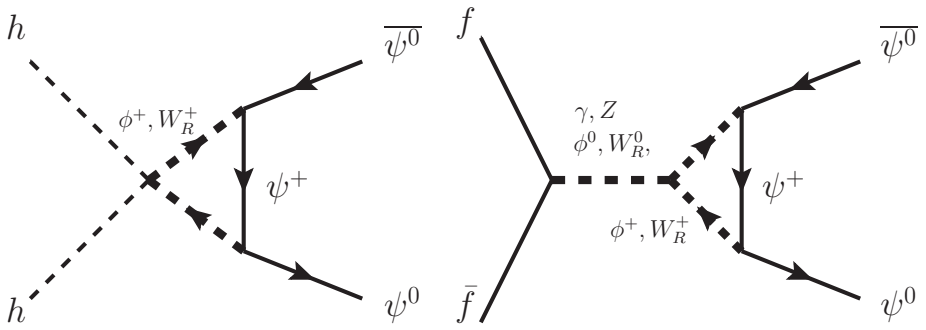

Figure 4.4: *Examples of diagrams responsible for the DM production in Model I.*

Next, we evaluate the relic abundance of the DM in Model I. In this case, there is no tree-level process for the DM production, since the DM does not couple to the singlet component ϕ^0 in the $(\mathbf{1},\mathbf{1},\mathbf{3})_R$. Therefore, the DM is produced at the loop level. In Fig. 4.4, we show examples of one-loop diagrams which give the dominant contribution to the DM production. The amplitude is then estimated as

$$\sum |\mathcal{M}|^2 \simeq \frac{c'}{(16\pi^2)^2} \, \frac{\hat{s} - 4M_{\rm DM}^2}{M_{\rm int}^2} \ , \tag{4.21}$$

where we have included the one-loop factor. After a similar computation, we obtain

$$Y_{\rm DM}^{(0)} \simeq \frac{c'}{64\pi^7 (16\pi^2)^2} \left(\frac{45}{\pi g_*} \right)^{\frac{3}{2}} \frac{M_{\rm Pl} T_{\rm RH}}{M_{\rm int}^2} \ , \tag{4.22}$$

and

$$T_{\rm RH} \simeq 4.6 \ {\rm GeV} \times \left(\frac{\Omega_{\rm DM} h^2}{0.12} \right) \left(\frac{g_*^{\frac{3}{2}} c'^{-1}}{10^5} \right) \left(\frac{M_{\rm DM}}{\rm GeV} \right)^{-1} \ , \tag{4.23}$$

on the assumption of $M_{\rm DM} \ll T_{\rm RH}$. Here, we have set $M_{\rm int} = 10^{8.08}$ GeV.

In Fig. 4.5, we plot the predicted reheating temperature as a function of the DM mass after numerically integrating Eq. (4.17). The left and right panels show the cases of Model I and II, respectively. The pink band shows the uncertainty of the calculation, which we estimate by varying the unknown factor by a factor of ten. It turns out that when $M_{\rm DM} \ll T_{\rm RH}$, in the case of Model I, only a small DM mass is allowed and the reheating temperature must be quite low. In Model II, on the other hand, DM with a mass of around the electroweak scale accounts for the observed DM density with an

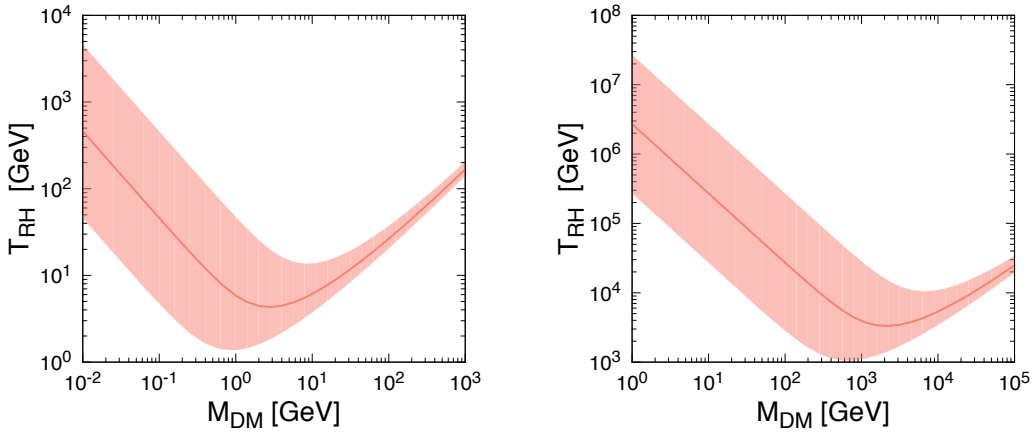

(a) Model I (b) Model II

Figure 4.5: *Reheating temperature as a function of DM mass. Pink band shows the theoretical uncertainty.*

acceptably high reheating temperature. For a larger $M_{\rm DM}$, in both models, the DM relic abundance can only be explained in the narrow strip region where $M_{\rm DM} \simeq T_{\rm RH}$.

Chapter 5

Weakly Interactive Massive Particles

In this chapter, we consider weakly interactive massive particles(WIMP) as dark matter candidates. Unlike NETDM, WIMP DM candidates interact with the thermal bath of the SM particles efficiently so that they are in thermal equilibrium in the early universe. The annihilation rate of the DM particle decreases as the universe expands until the plasma of the DM becomes so diluted that the annihilation no longer proceeds. After that, the total number of DM particle is freezed and the density only decreases as a result of the expansion of the universe. This mechanism is usually called the "freeze-out" mechanim in the literatures. In the following text, we will list models in which gauge coupling unification is achieved with appropriate GUT and intermediate scales. Then, we study the phenomenology of these models, such as the relic abundance of DM, the DM direct detection rate, the proton decay lifetime, and neutrino masses. It is found that the condition of gauge coupling unification, as well as the proton decay bounds, severely restricts the WIMP DM models in SO(10) GUTs. Still, we obtain some promising candidates, which can be probed in future DM searches and proton decay experiments.

5.1 WIMP DM candidates

We begin this chapter by identifying all possible WIMP DM candidates in Tabel 3.1. The WIMP scenario generally requires DM to be in thermal equilibrium with the SM particles before its abundance freezes out. This requires DM particles to interact with SM particles efficiently in the early universe. As a consequence, the fermionic singlets $\mathtt{F}^0_{\mathbf{1}}$ and $\widehat{\mathtt{F}}^0_{\mathbf{1}}$ are not good WIMP candidates since they are SM singlets and can only interact with SM particles through exchange of intermediate scale virtual particles. On the otherhand, the scalar singlet $\mathtt{S}^0_{\mathbf{1}}$ and triplet $\mathtt{S}^0_{\mathbf{3}}$ can interact with the SM Higgs boson efficiently through the quartic coupling and are potential good DM candidates to be discussed below. These can be taken to be either real or complex. For $\mathtt{S}^0_{\mathbf{1}}$, there is no difference in any of our results whether $\mathtt{S}^0_{\mathbf{1}}$ is real or complex. We have taken $\mathtt{S}^0_{\mathbf{3}}$ to be real, but there would be no qualitative difference in our results for complex $\mathtt{S}^0_{\mathbf{3}}$. In addition, $\mathtt{S}^0_{\mathbf{3}}$ couples to the SM particles via the weak interaction. Similarly, the fermion triplet $\mathtt{F}^0_{\mathbf{3}}$ is a wino-like DM candidate and will also be considered below. In general, the neutral component of a $\mathrm{SU}(2)_L \otimes \mathrm{U}(1)_Y$ multiplet can interact with SM particles through exchange of W or Z boson, and thus can be a good DM candidate. Such DM candidates have been widely studied in the literature [31–34, 36, 37, 39–42, 75].

There are also DM candidates which have non-zero hypercharge. These are: $\mathtt{F}^{1/2}_{\mathbf{2}}$, $\mathtt{F}^1_{\mathbf{3}}$, $\mathtt{F}^{1/2}_{\mathbf{4}}$, $\mathtt{F}^{3/2}_{\mathbf{4}}$, $\mathtt{S}^{1/2}_{\mathbf{2}}$, $\mathtt{S}^1_{\mathbf{3}}$, $\widehat{\mathtt{F}}^{1/2}_{\mathbf{2}}$, and $\widehat{\mathtt{F}}^1_{\mathbf{3}}$. These DM candidates are charged under the electroweak gauge group so they can be produced thermally in the early universe. However they are severely constrained by DM direct detection experiments since their scattering cross sections with a nucleon induced by Z-boson exchange are generally too large. Possible ways to evade this constraint are discussed in the following section.

5.2 Hypercharged DM

A DM candidate with $Y \neq 0$ needs to be a Dirac spinor or a complex scalar, depending on its matter parity. These hypercharged candidates are severely restricted by the direct detection experiments, since they elastically scatter nucleons via the vector interactions mediated by Z-boson exchange, whose scattering cross section turns out to be too large by many orders of magnitude. One possible way to evade the constraint is to generate mass splitting, Δm, between the neutral components of such a DM multiplet ψ and

to split it into two Majorana fermions or real scalars χ_1, χ_2. Then, the DM no longer suffers from large scattering cross sections since it does not have vector interactions. Such splitting occurs if the DM mixes with extra $\mathrm{SU}(2)_L \otimes \mathrm{U}(1)_Y$ multiplets after electroweak symmetry breaking. As we have assumed that only a single DM multiplet lies in the low-energy region, a natural mass scale for the extra $\mathrm{SU}(2)_L \otimes \mathrm{U}(1)_Y$ multiplets is the intermediate scale $M_{\rm int}$. The effects of these heavy particles on the low-energy theory are expressed in terms of effective operators induced after integrating them out.

Among them, the following operator is relevant for the generation of mass splitting of the DM:

$$\frac{c}{M_{\rm int}^n}\mathcal{O}_\psi H^{*p} \ , \tag{5.1}$$

where H is the SM Higgs field, $p = 4Y_\psi$ with $Y_\psi > 0$ being the hypercharge of the DM ψ, $\mathcal{O}_\psi = \overline{\psi^{\mathcal{C}}}\psi$ or $\psi\psi$, and $n = p-1$ or $p-2$ for Dirac fermion DM or complex scalar DM respectively. After the Higgs field acquires a VEV, the above operator generates a mass splitting between two Weyl fermions(real scalars) inside the neutral component of the DM multiplet. The splitting is given by $\Delta m \sim v^p/M_{\rm int}^n$ for fermionic DM and $v^p/(M_{\rm int}^n m_\psi)$ for scalar DM, with $v \simeq 174$ GeV being the Higgs VEV. m_ψ corresponds to the scalar mass term $m_\psi^2 \psi\psi^*$.

The operator (5.1) is suppressed if the intermediate scale is large [37]. When the mass splitting is sufficiently small, the DM can scatter off a nucleon N inelastically: $\chi_1 + N \to \chi_2 + N$. Since this process is induced by the vector interactions, the scattering cross section again becomes too large if the mass splitting Δm is smaller than the recoil energy sensitive to the direct detection experiments. This sets the bound $\Delta m \gtrsim 100$ keV. For this condition to be satisfied, $M_{\rm int} \lesssim 10^9$, 3×10^4, and 4×10^3 GeV are required for fermionic dark DM with $Y_\psi = 1/2$, 1 and 3/2, respectively [37]. In the case of scalar DM, the upper bound depends on the DM mass. For a 1 TeV DM mass, $M_{\rm int} \lesssim 10^5$ GeV for $Y_\psi = 1$. For a $Y_\psi = 1/2$ scalar DM candidate, on the other hand, the mass splitting can be generated with a renormalizable interaction and its effect on the mass splitting depends only on its dimensionless coefficient c. We will see later that this coefficient can still be very small, whose size is determined by the symmetry breaking pattern and its scale. This is because the operators relevant for the generation of the mass splitting are forbidden by the SO(10) symmetry. Thus, the constraint from inelastic scattering can again give a bound on the intermediate scale even for $Y_\psi = 1/2$ scalar DM candidates.

5.3 Scalar dark matter

In this section, we discuss scalar WIMP DM in SO(10) models with different intermediate subgroups. In this case, the DM candidates belong to either a **16** or a **144** representation. The masses of components in a DM multiplet in general need to be fine-tuned; if a charged component is nearly degenerate with the DM particle and decays to it only through an intermediate-scale gauge boson or Higgs field, this charged particle would be very long lived, as discuseed in Section 3.3. Thus, to be safe, we take the masses of these extra components to be $\mathcal{O}(M_{\rm GUT})$ or $\mathcal{O}(M_{\rm int})$, while the DM mass to be around TeV scale so that the thermal relic abundance of the DM agrees with the observed DM density. Here, we assume that the fine-tuning of DM masses be realized with a minimal choice of Higgs fields, that is, we exploit only R_1 and $R_2 = \mathbf{126}$ to generate desired mass spectrum with R_1 being an irreducible representation chosen from Table 2.1. This is possible because a **16** or **144** can couple to the **126** Higgs field. Then, we study whether each set of matter content and its mass spectrum offers gauge coupling unification with appropriate GUT and intermediate scales.

5.3.1 DM mass

To determine the renormalization group (RG) running of gauge couplings, we need to know the mass of DM candidates, since they affect the running above its mass scale. An exception is $\mathtt{S}_{\mathtt{1}}^{\mathtt{0}}$ as it is a SM singlet and does not contribute to the gauge coupling beta functions below $M_{\rm int}$ at the one-loop level. Scalar singlet DM is discussed in Ref. [44]. To roughly estimate favored mass region for such a singlet DM particle, consider the quartic interaction between the singlet DM ϕ and the SM Higgs field: $-\lambda_{H\phi}\phi^2|H|^2/2$. Through this coupling, the singlet DM particles annihilate into a pair of the SM Higgs bosons. The annihilation cross section $\sigma_{\rm ann}$ times the relative velocity between the initial state particles $v_{\rm rel}$ is evaluated as

$$\sigma_{\rm ann} v_{\rm rel} \simeq \frac{\lambda_{H\phi}^2}{16\pi m_{\rm DM}^2} \ , \tag{5.2}$$

assuming that the DM mass $m_{\rm DM}$ is much larger than the SM Higgs mass m_h and we neglect terms proportional to v^2. The DM relic abundance is, on the other hand, related

to the annihilation cross section by

$$\Omega_{\rm DM}h^2 \simeq \frac{3\times 10^{-27}\ {\rm cm}^3\ {\rm s}^{-1}}{\langle\sigma_{\rm ann}v_{\rm rel}\rangle}\ . \tag{5.3}$$

To account for the observed DM density $\Omega_{\rm DM}h^2 = 0.12$ [45], the DM mass should be $m_{\rm DM} \lesssim 10$ TeV for $\lambda_{H\phi} \lesssim 1$. This gives us a rough upper bound for the DM mass.

The other scalar DM candidates are $\mathrm{SU}(2)_L \otimes \mathrm{U}(1)_Y$ multiplets, which can interact with SM particles through gauge interactions besides the quartic coupling mentioned above. In particular, $\mathtt{S}_{\mathbf{2}}^{1/2}$ is known as the Inert Higgs Doublet Model and has been widely studied in the literature. To evaluate the effects of gauge interactions, let us first consider the limit of zero quartic couplings, where the dark matter particles mainly annihilates into gauge bosons. For $\mathtt{S}_{\mathbf{n}}^{\mathtt{Y}}$, the effective (averaged) annihilation cross section is given by [31]

$$\sigma_{\rm ann}v_{\rm rel} \simeq \frac{g^4(3-4n^2+n^4)+16Y^4g'^4+8g^2g'^2Y^2(n^2-1)}{64\pi c_n m_{\rm DM}^2}\ , \tag{5.4}$$

where g (g') are the $\mathrm{SU}(2)_L$ ($\mathrm{U}(1)_Y$) gauge couplings and $c_n = n$ ($2n$) for a real (complex) scalar. Here, we assume the DM mass to be much larger than the weak gauge boson masses. Again Eq. (5.3) tells us that the masses of the DM candidates should fall into a region from ~ 500 GeV to ~ 2 TeV. On the other hand, if the quartic coupling is larger than the gauge couplings, the annihilation into a pair of Higgs bosons becomes dominant and thus the DM abundance would be similar to that of the singlet DM candidate. In general, the DM mass should lie between 0.5 TeV to 10 TeV for $\mathtt{S}_{\mathbf{2}}^{1/2}$, $\mathtt{S}_{\mathbf{3}}^{0}$ and $\mathtt{S}_{\mathbf{3}}^{1}$.

More accurate estimations for the DM mass can be found in the literature [31,33,46] with various additional contributions taken into account. For $\mathrm{SU}(2)_L \otimes \mathrm{U}(1)_Y$ DM multiplets, the non-perturbative Sommerfeld enhancement is of great importance [47]. In the limit of zero quartic coupling, the DM masses with which the relic abundance agrees with the observed DM density are evaluated as $m_{\rm DM} = 0.5$ and 2.5 TeV for $\mathtt{S}_{\mathbf{2}}^{1/2}$ and $\mathtt{S}_{\mathbf{3}}^{0}$, respectively [46]. For $\mathtt{S}_{\mathbf{3}}^{1}$, as far as we know, there has been no calculation which includes the Sommerfeld enhancement; thus its mass would be larger than 1.6 TeV, which is obtained with only the perturbative contribution considered [31]. For the cases where the scalar DM multiplets have non-zero quartic coupling with the SM Higgs doublet, it was shown in Ref. [33] that the allowed DM mass can be extended to ~ 58 and 28 TeV for $\mathtt{S}_{\mathbf{2}}^{1/2}$ and $\mathtt{S}_{\mathbf{3}}^{0}$, respectively, when the quartic coupling $\lambda \sim 4\pi$. Such a large quartic

coupling is, however, in general inconsistent with GUTs since it immediately blows up at a scale much below the GUT and intermediate scales. Thus, we implicitly assume the quartic coupling should be rather small, *e.g.*, $\lesssim 1$, to avoid divergent couplings. In this case, the DM mass usually lies around $\mathcal{O}(1)$ TeV.

5.3.2 Candidates for scalar DM

We list all possible scalar DM candidates in Table 5.1. All of the candidates belong to either a **16** or a **144**. Here, the first column shows the model names with subscript representing the intermediate gauge group $G_{\rm int}$. The second column lists the $G_{\rm int}$ representations that contain the DM candidate multiplet $\mathtt{S}^{\mathtt{Y}}_{\mathbf{n}}$. All of the components in the representation except the DM multiplet $\mathtt{S}^{\mathtt{Y}}_{\mathbf{n}}$ shown in the third column will have masses tuned to $\mathcal{O}(M_{\rm int})$. The rest of the components in the SO(10) multiplet have masses of $\mathcal{O}(M_{\rm GUT})$. The case of $G_{\rm int} = {\rm SU}(4)_C \otimes {\rm SU}(2)_L \otimes {\rm SU}(2)_R \otimes D$ $({\rm SU}(3)_C \otimes {\rm SU}(2)_L \otimes {\rm SU}(2)_R \otimes {\rm U}(1)_{B-L} \otimes D)$ is identical to that of $G_{\rm int} = {\rm SU}(4)_C \otimes {\rm SU}(2)_L \otimes {\rm SU}(2)_R$ $({\rm SU}(3)_C \otimes {\rm SU}(2)_L \otimes {\rm SU}(2)_R \otimes {\rm U}(1)_{B-L})$ with additional multiplets required by the left-right symmetry introduced above the intermediate scale. Notice that $\mathtt{S}^{1/2}_{\mathbf{2}}$ is contained in both the model SB's and SC's. The difference between the models is the ${\rm SU}(2)_R$ (or additional U(1)) charge assignment; for instance, $\mathtt{SB}_{422}$ ($\mathtt{SC}_{422}$) includes the ${\rm SU}(2)_R$ singlet (triplet) DM. From Table 5.1, we find that a **16** contains only SA's and SB's, while a **144** has all of the candidates listed in the table.

Next, we perform the RGE analysis in the models presented in Table 5.1 to see if these models achieve gauge coupling unification with appropriate GUT and intermediate scales. The one-loop results for $M_{\rm GUT}$, $M_{\rm int}$, the unified gauge coupling $\alpha_{\rm GUT}$, and the proton lifetimes in the $p \to e^+\pi^0$ channel are shown in Table 5.2.[1] Here, $M_{\rm GUT}$ and $M_{\rm int}$ are given in GeV units, while the unit for proton lifetimes $\tau_p(p \to e^+\pi^0)$ is years. The DM mass is set to be $m_{\rm DM} = 1$ TeV. We have checked that altering the DM mass by an order of magnitude results in only a $\mathcal{O}(0.2)\%$ variation in the logarithmic masses of $M_{\rm int}$ and $M_{\rm GUT}$. The uncertainty of the lifetime reflects our innocence of the GUT-scale gauge boson mass M_X, which we take it to be within a range of $0.5 M_{\rm GUT} \lesssim M_X \lesssim 2 M_{\rm GUT}$. It turns out that most models have already been

[1] We restrict our attention to one-loop running as two loop effects become very model dependent on our choice of the scalar potential.

Table 5.1: *Summary of scalar DM multiplets. The second column shows the G_{int} representation with quantum numbers listed in the same order as the groups shown in the direct product. The case of $G_{\rm int} = SU(4)_C \otimes SU(2)_L \otimes SU(2)_R \otimes D$ ($SU(3)_C \otimes SU(2)_L \otimes SU(2)_R \otimes U(1)_{B-L} \otimes D$) is identical to that of $G_{\rm int} = SU(4)_C \otimes SU(2)_L \otimes SU(2)_R$ ($SU(3)_C \otimes SU(2)_L \otimes SU(2)_R \otimes U(1)_{B-L}$) with additional multiplets required by left-right symmetry introduced above the intermediate scale.*

Model	$R_{\rm DM}$	$\mathtt{S}^{\mathtt{Y}}_{\mathbf{n}}$	SO(10) representation
$G_{\rm int} = {\rm SU}(4)_C \otimes {\rm SU}(2)_L \otimes {\rm SU}(2)_R (\otimes D)$			
$\mathtt{SA}_{422(\mathtt{D})}$	$\mathbf{4}, \mathbf{1}, \mathbf{2}$	$\mathtt{S}^{0}_{\mathbf{1}}$	**16**, **144**
$\mathtt{SB}_{422(\mathtt{D})}$	$\mathbf{4}, \mathbf{2}, \mathbf{1}$	$\mathtt{S}^{1/2}_{\mathbf{2}}$	**16**, **144**
$\mathtt{SC}_{422(\mathtt{D})}$	$\mathbf{4}, \mathbf{2}, \mathbf{3}$	$\mathtt{S}^{1/2}_{\mathbf{2}}$	**144**
$\mathtt{SD}_{422(\mathtt{D})}$	$\mathbf{4}, \mathbf{3}, \mathbf{2}$	$\mathtt{S}^{1}_{\mathbf{3}}$	**144**
$\mathtt{SE}_{422(\mathtt{D})}$	$\mathbf{4}, \mathbf{3}, \mathbf{2}$	$\mathtt{S}^{0}_{\mathbf{3}}$	**144**
$G_{\rm int} = {\rm SU}(4)_C \otimes {\rm SU}(2)_L \otimes {\rm U}(1)_R$			
$\mathtt{SA}_{421}$	$\mathbf{4}, \mathbf{1}, -1/2$	$\mathtt{S}^{0}_{\mathbf{1}}$	**16**, **144**
$\mathtt{SB}_{421}$	$\mathbf{4}, \mathbf{2}, 0$	$\mathtt{S}^{1/2}_{\mathbf{2}}$	**16**, **144**
$\mathtt{SC}_{421}$	$\mathbf{4}, \mathbf{2}, 1$	$\mathtt{S}^{1/2}_{\mathbf{2}}$	**144**
$\mathtt{SD}_{421}$	$\mathbf{4}, \mathbf{3}, 1/2$	$\mathtt{S}^{1}_{\mathbf{3}}$	**144**
$\mathtt{SE}_{421}$	$\mathbf{4}, \mathbf{3}, -1/2$	$\mathtt{S}^{0}_{\mathbf{3}}$	**144**
$G_{\rm int} = {\rm SU}(3)_C \otimes {\rm SU}(2)_L \otimes {\rm SU}(2)_R \otimes {\rm U}(1)_{B-L} (\otimes D)$			
$\mathtt{SA}_{3221(\mathtt{D})}$	$\mathbf{1}, \mathbf{1}, \mathbf{2}, 1$	$\mathtt{S}^{0}_{\mathbf{1}}$	**16**, **144**
$\mathtt{SB}_{3221(\mathtt{D})}$	$\mathbf{1}, \mathbf{2}, \mathbf{1}, -1$	$\mathtt{S}^{1/2}_{\mathbf{2}}$	**16**, **144**
$\mathtt{SC}_{3221(\mathtt{D})}$	$\mathbf{1}, \mathbf{2}, \mathbf{3}, -1$	$\mathtt{S}^{1/2}_{\mathbf{2}}$	**144**
$\mathtt{SD}_{3221(\mathtt{D})}$	$\mathbf{1}, \mathbf{3}, \mathbf{2}, 1$	$\mathtt{S}^{1}_{\mathbf{3}}$	**144**
$\mathtt{SE}_{3221(\mathtt{D})}$	$\mathbf{1}, \mathbf{3}, \mathbf{2}, 1$	$\mathtt{S}^{0}_{\mathbf{3}}$	**144**

ruled out by the current experimental constraint $\tau(p \to e^+\pi^0) > 1.4 \times 10^{34}$ yrs [57, 58]. The models that possibly survive this constraint are $\mathtt{SA}_{422}$, $\mathtt{SB}_{422}$, $\mathtt{SA}_{3221}$, $\mathtt{SB}_{3221}$, $\mathtt{SC}_{3221}$, $\mathtt{SA}_{3221\mathtt{D}}$, and $\mathtt{SB}_{3221\mathtt{D}}$, which are highlighted in blue shading in the table. In terms of ${\rm SU}(2)_L \otimes {\rm U}(1)_Y$ assignments, only $\mathtt{S}^{0}_{\mathbf{1}}$ and $\mathtt{S}^{1/2}_{\mathbf{2}}$ are found to be viable candidates. Among them, models $\mathtt{SB}_{422}$, $\mathtt{SC}_{3221}$, $\mathtt{SA}_{3221\mathtt{D}}$, and $\mathtt{SB}_{3221\mathtt{D}}$ predict proton lifetimes close to the

Table 5.2: *One-loop result for scales, unified couplings, and proton lifetimes for models in table. 5.1. The DM mass is set to be $m_{DM} = 1$ TeV. The mass scales are given in GeV and the proton lifetimes are in units of years. Blue shaded models evade the proton decay bound, $\tau(p \to e^+\pi^0) > 1.4 \times 10^{34}$ yrs [57, 58].*

Model	$\log_{10} M_{\rm GUT}$	$\log_{10} M_{\rm int}$	$\alpha_{\rm GUT}$	$\log_{10} \tau_p(p \to e^+\pi^0)$
$G_{\rm int} = {\rm SU}(4)_C \otimes {\rm SU}(2)_L \otimes {\rm SU}(2)_R$				
$\mathtt{SA}_{422}$	16.33	11.08	0.0218	36.8 ± 1.2
$\mathtt{SB}_{422}$	15.62	12.38	0.0228	34.0 ± 1.2
$\mathtt{SC}_{422}$	14.89	11.18	0.0243	31.0 ± 1.2
$\mathtt{SD}_{422}$	14.11	13.29	0.0253	28.0 ± 1.2
$\mathtt{SE}_{422}$	14.73	13.72	0.0243	30.4 ± 1.2
$G_{\rm int} = {\rm SU}(4)_C \otimes {\rm SU}(2)_L \otimes {\rm SU}(2)_R \otimes D$				
$\mathtt{SA}_{422\mathtt{D}}$	15.23	13.71	0.0245	32.4 ± 1.2
$\mathtt{SB}_{422\mathtt{D}}$	15.01	13.71	0.0247	31.6 ± 1.2
$\mathtt{SC}_{422\mathtt{D}}$	14.50	13.71	0.0254	29.5 ± 1.2
$\mathtt{SD}_{422\mathtt{D}}$	13.95	13.47	0.0260	27.3 ± 1.2
$\mathtt{SE}_{422\mathtt{D}}$	14.55	13.96	0.0251	29.7 ± 1.2
$G_{\rm int} = {\rm SU}(4)_C \otimes {\rm SU}(2)_L \otimes {\rm U}(1)_R$				
$\mathtt{SA}_{421}$	14.62	10.96	0.0226	30.1 ± 1.2
$\mathtt{SB}_{421}$	14.55	11.90	0.0233	29.8 ± 1.2
$\mathtt{SC}_{421}$	14.15	10.92	0.0236	28.2 ± 1.2
$\mathtt{SD}_{421}$	13.91	12.80	0.0250	27.2 ± 1.2
$\mathtt{SE}_{421}$	14.45	13.12	0.0241	29.4 ± 1.2
$G_{\rm int} = {\rm SU}(3)_C \otimes {\rm SU}(2)_L \otimes {\rm SU}(2)_R \otimes {\rm U}(1)_{B-L}$				
$\mathtt{SA}_{3221}$	16.66	8.54	0.0217	38.1 ± 1.2
$\mathtt{SB}_{3221}$	16.17	9.80	0.0223	36.2 ± 1.2
$\mathtt{SC}_{3221}$	15.62	9.14	0.0230	34.0 ± 1.2
$\mathtt{SD}_{3221}$	14.49	12.07	0.0246	29.5 ± 1.2
$\mathtt{SE}_{3221}$	15.09	12.22	0.0237	31.9 ± 1.2
$G_{\rm int} = {\rm SU}(3)_C \otimes {\rm SU}(2)_L \otimes {\rm SU}(2)_R \otimes {\rm U}(1)_{B-L} \otimes D$				
$\mathtt{SA}_{3221\mathtt{D}}$	15.58	10.08	0.0231	33.8 ± 1.2
$\mathtt{SB}_{3221\mathtt{D}}$	15.40	10.44	0.0233	33.1 ± 1.2
$\mathtt{SC}_{3221\mathtt{D}}$	14.58	11.62	0.0245	29.8 ± 1.2
$\mathtt{SD}_{3221\mathtt{D}}$	14.07	12.13	0.0253	27.8 ± 1.2
$\mathtt{SE}_{3221\mathtt{D}}$	14.60	12.29	0.0245	29.9 ± 1.2

present limit, and thus can be tested in future proton decay experiments.

The desired mass spectum of the models can be obtained by fine-tuning the couplings of the potential as described in Section 3.3. For the above models, the representations in Eq. (3.7) are chosen as $R_2 = \mathbf{126}$ and $R_1 = \mathbf{210}$, $\mathbf{45}$, or $\mathbf{210}$ for $G_{\rm int} = {\rm SU}(4)_C \otimes {\rm SU}(2)_L \otimes {\rm SU}(2)_R$, ${\rm SU}(3)_C \otimes {\rm SU}(2)_L \otimes {\rm SU}(2)_R \otimes {\rm U}(1)_{B-L}$, and ${\rm SU}(3)_C \otimes {\rm SU}(2)_L \otimes {\rm SU}(2)_R \otimes {\rm U}(1)_{B-L} \otimes D$ respectively. Then, R' and R'' only needs to be summed over $\mathbf{45}$ and $\mathbf{210}$ for these choices of representations. For a concrete example, we show an explicit procedure for the fine-tuning in Appendix F, by taking $R_{DM} = \mathbf{16}$ and $G_{\rm int} = {\rm SU}(3)_C \otimes {\rm SU}(2)_L \otimes {\rm SU}(2)_R \otimes {\rm U}(1)_{B-L}$.

5.3.3 Mass splitting of hypercharged scalar dark matter

As discussed in Sec. 5.2, we need a mass splitting of $\Delta m \gtrsim 100$keV [37] between the neutral and charged components of the hypercharged DM candidates (models SB and SC) to avoid the direct detection bound. Since both of these models yield $\mathtt{S}_{\mathbf{2}}^{1/2}$ DM, the mass splitting can be induced by dimension-four operators like $\phi^2 H^{*2}$, where ϕ denotes the hypercharged scalar DM $\mathtt{S}_{\mathbf{2}}^{1/2}$. Such operators are, however, forbidden by the SO(10) GUT symmetry; in fact, as the $\mathtt{S}_{\mathbf{2}}^{1/2}$ DM and the SM Higgs field have $B-L = 1$ and 0, respectively, the operators contributing the mass splitting violate the $B-L$ symmetry. Thus, they can be induced only below the intermediate scale where the $B-L$ symmetry is spontaneously broken.

Such an operator is induced by the interactions with the coefficients κ_2 and $\lambda_{12}^{\mathbf{126}}$ in Eq. (3.7), since it requires violation of the particle number associated with the DM field ϕ. The required $B-L$ breaking is realized by the R_2 VEV. We find that the tree-level diagrams in Fig. 5.1 are relevant to the generation of mass splitting. Here, $R_H = \mathbf{10}$ contains the SM Higgs field. Since the κ_2 and $\lambda_{12}^{\mathbf{126}}$ interactions are symmetric with respect to the interchange of $R_{\rm DM}$, the component in R_2 which propagates in the upper two diagrams should be an ${\rm SU}(2)_L$ triplet. On the other hand, the component appearing in the inner lines in the lower two diagrams can be either an ${\rm SU}(2)_L$ singlet or triplet. The masses of these fields are dependent on the intermediate gauge groups; if $G_{\rm int} = {\rm SU}(4)_C \otimes {\rm SU}(2)_L \otimes {\rm SU}(2)_R$ or ${\rm SU}(3)_C \otimes {\rm SU}(2)_L \otimes {\rm SU}(2)_R \otimes {\rm U}(1)_{B-L}$, then these masses are $\mathcal{O}(M_{\rm GUT})$, while for $G_{\rm int} = {\rm SU}(3)_C \otimes {\rm SU}(2)_L \otimes {\rm SU}(2)_R \otimes {\rm U}(1)_{B-L} \otimes D$, they are $\mathcal{O}(M_{\rm int})$ because of the left-right parity D.

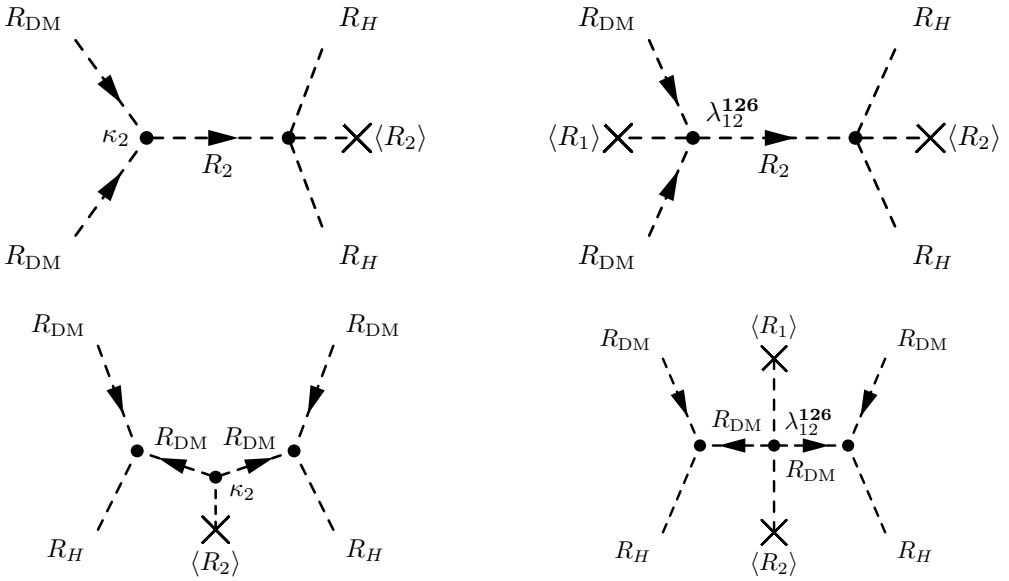

Figure 5.1: *Diagrams that generate the mass splitting between real components of hypercharged scalar DM.*

Let us first consider the former cases. In these cases, the coefficient of the dimension-four operator $\phi^2 H^{*2}$ is $\mathcal{O}(M_{\rm int}/M_{\rm GUT})$, as the dimensionful couplings in the Lagrangian are expected to be $\mathcal{O}(M_{\rm GUT})$. We note here that there is no requirement for the cancellation between κ_2 and $\lambda_{12}^{\mathbf{126}}\langle R_1\rangle$ to realize the desired mass spectrum since these couplings do not contribute to the mass splitting. Thus, this operator induces a mass splitting of

$$\Delta m \sim \frac{M_{\rm int} v^2}{m_{\rm DM} M_{\rm GUT}} \ . \tag{5.5}$$

The condition $\Delta m \gtrsim 100$ keV then becomes

$$\frac{M_{\rm int}}{M_{\rm GUT}} \gtrsim 3 \times 10^{-6} \times \left(\frac{m_{\rm DM}}{1\ {\rm TeV}}\right) \ . \tag{5.6}$$

From Table 5.2, we find that the model $\mathtt{SB}_{422}$ clearly satisfies this bound, while the intermediate scales in $\mathtt{SB}_{3221}$ and $\mathtt{SC}_{3221}$ lie slightly below this constraint. However, since this bound is just a rough estimation and the intermediate scales given in Table 5.2 are obtained with the one-loop RGEs, it is possible that the DM candidates in these models are just not yet reached by the current direct detection experiments. If so, these models can be probed in the near future.

For $\mathtt{SB}_{\mathtt{3221D}}$, on the other hand, the mass spectrum is altered because of the presence of the left-right parity. In this case, the charge of the DM candidate under $G_{\rm int}$ is $(\mathbf{1},\mathbf{2},\mathbf{1},-1)$, and the left-right symmetry requires the $(\mathbf{1},\mathbf{1},\mathbf{2},+1)$ to be also light. To that end, the fine-tuning between the κ_2 and $\lambda_{12}^{\mathbf{126}}$ terms in Eq. 3.7 is required such that $\kappa_2 + \lambda_{12}^{\mathbf{126}}\langle R_1\rangle \simeq M_{\rm int}$; otherwise, these terms give a mass of $\mathcal{O}(\sqrt{M_{\rm int}M_{\rm GUT}})$ to the $(\mathbf{1},\mathbf{1},\mathbf{2},+1)$ component, which is much higher than the intermediate scale. This fine-tuning also guarantees the absence of non-perturbative couplings at low energies; without this fine-tuning, the exchange of intermediate-scale particles with the κ_2 and $\lambda_{12}^{\mathbf{126}}\langle R_1\rangle$ vertices induces extremely large effective couplings, which destroy the perturbativity of the low-energy theory.

In the presence of the fine-tuning, the diagrams in Fig. 5.1 with the virtual states having a mass of $M_{\rm int}$ induce the effective operator $\phi^2 H^{*2}$ with a coefficient of $\mathcal{O}(1)$. Thus, the resultant mass splitting is well above 100 keV and the model $\mathtt{SB}_{\mathtt{3221D}}$ easily evades the constraints from the direct detection experiments.

To summarize, $\mathtt{SB}_{\mathtt{422}}$ and $\mathtt{SB}_{\mathtt{3221D}}$ are safe from the direct detection bound. $\mathtt{SB}_{\mathtt{3221}}$ and $\mathtt{SC}_{\mathtt{3221}}$ lie just around the margin of the bound, and they might be detected or completely excluded in future direct detection experiments.

5.4 Fermionic dark matter

Next, we consider the fermionic DM candidates. Again, we begin with showing the favored mass region for these DM candidates in Sec. 5.4.1. As already mentioned above, the singlet fermion candidates, $\mathtt{F}_{\mathtt{1}}^{\mathtt{0}}$ and $\widehat{\mathtt{F}}_{\mathtt{1}}^{\mathtt{0}}$, are not good candidates for WIMP DM since their annihilation cross sections are extremely suppressed (though they are good NETDM candidates). On the other hand, electroweakly charged DM can yield the desired relic abundance via gauge interactions. In this section, we will discuss the $Y = 0$ and $Y \neq 0$ cases respectively, and give some concrete examples for each case and perform RGE analysis to determine the intermediate/GUT scales of the models.

5.4.1 DM mass

Contrary to the case of the scalar DM, the thermal relic abundance of the fermionic DM candidates is completely determined by gauge interactions. Therefore, it is possible to

make a robust prediction for the DM mass favored by the present DM density. In the case of fermion DM, not only the gauge boson channels but also the SM fermions and the Higgs boson final states can contribute to s-wave annihilation. We obtain a similar expression to Eq. (5.4) for the effective annihilation cross section of $\mathtt{F}^{\mathtt{Y}}_{\mathbf{n}}$ as [31]

$$\sigma_{\rm ann} v_{\rm rel} \simeq \frac{g^4(2n^4+17n^2-19)+4Y^2g'^4(41+8Y^2)+16g^2g'^2Y^2(n^2-1)}{128\pi c_n m_{\rm DM}^2} \,, \qquad (5.7)$$

with $c_n = 2n$ $(4n)$ for a Majorana (Dirac) fermion. In addition, the Sommerfeld enhancement again affects the annihilation cross section significantly. With this effect taken into account, the thermal relic abundance of $\mathtt{F}^{\mathtt{0}}_{\mathbf{3}}$ is computed in Ref. [35] and found to be consistent with the observed DM density if $m_{\rm DM} \simeq 2.7$ TeV as in the case of supersymmetric winos. As for $\mathtt{F}^{\mathtt{1/2}}_{\mathbf{2}}$ and $\widehat{\mathtt{F}}^{\mathtt{1/2}}_{\mathbf{2}}$, the favored mass value is $\simeq 1.1$ TeV [31] as in the case of supersymmetric Higgsinos. As far as we know, there is no calculation for the other fermionic DM candidates that includes the Sommerfeld enhancement; without the effect, the thermal relic of $\mathtt{F}^{\mathtt{1}}_{\mathbf{3}}$, $\widehat{\mathtt{F}}^{\mathtt{1}}_{\mathbf{3}}$, $\mathtt{F}^{\mathtt{1/2}}_{\mathbf{4}}$, and $\mathtt{F}^{\mathtt{3/2}}_{\mathbf{4}}$ is consistent with the observed value if $m_{\rm DM} \simeq 1.9$ TeV, 1.9 TeV, 2.4 TeV, and 2.6 TeV, respectively [46].

5.4.2 Real triplet DM

We begin our discussion of fermionic DM models with the $Y = 0$ case. As discussed earlier, these are less constrained by direct detection experiments. According to Table 3.1, such candidates belong to $\mathrm{SU}(2)_L$ triplets in a **45**, **54** or **210** of SO(10). A summary of $\mathrm{SU}(4)_C \otimes \mathrm{SU}(2)_L \otimes \mathrm{SU}(2)_R$ quantum numbers of these DM multiplets are listed in Table. 5.3. Note that the $B-L$ and T_R^3 charges for all of these DM candidates vanish, and therefore they are regarded as real Majorana fermions. As in the scalar DM scenario, the DM multiplet in the **54** or **210** is degenerate with other components with respect to $G_{\rm int}$, and we are required to break this degeneracy to avoid unwanted long-lived colored/charged particles. In the fermionic case, however, a renormalizable Yukawa term like $\overline{R}_{\rm DM} R_{\rm DM} \mathbf{126}_H$ is forbidden by SO(10) symmetry and the choice of DM representation [29], and thus we are unable to use the **126** Higgs to break the degeneracy. Therefore, we need to introduce additional Higgs fields at the intermediate scale in these cases.

For simplicity, we restrict ourselves to the cases where the intermediate scale VEVs develop in the SM singlet direction of R_1 and/or $R_2 = \mathbf{126}$. One of the SM singlet

Table 5.3: *Real triplet DM candidates in various SO(10) representations.*

SO(10) representation	$\mathrm{SU}(4)_C \otimes \mathrm{SU}(2)_L \otimes \mathrm{SU}(2)_R$
45	$(\mathbf{1}, \mathbf{3}, \mathbf{1})$
54	$(\mathbf{1}, \mathbf{3}, \mathbf{3})$
210	$(\mathbf{15}, \mathbf{3}, \mathbf{1})$

components of R_1 should have a VEV of $\mathcal{O}(M_{\rm GUT})$ to break SO(10) into $G_{\rm int}$. The R_2 Higgs field acquires an $\mathcal{O}(M_{\rm int})$ VEV to break $G_{\rm int}$, but it is not able to give mass differences among the components in $R_{\rm DM}$, as mentioned above. Thus, we need to exploit an extra SM singlet component in R_1 which remains light compared to the GUT scale, to induce intermediate-scale mass terms for $R_{\rm DM}$, which are to be used to generate the required mass splitting, as we described in Section 3.3.

We summarize in Table 5.4 the multiplets in R_1 that may develop a VEV of $\mathcal{O}(M_{\rm int})$ for different $G_{\rm int}$. The multiplets are labeled by the quantum numbers of $G_{\rm int}$. It turns out that there is no extra SM singlet component in **54**, which is indicated by a hyphen in the table. As a consequence, there is no way to fine-tune the mass of the (**1**, **3**, **3**) DM candidate originating from the **54** and we drop it from further discussion. Here, we note that the cases of $G_{\rm int} = \mathrm{SU}(3)_C \otimes \mathrm{SU}(2)_L \otimes \mathrm{SU}(2)_R \otimes \mathrm{U}(1)_{B-L}$ and $\mathrm{SU}(3)_C \otimes \mathrm{SU}(2)_L \otimes \mathrm{SU}(2)_R \otimes \mathrm{U}(1)_{B-L} \otimes D$ are disfavored before further analysis: the addition of a real triplet DM lowers the unification scale to unacceptable values and in these cases there is neither any new-physics contribution to the $\mathrm{SU}(3)_C$ gauge coupling beta function nor any new positive contribution to the $\mathrm{SU}(2)_L$ beta function above $M_{\rm int}$. Therefore, the resultant $M_{\rm GUT}$ is always smaller than the unification scale of the $\mathrm{SU}(3)_C$ and $\mathrm{SU}(2)_L$ gauge couplings in the SM plus a real triplet DM, which is below 10^{15} GeV and thus too low to evade the proton decay constraint.[2] For this reason, we do not consider these cases in Table 5.4.

We now perform the RG analysis to look for promising models with additional intermediate Higgs multiplets given in Table 5.4. The one-loop results for $M_{\rm GUT}$, $M_{\rm int}$,

[2] Note that scalar doublet DM is allowed under these intermediate symmetries as shown in Table 5.2, since its contribution to the beta functions is much smaller than that from a fermionic real triplet, thus allowing for a higher unification scale.

Table 5.4: *Possible components in R_1 that can develop a VEV of $\mathcal{O}(M_{int})$.*

$G_{\rm int}$	R_1	Intermediate scale multiplets
$\mathrm{SU}(4)_C \otimes \mathrm{SU}(2)_L \otimes \mathrm{SU}(2)_R$	**210**	$(\mathbf{15},\mathbf{1},\mathbf{1})$
		$(\mathbf{15},\mathbf{1},\mathbf{3})$
$\mathrm{SU}(4)_C \otimes \mathrm{SU}(2)_L \otimes \mathrm{SU}(2)_R \otimes D$	**54**	–
$\mathrm{SU}(4)_C \otimes \mathrm{SU}(2)_L \otimes \mathrm{U}(1)_R$	**45**	$(\mathbf{15},\mathbf{1},0)$

Table 5.5: *The one-loop results for M_{GUT}, M_{int}, α_{GUT}, and proton lifetimes for real triplet fermionic DM models. Here we set the DM mass to be 1 TeV. The mass scales and proton decay lifetime are in unit of GeV and years, respectively. In the blue shaded model, gauge coupling unification is achieved with a sufficiently high GUT scale.*

$R_{\rm DM}$	Additional Higgs in R_1	$\log_{10}M_{\rm int}$	$\log_{10}M_{\rm GUT}$	$\alpha_{\rm GUT}$	$\log_{10}\tau_p(p\to e^+\pi^0)$
$G_{\rm int} = \mathrm{SU}(4)_C \otimes \mathrm{SU}(2)_L \otimes \mathrm{SU}(2)_R$					
$(\mathbf{1},\mathbf{3},\mathbf{1})$	–	15.50	13.69	0.0263	–
$(\mathbf{1},\mathbf{3},\mathbf{1})$	$(\mathbf{15},\mathbf{1},\mathbf{3})$	–	–	–	–
$(\mathbf{1},\mathbf{3},\mathbf{1})$	$(\mathbf{15},\mathbf{1},\mathbf{1})$	15.65	13.47	0.0263	–
$(\mathbf{1},\mathbf{3},\mathbf{1})$	$(\mathbf{15},\mathbf{1},\mathbf{1})$	6.54	17.17	0.0252	39.8 ± 1.2
	$(\mathbf{15},\mathbf{1},\mathbf{3})$				
$(\mathbf{15},\mathbf{3},\mathbf{1})$	$(\mathbf{15},\mathbf{1},\mathbf{1})$	14.44	14.10	0.0246	–
$(\mathbf{15},\mathbf{3},\mathbf{1})$	$(\mathbf{15},\mathbf{1},\mathbf{1})$	14.52	14.11	0.0243	–
	$(\mathbf{15},\mathbf{1},\mathbf{3})$				
$G_{\rm int} = \mathrm{SU}(4)_C \otimes \mathrm{SU}(2)_L \otimes \mathrm{SU}(2)_R \otimes D$					
$(\mathbf{1},\mathbf{3},\mathbf{1})$	–	14.78	14.04	0.0250	–
$G_{\rm int} = \mathrm{SU}(4)_C \otimes \mathrm{SU}(2)_L \otimes \mathrm{U}(1)_R$					
$(\mathbf{15},\mathbf{3},0)$	$(\mathbf{15},\mathbf{1},\mathbf{0})$	14.55	14.21	0.0246	–

$\alpha_{\rm GUT}$, and proton lifetimes for different combination of $R_{\rm DM}$ and the Higgs fields are

listed in Table 5.5.[3] Here, we set the DM mass to be 1 TeV. The second column lists the extra Higgs fields in R_1 at $M_{\rm int}$ in addition to R_2. We suppressed combinations of Higgs multiplets that cannot split the degeneracy of DM multiplet as in Eq. (3.8). The mass scales and proton decay lifetime are in units of GeV and years, respectively. We find that there is only one promising model with $G_{\rm int} = {\rm SU}(4)_C \otimes {\rm SU}(2)_L \otimes {\rm SU}(2)_R$, which is highlighted by blue shading in Table. 5.5. In this case, since the DM multiplet is a singlet under both ${\rm SU}(4)_C$ and ${\rm SU}(2)_R$, the additional Higgs fields are not necessary from the viewpoint of the mass splitting for the DM multiplet; namely, there is no degeneracy problem for this model. Rather, they are required so that the model achieves a good unification scale beyond proton decay constraint. The model has, however, a quite low intermediate scale that results in large neutrino masses through the type-I seesaw mechanism since the Dirac mass terms for neutrinos are related to the up-type Yukawa couplings in this setup. A simple way to evade this problem is to introduce a complex $(\mathbf{15}, \mathbf{2}, \mathbf{2})_C$ Higgs field in a **126** to modify the relation as what we have done in the case of NETDM. [4] If a $(\mathbf{15}, \mathbf{2}, \mathbf{2})_C$ Higgs is also present at the intermediate scale, it turns out that gauge coupling unification is still realized, with $\log_{10} M_{\rm int} = 9.28$, $\log_{10} M_{\rm GUT} = 16.38$, $\alpha_{\rm GUT} = 0.038$, and $\log_{10} \tau_p(p \to e^+\pi^0) = 35.9$. Here again, the mass scales and proton decay lifetime are expressed in units of GeV and years, respectively. Finally, we note that the addition of $(\mathbf{15}, \mathbf{2}, \mathbf{2})_C$ will not resurrect the failed models in Table 5.5.

5.4.3 Hypercharged DM

Hypercharged DM is a natural step forward after considering real triplet DM. In this section, we still restrict the Higgs content as in the previous section. As we discussed in Sec. 5.2, hypercharged DM is strongly constrained by direct detection experiments. To evade this constraint, we need to split the mass of the Weyl components of the hypercharged Dirac DM by ~ 100 keV. There are two possible ways to generate an effective operator in Eq. (5.1) through exchange of a field at the intermediate scale at tree level, depending on whether it is a scalar or a fermion. In the former case,

[3] We again restrict our attention to one-loop RGEs to avoid any model dependence due to the Yukawa coupling with the additional Higgs in R_1.

[4] For the effects of a $(\mathbf{15}, \mathbf{2}, \mathbf{2})_C$ Higgs field on the Yukawa couplings, see Refs. [14, 50].

the effective operator is induced by the exchange of intermediate-scale Higgs fields, as illustrated in Fig. 5.2(a). This requires the hypercharge of the virtual Higgs field to be at least one and $M_{\rm int} \lesssim 10^9$ GeV. According to Table 5.4, the only candidate for such a Higgs field belongs to $(\mathbf{15},\mathbf{1},\mathbf{3})$ in the $\mathbf{210}$ when $G_{\rm int} = {\rm SU}(4)_C \otimes {\rm SU}(2)_L \otimes {\rm SU}(2)_R$. The DM candidate should then be in a $(\mathbf{15},\mathbf{2},\mathbf{2})$ or $(\overline{\mathbf{10}},\mathbf{2},\mathbf{2}) \oplus (\mathbf{10},\mathbf{2},\mathbf{2})$ representation of ${\rm SU}(4)_C \otimes {\rm SU}(2)_L \otimes {\rm SU}(2)_R$. We performed a scan for models that contain above content, and found that none of them gives appropriate $M_{\rm int}$ and $M_{\rm GUT}$. The latter possibility is to introduce another fermionic real multiplet at the intermediate scale, so that the DM candidate is a mixture of a hypercharged field and a Majorana field. This mechanism is demonstrated in Fig. 5.2(b), where $R_{\rm DM}$ is the main component of the DM candidate which is hypercharged and has a mass term of TeV scale; $R'_{\rm DM}$ is the Majorana field at the intermediate scale. The cross mark in Fig. 5.2(b) represents the chiral flipping in the propagator of the Majorana field $R'_{\rm DM}$. $R_{\rm DM}$ and $R'_{\rm DM}$ couple to the SM Higgs field through terms like

$$\mathcal{L}_{\rm mix} \propto \overline{R}_{\rm DM} R'_{\rm DM} R_H + {\rm h.c.} \tag{5.8}$$

Since $R'_{\rm DM}$ is a Majorana field, it can only belong to either a singlet or a real triplet among the possible candidates in Table 3.1. As a result, DM can only belong to a doublet ($\mathtt{F}_{\mathbf{2}}^{1/2}$ or $\widehat{\mathtt{F}}_{\mathbf{2}}^{1/2}$) or a quartet ($\mathtt{F}_{\mathbf{4}}^{1/2}$), with hypercharge 1/2. This requires $M_{\rm int} \lesssim 10^9$ GeV according to the discussion in Sec. 5.2. Note that the $Y \geq 1$ DM candidates, $\mathtt{F}_{\mathbf{3}}^{\mathbf{1}}$, $\widehat{\mathtt{F}}_{\mathbf{3}}^{\mathbf{1}}$, and $\mathtt{F}_{\mathbf{4}}^{3/2}$, require at least $2Y$ additional fermions at the intermediate scale to generate the effective operator in Eq. (5.1). To minimize our model content, we do not consider these possibilities in the following discussion.

Taking the above discussion into account, we list the possible SO(10) representations for $R_{\rm DM}$ in the upper part of Table 5.6; the singlet and real triplet candidates for $R'_{\rm DM}$ are listed in the lower part of Table 5.6 and Table 5.3, respectively. The quantum numbers of the DM candidates with respect to the intermediate gauge groups we consider can be inferred from the ${\rm SU}(4)_C \otimes {\rm SU}(2)_L \otimes {\rm SU}(2)_R$ and $B-L$ quantum numbers listed in the table.

Now, we perform a one-loop calculation of $M_{\rm int}$, $M_{\rm GUT}$ and the proton decay lifetime for various combination of $R_{\rm DM}$, $R'_{\rm DM}$ and intermediate scale Higgs fields. Then, we pick up the models that are not yet ruled out by proton decay experiments, and at the

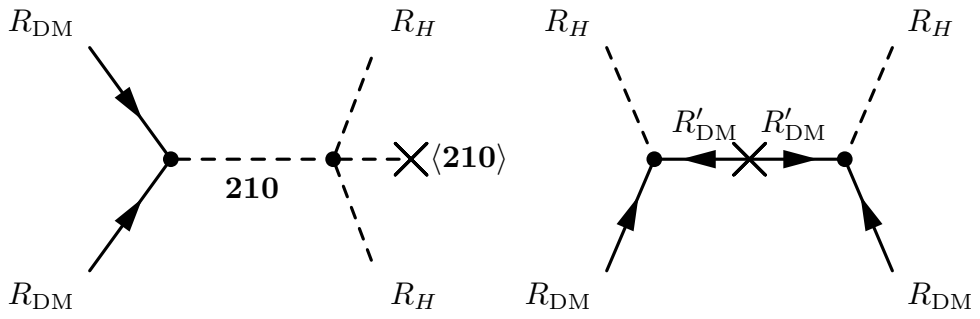

(a) Scalar exchange (b) Fermion exchange

Figure 5.2: *Diagrams that generate the mass splitting between the Weyl components of hypercharged Dirac DM through the exchange of an intermediate-scale (a) scalar (b) fermion.*

Table 5.6: *The upper half of the table shows the fermionic $Y = 1/2$ candidates for R_{DM} in various SO(10) representations; the lower half of the table shows the fermionic singlet candidates for R'_{DM}.*

SO(10) representation	$\mathrm{SU}(4)_C \otimes \mathrm{SU}(2)_L \otimes \mathrm{SU}(2)_R$	$B - L$
10, **120**, **210′**	$(\mathbf{1}, \mathbf{2}, \mathbf{2})$	0
120, **126**	$(\mathbf{15}, \mathbf{2}, \mathbf{2})$	0
210	$(\mathbf{10}, \mathbf{2}, \mathbf{2}) \oplus (\overline{\mathbf{10}}, \mathbf{2}, \mathbf{2})$	± 2
210′	$(\mathbf{1}, \mathbf{4}, \mathbf{4})$	0
54, **210**	$(\mathbf{1}, \mathbf{1}, \mathbf{1})$	0
45	$(\mathbf{1}, \mathbf{1}, \mathbf{3})$	0
45, **210**	$(\mathbf{15}, \mathbf{1}, \mathbf{1})$	0
210	$(\mathbf{15}, \mathbf{1}, \mathbf{3})$	0
126	$(\mathbf{10}, \mathbf{1}, \mathbf{3})$	2

same time have a relatively low intermediate scale $M_{\rm int} \lesssim 10^9$. We also require that the models have appropriate particle and Higgs content, so that the DM acquires the right mass through Eq. (3.8) and Eq. (5.8). It turns out that the viable models are limited to $G_{\rm int} = \mathrm{SU}(4)_C \otimes \mathrm{SU}(2)_L \otimes \mathrm{SU}(2)_R$ or $\mathrm{SU}(4)_C \otimes \mathrm{SU}(2)_L \otimes \mathrm{U}(1)_R$. These models are listed

in Table 5.7 and no quartic models ($\mathtt{F}_{\mathbf{4}}^{1/2}$) were found. The model $\mathtt{FA}_{422}$ is incompatible with small neutrino masses, since the Yukawa coupling for the **16** of this model is unified at $M_{\rm GUT}$. For models $\mathtt{FA}_{421}$ and $\mathtt{FB}_{422}$, on the other hand, we can avoid the neutrino mass problem by fine-tuning the Yukawa couplings with additional Higgs fields at the intermediate scale, as discussed in Sec. 5.4.2. Among them, the model $\mathtt{FA}_{421}$ has a phenomenologically interesting consequence. Since $M_{\rm int} \simeq 3$ TeV, this model predicts a new massive neutral gauge boson, Z', and vector leptoquarks whose masses are around a few TeV.

Table 5.7: *Possible hypercharged fermionic DM models that is not yet excluded by current proton decay experiments. The quantum numbers are labeled in the same order as G_{int}. The subscripts D and W refer to Dirac and Weyl respectively. The numerical results are calculated for DM mass of 1 TeV. The mass scales and proton decay lifetime are in unit of GeV and years, respectively.*

Model	$R_{\rm DM}$	$R'_{\rm DM}$	Higgs	$\log_{10}M_{\rm int}$	$\log_{10}M_{\rm GUT}$	$\alpha_{\rm GUT}$	$\log_{10}\tau_p$
$G_{\rm int} = {\rm SU}(4)_C \otimes {\rm SU}(2)_L \otimes {\rm U}(1)_R$							
$\mathtt{FA}_{421}$	$(\mathbf{1},\mathbf{2},1/2)_D$	$(\mathbf{15},\mathbf{1},0)_W$	$(\mathbf{15},\mathbf{1},0)_R$ $(\mathbf{15},\mathbf{2},1/2)_C$	3.48	17.54	0.0320	40.9 ± 1.2
$G_{\rm int} = {\rm SU}(4)_C \otimes {\rm SU}(2)_L \otimes {\rm SU}(2)_R$							
$\mathtt{FA}_{422}$	$(\mathbf{1},\mathbf{2},\mathbf{2})_W$	$(\mathbf{1},\mathbf{3},\mathbf{1})_W$	$(\mathbf{15},\mathbf{1},\mathbf{1})_R$ $(\mathbf{15},\mathbf{1},\mathbf{3})_R$	9.00	15.68	0.0258	34.0 ± 1.2
$\mathtt{FB}_{422}$	$(\mathbf{1},\mathbf{2},\mathbf{2})_W$	$(\mathbf{1},\mathbf{3},\mathbf{1})_W$	$(\mathbf{15},\mathbf{1},\mathbf{1})_R$ $(\mathbf{15},\mathbf{2},\mathbf{2})_C$ $(\mathbf{15},\mathbf{1},\mathbf{3})_R$	5.84	17.01	0.0587	38.0 ± 1.2

Chapter 6

Asymmetric Dark Matter

Among the components of the current universe, the density of baryons, $\Omega_B h^2 = 0.022$, and the density of cold dark matter, $\Omega_c h^2 = 0.12$ are found to be comparable to each other. This leads to the idea that the cold dark matter and the baryon asymmetry have the same origin in the early universe. In an SO(10) model with an intermediate scale, the generation of baryon-antibaryon asymmetry can be explained by the well studied framework of leptogenesis: the lepton-antilepton asymmetry is first generated by the out-of-equilibrium of right-handed neutrinos, this asymmetry is then transfered to the baryon density by the sphaleron process that violates the baryon and the lepton number conservation.

In this chapter, we consider the possibility that the SO(10) dark matter candidate possesses an asymmetry in its number density. Unlike NETDM and WIMP models where the DM candidate has equal matter and anti-matter densities, the asymmetric dark matter which accounts for the observed relic density is much more abundant than the anti-dark matter. The asymmetry in the dark matter states can be obtained by transferring a part of the asymmetry in the SM sector, which is generated by leptogenesis [60], to the dark matter sector. Preservation of this asymmetry in the background of sphaleron interactions, and possible dark matter-anti matter oscillations will impose stringent constraints on the possible models.

6.1 Asymmetric dark matter in SO(10)

6.1.1 Generation of asymmetries

As we have seen in the previous chapters of this thesis, the SO(10) unification models we considered generally particles with masses of $M_{\rm int}$, such as the right-handed neutrinos, the components of R_2 that breaks $G_{\rm int}$ and some componnets of the dark matter multiplet.

The decay of such intermediate-scale particles can generate a $B-L$ asymmetry. The $B-L$ charge in the decay process may not be conserved if the relevant diagrams contain the **126** VEV. C and CP invariance can also be violated if the vertices in the diagrams include CP phases. Thus, if this decay occurs out-of-equilibrium, a $B-L$ asymmetry can be generated. A well-known example is the generation of a lepton-number (and thus $B-L$) asymmetry via the out-of-equilibrium decay of right-handed neutrinos—leptogenesis [60, 61]. If there are no other $B-L$ violating processes in equilibrium, the generated $B-L$ asymmetry remains non-zero, which results in non-zero baryon and lepton asymmetries with the help of electroweak sphaleron processes [62, 63].

Such heavy particles may also decay into dark matter particles and generate an asymmetry in its density. This possibility is often called "cogenesis" in the literature and has been widely studied. The asymmetry production in this type of ADM models relies on the CP violating phase in the interaction between the decaying intermediate scale particle and the DM and is therefore highly model dependent.

Our focus of this section is on the so called "transfer" scenario, where the DM does not obtain an asymmetry when it is initially produced. Rather, $B-L$ asymmetry in the SM sector can be transferred to the dark matter sector. For this to occur, some interactions that communicate the asymmetries between these sectors should be in thermal equilibrium after the leptogenesis. As we shall see below, in this case the thermalization conditions give strong constraints on dark matter models that must be shared by all of our SO(10) dark matter candidates.

6.1.2 Thermal conditions for transfer and the dark matter mass

The $B-L$ asymmetry generated by leptogenesis is transferred to the dark sector via effective operators of the form

$$\mathcal{L}_{\rm eff} = \frac{c_d}{\Lambda^{d-4}}\mathcal{O}_{\rm DM}\mathcal{O}_{\rm SM} + \text{h.c.}\ , \tag{6.1}$$

if they are in thermal equilibrium, where $\mathcal{O}_{\rm DM}$ is an operator which contains only the dark matter fields and has a non-zero dark-matter number while $\mathcal{O}_{\rm SM}$ consists of SM fields only; $d \geq 4$ is the mass dimension of the operator; Λ denotes the scale at which the effective operator is generated (in particular, $\Lambda = M_{\rm int}$ in the models discussed below); c_d is a dimension-less constant, which may involve additional suppression factors such as small Yukawa couplings. The necessary condition for the interaction induced by the operator to be in thermal equilibrium is then given by

$$\begin{cases} T < T_{\rm eq} & \text{for} \quad d = 4 \\ T > T_{\rm eq} & \text{for} \quad d \geq 5 \end{cases}\ , \tag{6.2}$$

where the decoupling temperature $T_{\rm eq}$ is determined by the condition

$$\Gamma_{\mathcal{L}_{\rm eff}}\big|_{T_{\rm eq}} \simeq \frac{1}{8\pi^3}\frac{c_d^2}{\Lambda^{2(d-4)}}T_{\rm eq}^{2(d-4)+1} = \frac{\mathcal{C}T_{\rm eq}^2}{M_P} \simeq H\big|_{T_{\rm eq}}\ , \tag{6.3}$$

which gives

$$T_{\rm eq} \equiv \Lambda\left[\frac{8\pi^3\mathcal{C}\Lambda}{c_d^2 M_P}\right]^{\frac{1}{2(d-4)-1}}\ . \tag{6.4}$$

Hence, for non-renormalizable operators, if $T_{\rm eq} < T_{BL}$, there is a period during which they are in equilibrium. If the operator is renormalizable, then even though it is out-of-equilibrium at $T = T_{BL}$, it will come into thermal equilibrium when the temperature becomes lower than $T_{\rm eq}$.

The presence of such interactions in thermal equilibrium gives rise to a condition between the chemical potentials of SM fields and that of the dark matter field, which relates the $B-L$ asymmetry to the asymmetry in the dark-matter number. We focus on the dominant operator in Eq. (6.1), and assume that $\mathcal{O}_{\rm DM}$ contains $N_{\rm DM}$ dark matter fields (or, strictly speaking, the number of dark matter fields minus the number of anti-dark-matter fields) and $\mathcal{O}_{\rm SM}$ consists of N_Q, N_{u_R}, N_{d_R}, N_L, N_{e_R}, N_H numbers of

the left-handed quarks, right-handed up quarks, right-handed down quarks, left-handed leptons, right-handed charged leptons, and Higgs fields, respectively. The dark matter field is a $n_{\rm DM}$-dimensional representation of $\mathrm{SU}(2)_L$ and has the hypercharge $Y_{\rm DM}$ and $B-L$ charge $Q^{\rm DM}_{B-L}$. By assigning each particle species a chemical potential, and using gauge and Higgs interactions as conditions on these potentials one can write down a simple set of equations for various charge densities [67, 68]. Above the electroweak phase transition temperature, the conservation of the electroweak symmetry makes the chemical potential of the W boson vanish: $\mu_W = 0$. In equilibrium, the sphaleron process then yields the additional condition,[1]

$$3\mu_{u_L} + \mu_{\nu_L} = 0 \ , \tag{6.5}$$

where μ_{u_L} and μ_{ν_L} are the chemical potentials for the left-handed up quark and left-handed neutrino, respectively. The chemical equilibrium condition with respect to the interaction $\mathcal{L}_{\rm eff}$ reads

$$N_{\rm DM}\mu_{\rm DM} + (N_Q + N_{u_R} + N_{d_R})\mu_{u_L} + (N_L + N_{e_R})\mu_{\nu_L} + (N_H + N_{u_R} - N_{d_R} - N_{e_R})\mu_0 = 0 \ , \tag{6.6}$$

where $\mu_{\rm DM}$ and μ_0 are the chemical potentials for the dark matter and the Higgs field. In this paper, we focus on the case where the low-energy effective theory contains one $\mathrm{SU}(2)_L$ doublet Higgs boson; however, for one's convenience, in this section we keep the number of the Higgs doublets to be arbitrary and denote it by n_H, with the assumption that all of the Higgs fields have the same chemical potential μ_0. In addition, since $\mathcal{L}_{\rm eff}$ should be neutral under $\mathrm{U}(1)_Y$, we have

$$Y_{\rm DM}N_{\rm DM} + \frac{1}{6}N_Q + \frac{2}{3}N_{u_R} - \frac{1}{3}N_{d_R} - \frac{1}{2}N_L - N_{e_R} + \frac{1}{2}N_H = 0 \ . \tag{6.7}$$

On the other hand, it is not necessary for the interaction $\mathcal{L}_{\rm eff}$ to conserve $B-L$ as we will see below. Let us denote the entire $B-L$ charge of $\mathcal{L}_{\rm eff}$ by Δ_{B-L}.

$$Q^{\rm DM}_{B-L}N_{\rm DM} + \frac{1}{3}N_Q + \frac{1}{3}N_{u_R} + \frac{1}{3}N_{d_R} - N_L - N_{e_R} = \Delta_{B-L} \ . \tag{6.8}$$

By using Eqs. (6.5), (6.6), (6.7), and (6.8), we then obtain

$$\mu_{\rm DM} = 3X_{\rm DM}\mu_{u_L} + (2Y_{\rm DM} - X_{\rm DM})\,\mu_0 \ , \tag{6.9}$$

[1] Here, we assume that the dark matter field is either a complex scalar or a Dirac fermion. In this case, the dark matter does not contribute to the condition (6.5).

with

$$X_{\rm DM} \equiv Q^{\rm DM}_{B-L} - \frac{\Delta_{B-L}}{N_{\rm DM}} \ . \tag{6.10}$$

The electric charge density Q in units of $T^2/6$ is given by

$$\begin{aligned} Q &= 6\mu_{u_L} - 6\mu_{\nu_L} + (12+2n_H)\mu_0 + 2\mu_{\rm DM} k(z) \sum_{j=-J_{\rm DM}}^{J_{\rm DM}} (j + Y_{\rm DM}) \\ &= 24\mu_{u_L} + (12+2n_H)\mu_0 + 2\mu_{\rm DM} n_{\rm DM} Y_{\rm DM} k(z) \ , \end{aligned} \tag{6.11}$$

where $J_{\rm DM} \equiv (n_{\rm DM}-1)/2$, $z \equiv m_{\rm DM}/T$ with $m_{\rm DM}$ the dark matter mass, and

$$k(z) = \begin{cases} \frac{3}{4\pi^2} \int_0^\infty \frac{x^2 dx}{\sinh^2\left(\frac{\sqrt{x^2+z^2}}{2}\right)} & \text{for complex scalar} \\ \frac{3}{2\pi^2} \int_0^\infty \frac{x^2 dx}{\cosh^2\left(\frac{\sqrt{x^2+z^2}}{2}\right)} & \text{for Dirac fermion} \end{cases} \ . \tag{6.12}$$

Note that $k(z) \to 1$ for $z \to 0$, while $k(z) \propto e^{-z}$ for $z \gg 1$. On the other hand, the dark matter multiplet does not give a contribution to the $\mathrm{SU}(2)_L$ charge T_3 due to $\mathrm{Tr}(T_3) = 0$. By using Eqs. (6.9) and (6.11) with the condition $Q = 0$, we can express $\mu_{\rm DM}$ in terms of μ_{u_L}:

$$\mu_{\rm DM} = \frac{3\left[(10+n_H)X_{\rm DM} - 8Y_{\rm DM}\right]}{6 + n_H + (2Y_{\rm DM} - X_{\rm DM}) n_{\rm DM} Y_{\rm DM} k(z)} \mu_{u_L} \ . \tag{6.13}$$

We can also express the $B-L$ charge density in terms of μ_{u_L}. For later convenience, let us denote the contributions of the SM and dark matter particles to the $B-L$ charge density by $(B-L)_{\rm SM}$ and $(B-L)_{\rm DM}$, respectively, and obtain a relation between $(B-L)_{\rm SM}$ and the asymmetry in the dark matter sector. To that end, first we express $(B-L)_{\rm SM}$ in units of $T^2/6$ in terms of μ_{u_L}. By using Eq. (6.5), the condition $Q = 0$, and Eq. (6.13), we have

$$\begin{aligned} (B-L)_{\rm SM} &= 3\left(4\mu_{u_L} - 3\mu_{\nu_L} + \mu_0\right) \\ &= \frac{3\left[13n_H + 66 + 2n_{\rm DM} Y_{\rm DM} k(z)\left(13Y_{\rm DM} - 8X_{\rm DM}\right)\right]}{6 + n_H + (2Y_{\rm DM} - X_{\rm DM}) n_{\rm DM} Y_{\rm DM} k(z)} \mu_{u_L} \ . \end{aligned} \tag{6.14}$$

Thus, the asymmetry in the dark matter sector in units of $T^2/6$, $\Delta_{\rm DM}(z) \equiv 2n_{\rm DM} k(z) \mu_{\rm DM}$,[2] is related to $(B-L)_{\rm SM}$ as

$$\Delta_{\rm DM}(z) = \frac{2n_{\rm DM} k(z)\left[(10+n_H)X_{\rm DM} - 8Y_{\rm DM}\right]}{13n_H + 66 + 2n_{\rm DM} Y_{\rm DM} k(z)(13Y_{\rm DM} - 8X_{\rm DM})} (B-L)_{\rm SM} \ . \tag{6.15}$$

[2] We include a factor of $n_{\rm DM}$ in the definition of $\Delta(\mathrm{DM})$ since all of the charged states in the dark matter multiplet decay into the neutral component in the end.

This expression shows that the interaction $\mathcal{L}_{\rm eff}$ should decouple at some point; otherwise, $\Delta_{\rm DM}(z)$ is suppressed due to the factor $k(z)$. In the calculation above, we assume that the interaction $\mathcal{L}_{\rm eff}$ decouples before the electroweak phase transition. After decoupling, the dark matter asymmetry freezes with a value of $\Delta_{\rm DM} \equiv \Delta_{\rm DM}(z_{\rm dec})$ where $z_{\rm eq} \equiv m_{\rm DM}/T_{\rm dec}$.

$(B-L)_{\rm SM}$ in Eq. (6.15) is related to the baryon and lepton asymmetries in the SM sector, $B_{\rm SM}$ and $L_{\rm SM}$, respectively, through the ordinary procedure [67, 68]. By using Eq. (6.5) and $Q = 0$ with the dark matter contribution removed from Eq. (6.11), we can express $B_{\rm SM}$ and $L_{\rm SM}$ in terms of μ_{u_L} (in units of $T^2/6$) as

$$\begin{aligned} B_{\rm SM} &= 12\mu_{u_L} \ , \\ L_{\rm SM} &= 9\mu_{\nu_L} - 3\mu_0 = -\frac{3(42+9n_H)}{6+n_H}\mu_{u_L} \ . \end{aligned} \tag{6.16}$$

The sphaleron processes decouple after the electroweak transition [69] so that $\mu_0 = 0$ as the Higgs boson now develops a VEV, while now μ_W is non-vanishing. In this case, the electric charge is given by

$$Q = 6\mu_{u_L} - 6\mu_{\nu_L} - 2(8+n_H)\mu_W \ . \tag{6.17}$$

while the sphaleron condition reads

$$3\mu_{u_L} + 2\mu_W + \mu_{\nu_L} = 0 \ . \tag{6.18}$$

Again, by imposing the electric neutrality $Q = 0$, we can find the relation

$$B_{\rm SM} = \frac{4(8+n_H)}{98+13n_H}(B-L)_{\rm SM} \ . \tag{6.19}$$

Provided that the symmetric part of the dark matter sector is removed via annihilation, the present dark matter abundance is simply given by $\Delta_{\rm DM}$. Since it is related to $(B-L)_{\rm SM}$, which is conserved after decoupling of the transfer interaction, we can relate it to the baryon number density today via (6.19). Therefore, to explain the observed dark matter energy density, the dark matter mass should be

$$m_{\rm DM} = m_N \left(\frac{\Omega_c h^2}{\Omega_B h^2}\right) \left|\frac{13n_H + 66 + 2n_{\rm DM}Y_{\rm DM}k(z_{\rm dec})(13Y_{\rm DM} - 8X_{\rm DM})}{2n_{\rm DM}k(z_{\rm dec})\left[(10+n_H)X_{\rm DM} - 8Y_{\rm DM}\right]}\right| \left[\frac{B_{\rm SM}}{(B-L)_{\rm SM}}\right] , \tag{6.20}$$

where m_N is the nucleon mass.

6.1.3 Hypercharged asymmetric dark matter

In Section 5.2 we discussed the constraint of direct detenction experiments on hypercharged. This constraint applies to all kinds of hypercharged dark matter candidates since it is independent of the production mechanism. To evade the constraint, the masses of the two real(majorana) components of the complex scalar(Dirac fermionic) hypercharged dark matter should be splitted from each other by the operator (5.1).

For a Dirac fermion ψ with hypercharge Y, the operator takes the form:

$$\mathcal{L}_{\Delta m} = \frac{c_{\Delta m}}{2\Lambda^{(4Y-1)}}(H^*)^{4Y}\overline{\psi^c}\psi + \text{h.c.}\ , \tag{6.21}$$

where all the Clebsch-Gorden coefficients have been absorbed in $c_{\Delta m}$. This operator has the form (6.1), and thus can communicate asymmetry in the SM sector to the dark matter sector [73, 74]. Hence, hypercharged dark matter can be a good candidate for asymmetric dark matter. As it turns out, however, there are two challenges in this scenario, besides the direct detection bound mentioned above. First, if the operator (6.21) remains in thermal equilibrium below the electroweak phase transition temperature, then it washes out the dark matter asymmetry. The chemical equilibrium condition for this interaction gives an additional relation between the dark matter and Higgs chemical potentials: $4Y\mu_0 + 2\mu_{\rm DM} = 0$. After electroweak symmetry breaking, $\mu_0 = 0$, and thus this condition implies $\mu_{\rm DM} = 0$. To avoid this, the interaction (6.21) should decouple before electroweak symmetry breaking. Second, the operator (6.21) causes particle-antiparticle oscillations after electroweak symmetry breaking, which may wash out the asymmetry in the dark sector. To prevent this, we need to make the oscillation rate sufficiently small or assure the decoupling of dark matter from thermal bath before the electroweak phase transition. In the latter case, there is no asymmetry in the dark matter sector at present, but still the dark matter abundance is (mainly) determined by the asymmetry of dark matter before the electroweak symmetry breaking.

Let us give a rough estimation for the above conditions. First, according to Eq. (6.4), $T_{\rm eq}$ for the operator (6.21) is given by

$$T_{\rm eq} = \left[\frac{8\pi^3\mathcal{C}\Lambda^{2(4Y-1)}}{c_{\Delta m}^2 M_P}\right]^{\frac{1}{2(4Y-1)-1}} = \left[\frac{8\pi^3\mathcal{C}v^{8Y}}{4^{(2Y-1)}M_P\Delta m^2}\right]^{\frac{1}{2(4Y-1)-1}}\ . \tag{6.22}$$

For $Y = 1/2$, for instance, this reads

$$T_{\rm eq} \simeq 100\ {\rm GeV} \times \left(\frac{100\ {\rm keV}}{\Delta m}\right)^2 . \tag{6.23}$$

This result shows that the requirement $\Delta m \gtrsim 100$ keV to evade the direct detection bound may cause the operator (6.21) to remain in equilibrium down to the electroweak phase transition. We however note that the formula (6.4) is based on the assumption that all of the relevant particles are relativistic. Thus, if the dark matter mass is much larger than the electroweak scale, the above consequence may be modified significantly.

The second condition follows from $\Gamma_{\rm osc} < H|_{T_{\rm EW}}$ where $\Gamma_{\rm osc} = \Delta m/2$ is the rate of particle-antiparticle oscillations and $T_{\rm EW}$ is the temperature at the electroweak phase transition. This leads to

$$\Delta m < \frac{2\mathcal{C}T_{\rm EW}^2}{M_P} \simeq 3 \times 10^{-14}\ {\rm GeV} \times \left(\frac{T_{\rm EW}}{100\ {\rm GeV}}\right)^2 . \tag{6.24}$$

Obviously, this conflicts with the direct detection bound. Thus, to avoid particle-antiparticle oscillations from erasing the dark matter asymmetry, the dark matter should decouple from thermal bath above $T_{\rm EW}$. Since the freeze-out temperature of dark matter is given by $\simeq m_{\rm DM}/25$, this condition requires $m_{\rm DM} \gtrsim 25 T_{\rm EW}$.

As we have just seen, the above conditions may be evaded if $m_{\rm DM} \gg T_{\rm EW}$. On the other hand, there is an upper bound on the dark matter mass which follows from the requirement that the symmetric part of dark matter be annihilated away so that the asymmetric part accounts for the (dominant part of the) dark matter abundance. For example, for the $\mathrm{SU}(2)_L$ doublet $Y = 1/2$ Dirac dark matter, the annihilation is effective if $m_{\rm DM} < 1$ TeV. On the other hand, the second condition discussed above requires $m_{\rm DM} \gtrsim 25 T_{\rm EW} > 1$ TeV, and thus the doublet Dirac fermion is unable to be asymmetric dark matter [73]. For the $\mathrm{SU}(2)_L$ doublet scalar dark matter, the upper bound on the dark matter mass is relaxed if the dark matter-Higgs quartic coupling is large. Even in this case, however, the dark matter asymmetry is found to be much smaller than the observed dark matter density once the perturbativity condition is imposed on the quartic coupling [76]. Other cases for hypercharged dark matter candidates are discussed in Ref. [75], and found that the $Y > 1$ cases are excluded. As a consequence, only the $Y = 1$ cases can be promising candidates for hypercharged asymmetric dark matter.

6.1.4 Candidate models for SO(10) asymmetric dark matter

Let us summarize the discussion in this section, and list up promising candidates for asymmetric dark matter in SO(10) GUTs. First, we consider the "minimal models", namely, we require that besides the SM particles only the dark matter multiplet has a mass much lighter than the intermediate scale. In this case, the low-energy effective theory only contains the SM particles and the dark matter, and the relevant non-renormalizable operators are generated at the intermediate or GUT scale.

As discussed in the previous subsection, the $Y = 1/2$ and $3/2$ candidates in Table 3.1 have already been excluded. In addition, the analysis in Chapter 5 shows that $\mathtt{S}^0_{\mathbf{3}}$, $\mathtt{S}^1_{\mathbf{3}}$, $\mathtt{F}^1_{\mathbf{3}}$, $\widehat{\mathtt{F}}^0_{\mathbf{1}}$, $\widehat{\mathtt{F}}^1_{\mathbf{3}}$ are not good candidates for SO(10) dark matter models. This is because none of these models are consistent with gauge coupling unification with reasonable values of $M_{\rm int}$ and/or $M_{\rm GUT}$ with minimal field content. As a result, only $\mathtt{S}^0_{\mathbf{1}}$ can be a promising candidate for SO(10) asymmetric dark matter. We will discuss this candidate in the subsequent section. Then, we discuss some next-to-minimal extensions in Sec. 6.3.

6.2 Scalar Singlet Asymmetric Dark Matter

As we discussed in the previous section, singlet scalar dark matter is the only candidate for asymmetric dark matter in SO(10) if we require the minimality. We discuss this possibility in this section. In Sec. 5.3.2, we have calculated $M_{\rm int}$, $M_{\rm GUT}$, unified coupling and the proton decay lifetime for various $G_{\rm int}$ for the WIMP scenario. The ADM model under consideration in this section has different DM particle mass since it is sensitive to the production mechanism. However, the rest of the spectrum is the same as those considered in Sec. 5.3.2. Thus the result obtained for the WIMP scenario is also valid for the ADM model considered here, because a singlet does not affect the RGE-running. Only three models accommodate a sufficiently high GUT scale that is required to evade the proton decay bound. These models are called $\mathtt{SA}_{422}$, $\mathtt{SA}_{3221}$, and $\mathtt{SA}_{3221\mathtt{D}}$. To be specific, we focus on the $\mathtt{SA}_{3221}$ case in the following analysis, but similar discussions can also be applied to the other cases. For convenience, the DM field is noted as S in the rest of this section.

6.2.1 Particle-antiparticle oscillations

Since S is a singlet under the SM gauge group, in addition to the particle-number-conserving mass term $|S|^2$, it can also have the particle-number-violating mass terms S^2 and S^{*2}. These mass terms induce particle-antiparticle oscillations $S \leftrightarrow S^*$, which are problematic as they erase the asymmetry in the dark matter sector. To avoid this problem, the oscillation rate has to be small, namely,

$$\Gamma_{\rm osc} = \frac{\Delta m}{2} \lesssim \frac{\mathcal{C}}{M_P}\left(\frac{m_{\rm DM}}{25}\right)^2 , \tag{6.25}$$

where Δm denotes the mass splitting between the dark matter particle and its antiparticle induced by the particle-number-violating mass terms, and the right-hand side is the Hubble parameter when the dark matter decouples from the thermal bath. In the presence of the mass terms $\mu^2(S^2 + S^{*2})/2$, the mass splitting is given by $\Delta m = \mu^2/m_{\rm DM}$, and thus Eq. (6.25) leads to

$$\mu \lesssim \frac{m_{\rm DM}}{25}\left(\frac{2\mathcal{C}m_{\rm DM}}{M_P}\right)^{\frac{1}{2}} \simeq 2\times 10^{-6}\times\left(\frac{m_{\rm DM}}{1\ {\rm TeV}}\right)^{\frac{3}{2}}\ {\rm GeV}\ . \tag{6.26}$$

In SO(10), both $\mathbf{16}^2$ and $\mathbf{144}^2$ are forbidden by the gauge symmetry, and thus the particle-number-violating mass terms are absent. The intermediate gauge symmetries also forbid such mass terms. Below the intermediate gauge scale, however, the VEV of the **126** Higgs field can generate the particle-number-violating mass terms via the interactions

$$\mathcal{L}_{\rm int} = -\kappa_2 R_{\rm DM} R_{\rm DM} R_2^* - \lambda_{12}^{\mathbf{126}}(R_{\rm DM}R_{\rm DM})(R_1 R_2^*)_{\overline{\mathbf{126}}} + {\rm h.c.}\ , \tag{6.27}$$

where $R_{\rm DM} = \mathbf{16}$ or $\mathbf{144}$ denotes the dark matter multiplet, R_1 is the GUT Higgs field, $R_2 = \mathbf{126}$ is the intermediate-scale Higgs field, and the subscripts after the parentheses denote the SO(10) representation formed by the product in them. To satisfy the bound (6.26), we need to suppress the couplings κ_2 and $\lambda_{12}^{\mathbf{126}}$. Once they are taken to be small, they remain small under the renormalization flow. By making these couplings small, we can also suppress the particle-number-violating couplings with the Higgs boson, such as $S^2|H|^2$, which are induced by the exchange of the **126** Higgs and lead to the particle-number-violating mass terms after electroweak symmetry breaking.

6.2.2 Thermal transfer

If the asymmetry in the dark sector is transferred from the $B-L$ asymmetry in the SM sector through effective interactions (6.1), the dark matter mass is uniquely determined by the thermal relation (6.20). The lowest-dimension effective operator which has the form of (6.1) is

$$\mathcal{L}_{\rm eff}^{(7)} = \frac{c_7}{\Lambda^3} S^2 H^2 \overline{L^c} L + \text{h.c.} \ , \tag{6.28}$$

which can be induced by the exchange of the intermediate-scale particles. We thus take $\Lambda = M_{\rm int}$ with other possible suppression factors included in the coefficient c_7. $T_{\rm eq}$ for this operator is then given by Eq. (6.4):

$$T_{\rm eq} = M_{\rm int} \left[\frac{8\pi^3 \mathcal{C} M_{\rm int}}{c_7^2 M_P} \right]^{\frac{1}{5}} \ . \tag{6.29}$$

If $T_{\rm eq} \gg m_{\rm DM}$, this interaction decouples from the thermal bath much before the decoupling of the dark matter, and in particular we can set $k(z_{\rm dec}) = 1$ in Eq. (6.20). By setting $n_{\rm DM} = 1$, $n_H = 1$, $Y_{\rm DM} = 0$, and $X_{\rm DM} = Q_{B-L}^{\rm DM} = 1$, we then obtain

$$m_{\rm DM} = m_N \frac{79}{22} \left(\frac{\Omega_c h^2}{\Omega_B h^2} \right) \left[\frac{B_{\rm SM}}{(B-L)_{\rm SM}} \right] \simeq 6.0 \text{ GeV} \ , \tag{6.30}$$

where we have used Eq. (6.19). However, such a small dark matter mass has already been excluded by the constraint on the Higgs invisible decay width. The symmetric part of the dark matter density is annihilated through the quartic interaction

$$\mathcal{L}_{\rm int} = -\lambda_{SH} |S|^2 |H|^2 \ , \tag{6.31}$$

If the mass of the dark matter singlet is smaller than $m_h/2$, the SM Higgs boson can decay into a pair of the dark matter particles through the interaction (6.31). This decay mode is invisible at the LHC, and reduces the branching fractions of the other decay channels, which is severely restricted by the Higgs measurements at the LHC [77]. As a result, the singlet dark matter candidate with such an interaction with the Higgs boson has been ruled out for $m_S < m_h/2$. [102]

If $T_{\rm eq} \lesssim m_{\rm DM}$, on the other hand, the dark matter mass given by Eq. (6.20) can be increased due to the Boltzmann factor $k(z_{\rm dec})$. In terms of the intermediate scale $M_{\rm int}$, the inequality $T_{\rm eq} \lesssim m_{\rm DM}$ reads

$$M_{\rm int} \lesssim m_{\rm DM}^{\frac{5}{6}} \left[\frac{c_7^2 M_P}{8\pi^3 \mathcal{C}} \right]^{\frac{1}{6}} \simeq c_7^{\frac{1}{3}} \times \left(\frac{m_{\rm DM}}{1 \text{ TeV}} \right)^{\frac{5}{6}} \times 10^5 \text{ GeV} \ . \tag{6.32}$$

As discussed in Sec. 5.3.2, however, there is no candidate in a model with minimal field content which predicts such a low intermediate scale.[3] We therefore conclude that the thermal transfer scenario does not work for the scalar singlet asymmetric dark matter candidate in SO(10).

6.3 Next-to-minimal models

In the model we considered in the previous section, the dark matter particle develops an asymmetric part in its density through transfer from an asymmetry of the SM particles and preserves it as (a part of) the dark matter relic observed today. As we have seen, these models are severely constrained leaving only the scalar singlet dark matter model which is in conflict with collider search if we assume a minimal particle content. However, we may find additional models if we relax the notion of the asymmetric dark matter—namely, the constraints discussed above can be relieved if the dark matter relic abundance is only required to have an asymmetric origin while it can be totally symmetric today. We discuss this possibility in this section.

More specifically, we consider dark matter models that achieve the relic density in two steps, similar to models considered in Refs. [74, 76]. In these models, two $\mathbb{Z}_2$-odd particles (or multiplets) X_1 and X_2 are introduced near the TeV scale. X_1 is the lighter one whose relic density eventually originates from the $B-L$ asymmetry in two steps: i) X_2 obtains asymmetric density by asymmetry transfer from SM particles, and then ii) the asymmetric density in X_2 is converted to the relic density of X_1 through X_2 decay. In order to annihilate the symmetric part of the thermal abundance efficiently, X_1 needs to have sizable couplings with the SM sector. To that end, we assume that X_1 has a charge under the $\mathrm{SU}(2)_L \otimes \mathrm{U}(1)_Y$ gauge interactions. In the model we present below, X_1 is a Majorana fermion. X_2 needs to have a long enough lifetime to decay after depletion of X_1 symmetric density; otherwise the determination of X_1 relic density is similar to that in the usual thermal relic scenario.

In the rest of this section we will consider the scenario where the asymmetry in X_2 is obtained from a Yukawa coupling of the form $X_2\overline{X}_1 f$ with f representing the

[3] One can construct a non-minimal model with a low intermediate scale. This can be done for example, if the intermediate gauge group is broken in two steps to the SM. While one of the intermediate scales remains relatively large, the second may be as low as ~ 1 TeV.

SM fermions. X_1 and X_2 are taken to be a Majorana fermion and a complex scalar multiplet, respectively. The chemical potentials of X_1 and X_2 are determined by the neutrality of the Majorana particle X_1 and by this Yukawa interaction, respectively:

$$\mu_{X_1} = 0, \qquad \mu_{X_2} = -\mu_f \ . \tag{6.33}$$

As stated above, X_2 is supposed to decay into X_1 after the X_1–X_1 and X_2–X_2^* annihilation processes decouple. If these annihilation processes deplete X_1 and the symmetric part of X_2 density efficiently, the relic abundance will be determined by the asymmetric part of the X_2 density before its decay. As we will see, the slow decay $X_2 \to X_1 + \bar{f}$ requires a small mass gap between X_2 and X_1. At low temperature $T < m_{X_1}$, the asymmetry is transferred through the scattering $f + X_{1,2} \to A + X_{2,1}$ with SM fermions propagating in the t-channel and A is any light gauge boson which couples to f. The decoupling temperature of the asymmetric transfer $T_{\rm dec}$ is thus determined by the decoupling of this t-channel scattering process.

For a concrete model, we choose X_2 as a right-handed stop-like particle $\widetilde{t}_R$, which is a color triplet, weak isospin singlet and has hypercharge $2/3$. X_1 is chosen as a mixture of a singlet Majorana fermion ψ_S and the neutral component of a doublet ψ_D^0. The lighter component of the mixture is the dark matter candidate and we will write it as χ for convenience. Furthermore, we assume $\widetilde{t}_R$ only couples to the right-handed top quark t_R through the Yukawa coupling

$$\mathcal{L} = \lambda_t \bar{t}_R \psi_S \widetilde{t}_R + \text{h.c.} \ , \tag{6.34}$$

which resembles the bino-stop-top coupling in the minimal supersymmetric Standard Model.

The SO(10) completion of this model on top of the three generations of the SM **16** is summarized in Table 6.1. The SO(10) symmetry is broken by a $\mathbf{210}_R$ to $G_{\rm int} = {\rm SU}(4)_C \otimes {\rm SU}(2)_L \otimes {\rm SU}(2)_R$, which is broken subsequently to $G_{\rm SM}$ by the VEV of $(\mathbf{10}, \mathbf{1}, \mathbf{3})_C$ in a $\mathbf{126}_C$. ψ_S, ψ_D and $\widetilde{t}_R$ belong to Weyl **45**, Weyl **10**, and complex scalar **16** representations, respectively.[4] The Yukawa interaction (6.34) comes from the coupling $\mathbf{16}^* \mathbf{16}_f \mathbf{45}_W$ where $\mathbf{16}_f$ is the multiplet composed of the third generation

[4] We are required here to consider a higher representation for ψ_S to achieve gauge coupling unification with a sufficiently high GUT scale.

Table 6.1: *Particle content of the stop mediated asymmetry transfer model. The first column shows the particle content around the electroweak or TeV scale. The second column and the third column show the quantum number under G_{int} and the SO(10) representation respectively.*

EW	$\mathrm{SU}(4)_C \otimes \mathrm{SU}(2)_L \otimes \mathrm{SU}(2)_R$	SO(10)
$\widetilde{t}_R$	$(\mathbf{4},\mathbf{1},\mathbf{2})_C$	$\mathbf{16}_C$
ψ_D	$(\mathbf{1},\mathbf{2},\mathbf{2})_W$	$\mathbf{10}_W$
ψ_S	$(\mathbf{1},\mathbf{1},\mathbf{3})_W$	$\mathbf{45}_W$
H	$(\mathbf{15},\mathbf{2},\mathbf{2})_C$	$\mathbf{126}_C$
H	$(\mathbf{10},\mathbf{2},\mathbf{2})_C$	$\mathbf{210}_R$
H	$(\mathbf{1},\mathbf{2},\mathbf{2})_C$	$\mathbf{10}_C$
	$(\mathbf{10},\mathbf{1},\mathbf{3})_C$	$\mathbf{126}_C$

SM fermions and right-handed neutrino. G_{SM} is broken by the VEV of the following doublets: $(\mathbf{1},\mathbf{2},\mathbf{2})_R$ of $\mathbf{10}_R$, $(\mathbf{15},\mathbf{2},\mathbf{2})_C$ of $\mathbf{126}_C$, and $(\mathbf{10},\mathbf{2},\mathbf{2})_C$ of $\mathbf{210}_R$. The SM Higgs doublet is a mixture of the above doublets. The latter two multiplets at the intermediate scale are necessary for achieving a sufficiently high unification scale. With this particle content, the one-loop result for the scales and unification coupling are

$$M_{\mathrm{int}} = 10^{11.3}\ \mathrm{GeV}, \qquad M_{\mathrm{GUT}} = 10^{15.7}\ \mathrm{GeV}, \qquad \alpha_{\mathrm{GUT}} = 0.035\ . \tag{6.35}$$

Now we consider the constraint placed on the coupling strength λ_t and the particle masses. An upper bound on the mass of χ can be set by requiring its symmetric density to be small before the decay of X_2. The relic abundance of an $\mathrm{SU}(2)_L$ doublet Dirac dark matter candidate is saturated by the symmetric part if its mass is about 1 TeV. Thus, if we require that the density of asymmetric origin makes up over 90% of the total relic density, we can set a bound on the dark matter particle mass $m_\chi \lesssim 1\ \mathrm{TeV}/\sqrt{10} \sim 350\mathrm{GeV}$.[5] The DM-nucleon scattering cross section for almost pure $\mathrm{SU}(2)_L$ doublet

[5] As we see below, the coupling λ_t is required to be very small, and thus the contribution of the interaction (6.34) to the annihilation of the dark matter particles is negligible. Moreover, since the conversion process $t\chi \leftrightarrow g\widetilde{t}_R$ decouples before the decoupling of the dark matter (see the discussion below), coannihilation with $\widetilde{t}_R$ is ineffective.

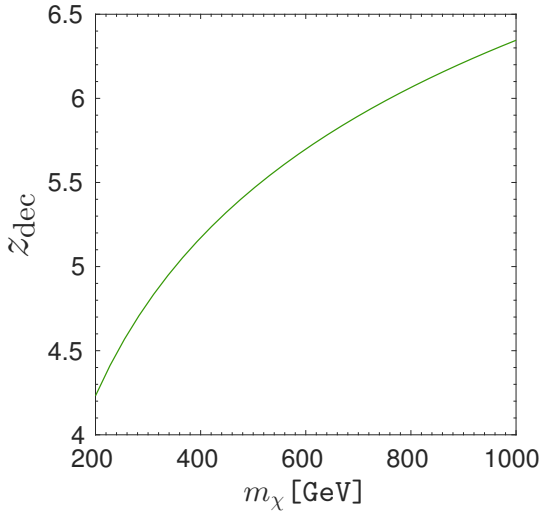

Figure 6.1: $z_{\rm dec} = m_{\tilde{t}_R}/T_{\rm dec}$ *as a function of* m_χ*, determined by dark matter relic density.*

dark matter is found to be very small ($\sigma_{\rm SI} \lesssim 10^{-49}$ cm^2) [103] and thus this candidate can evade the direct detection limits.[6]

The relationship between the relic density and the dark matter mass is given by Eq. (6.20), with the relevant quantities for dark matter in Eq. (6.20) replaced with the corresponding quantities for $\widetilde{t}_R$; namely, we set $n_H = 1$, $n_{\rm DM} = 1$, $Y_{\rm DM} = 2/3$, $X_{\rm DM} = 1/3$, and replace $k(z_{\rm dec})$ with $3k(z_{\rm dec})$ to take the color factor for $\widetilde{t}_R$ into account.[7] We then have

$$m_\chi \simeq m_N \left(\frac{\Omega_c}{\Omega_B}\right) \frac{474 + 144k(z_{\rm dec})}{185k(z_{\rm dec})} \ , \tag{6.36}$$

where $z_{\rm dec} = m_{\tilde{t}_R}/T_{\rm dec}$ with $T_{\rm dec}$ the decoupling temperature of the Yukawa interaction,

[6] If χ is a well-mixed state of singlet and doublet components, the dark matter-nucleon scattering is induced by the Higgs boson exchange process, which is severely constrained by the direct detection experiments. However, there is a specific parameter region, so-called blind spot [78–80], where the direct detection bound is evaded even though the singlet-doublet mixing is sizable. In this region, the symmetric part of dark matter relic agrees with the observed dark matter density even if the dark matter mass is as large as ~ 1.5 TeV [81]; therefore, for the symmetric origin of the dark matter abundance to be less than 10%, $m_{\rm DM} \lesssim 1.5$ TeV$/\sqrt{10} \sim 500$ GeV is required in the case of the blind spot.

[7] Strictly speaking, we may not directly apply Eq. (6.20) to the present case as $\widetilde{t}_R$ can be in thermal bath until the time of the sphaleron decoupling, though this effect does not affect our discussion significantly.

and we have used Eq. (6.19). The required value for $z_{\rm dec}$ is then obtained from the observed dark matter density using this relation, as shown in Fig. 6.1. We find that it is in the range of 4–6.5 for m_χ of 200 GeV–1 TeV.

According to Fig. 6.1, around the decoupling temperature of the Yukawa interaction (6.34), the temperature is as low as ~ 100 GeV and thus even the dominant t-channel scattering process $t + \chi \leftrightarrow g + \widetilde{t}_R$, with g a gluon, is exponentially suppressed. The reaction rate is estimated by the target density n_t times the cross section for the process $\langle \sigma v \rangle_{t\chi}$, which is approximated by

$$\Gamma(t\chi \leftrightarrow g\widetilde{t}_R) \simeq \frac{g_3^2 \lambda_t^2}{\pi m_\chi m_t} \cdot \frac{T}{m_t} \cdot \left(\frac{m_t T}{2\pi} \right)^{3/2} e^{-m_t/T} \ , \tag{6.37}$$

where we neglect the ψ_S–ψ_D mixing for simplicity. This does not change the following discussion qualitatively. Through this process, any asymmetry in tops (baryon asymmetry) is transferred to an asymmetry in the $\widetilde{t}_R$ which subsequently decay to χ. The decoupling temperature is estimated from $\Gamma(t\chi \leftrightarrow g\widetilde{t}_R) \simeq H$ and using the result in Fig. 6.1, we then obtain $\lambda_t \simeq 2.5\ (1.2) \times 10^{-6}$ for $m_\chi = 200\ (1000)$ GeV.

Now let us consider the condition that $\widetilde{t}_R$ has a lifetime long enough to decay after the annihilation of the symmetric part of χ is over. To ensure such slow decay, we need to set $\Delta m \equiv m_{\widetilde{t}_R} - m_\chi < m_t$ so that the two-body decay channel $\widetilde{t}_R \to t\chi$ is kinematically forbidden.[8] The dominant decay channel is then the three-body decay $\widetilde{t}_R \to bW\chi_i$, $i = 1, 2, 3$ represents three mass eigenstates of $\psi_D^0 - \psi_S$ mixing, and for simplicity we assume $\widetilde{t}_R$ can decay to all of them, so that the decay rate is not suppressed by the mixing angle. The decay occurs after χ–χ annihilation if $\Gamma_{\tilde{t}_R} < H|_{T_f}$, where $m_\chi/T_f \sim 20$ is the decoupling temperature of the annihilation. Numerical calculation of the decay rate gives a bound of $\Delta m \lesssim 100\ (160)$ GeV for $m_{X_1} = 200\ (1000)$ GeV, assuming the three χ_i are degenerate in mass.

Finally we remark that the framework of transferring the asymmetry through Yukawa interactions can also be applied straightforwardly to other choices of $\mathbb{Z}_2$-odd particles. For example, we can also choose X_1 as a single Majorana triplet (thus avoiding the need for mixing among two multiplets) and X_2 as a slepton-like doublet. The asymmetry is transferred to X_2 from the lepton doublet. The decoupling temperature of asymmetry

[8] Such a small mass difference also allows $\widetilde{t}_R$ to evade the strong limits from stop searches at the LHC [83, 84].

transfer in this case is however exponentially sensitive to the Yukawa coupling, since the asymmetry transfer scattering $X_1 + \ell^- \leftrightarrow \gamma + X_2$ is mediated by a lepton and the reaction rate is dependent on $\log(T/m_\ell)/T$ when $m_\ell \ll T \ll X_1$. We will not discuss this model in more detail here.

Chapter 7

Improvement of Vacuum Stability

In this chapter we consider the stability of the Higgs VEV. The scalar potential of the SM Higgs doublet is

$$V_{\rm SM} = \mu^2|H|^2 + \frac{\lambda}{2}|H|^4. \tag{7.1}$$

where the parameter λ and μ are determined by the value of the Higgs VEV and the mass of the Higgs particle $m_h = 125.09 \pm 0.24$ GeV. If the SM is valid up to an arbitary high scale, we can ran the quartic coupling with the SM RGE as shown by the green dotted curve in Fig. 7.1. λ becomes negative around the scale of 10^{10} GeV. Thus the scalar potential of the SM is unbounded from below for large value of H and the vacuum of the electroweak theory is unstable. This is an implication for new physics beyond the SM at a scale lower than 10^{10} GeV. In an SO(10) unification model, the dark matter candidate and an intermediate scale below 10^{10} GeV introduce new particles beyond the SM that may modify the running of λ so that it stays positive all the way up to the PLANCK scale. For simplicity, we consider here a SM singlet dark matter candidate originating from a **16** of SO(10) as in model $\texttt{SA}_{3221}$ in Chapter 5 based on the intermediate gauge group $\mathrm{SU}(3)_C \otimes \mathrm{SU}(2)_L \otimes \mathrm{SU}(2)_R \otimes \mathrm{U}(1)_{B-L}$. In this model, the intermediate scale is found to be $M_{\rm int} \simeq 10^9$ GeV and is small enough to allow the couplings of the **126** Higgs field to the SM Higgs to lift the Higgs quartic coupling through the threshold corrections before it turns negative.

Moreover, we also consider the running of the quadratic coupling μ^2 in this model. In this SM this parameter is taken to be negative at the electroweak scale for the purpose of spontaneous symmetry breaking. In a supersymmetric SM, the electroweak symmetry

is broken radiatively, where the quartic couplings are initial positive at a high energy scale, but is driven negative at a low energy scale. We will also reproduce this feature in our non-supersymmetric SO(10) model by requiring μ^2 runs positive at a high energy scale.

7.1 Renormalization group evolution of the Higgs couplings

The renormalization group evolution between the weak scale and intermediate scale is almost identical to the SM. The only difference comes from the inclusion of the SM singlet dark matter candidate, $s \equiv \mathrm{Re}[\tilde{\nu}_R]$. Below the intermediate scale, the scalar potential is relatively simple,

$$V_{\mathrm{blw}} = \mu^2|H|^2 + \frac{1}{2}\mu_s^2 s^2 + \frac{\lambda}{2}|H|^4 + \frac{\lambda_{sH}}{2}|H|^2 s^2 + \frac{\lambda_s}{4!}s^4 \ . \tag{7.2}$$

In many ways, this resembles the minimal dark matter model often referred to as the Higgs portal. The mass of our dark matter candidate is given by $m_{\mathrm{DM}}^2 = \lambda_{sH} v^2/2 + \mu_s^2$. Furthermore, fixing the dark matter mass will also fix λ_{sH} at the weak scale (taken here to be m_t) through the relic density (assuming standard thermal freeze-out): $m_{\mathrm{DM}} \simeq 3.3\lambda_{sH}$ TeV. The evolution of the Higgs quartic coupling in the SM with and without the inclusion of the scalar s is shown in Fig. 7.1 by the green solid and dotted curves, respectively. The renormalization group equations (RGE) are run at the two-loop level[1]

and one sees that the SM quartic coupling runs negative just above 10^{10} GeV [85] without the scalar contribution. With the scalar contribution, the running of λ would remain positive out to the GUT scale. Note that at the intermediate scale (determined by the conditions for gauge coupling unification; the running of the gauge couplings in $\mathtt{SA}_{3221}$ is shown by thin black lines in Fig. 7.1), $M_{\mathrm{int}} \simeq 10^9$ GeV, $\lambda > 0$. Gauge coupling unification also determines the GUT scale to be $M_{\mathrm{GUT}} \simeq 1.5 \times 10^{16}$ GeV, which is high enough to evade the proton decay limit. Also shown is the running of λ_s (blue dash-dotted) and λ_{sH} (brown dashed).

[1] We use the three-loop RGEs for the top Yukawa and Higgs quartic couplings. We also include the two-loop electroweak threshold corrections according to Ref. [85]. We use the $\overline{\mathrm{MS}}$ scheme up to the intermediate scale, and switch to the $\overline{\mathrm{DR}}$ scheme at M_{int}.

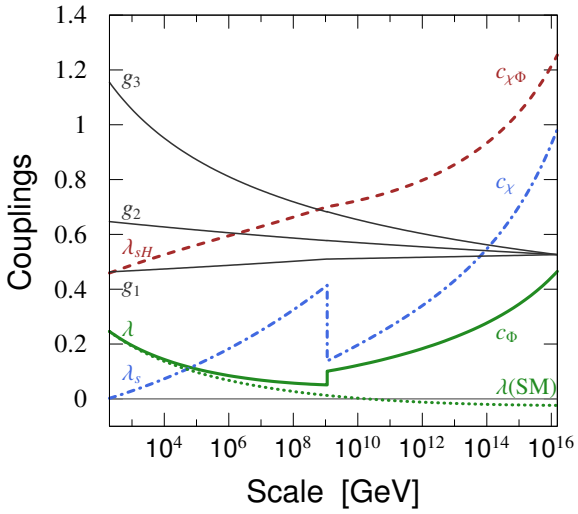

Figure 7.1: *Running of the quartic couplings of Higgs field, for selected inputs. The green solid, brown dashed, and blue dash-dotted lines show the running of* λ, λ_{sH}, *and* λ_s, *respectively, while the green dotted curve shows the running of* λ *in the SM. The gauge coupling running is also shown in thin black lines. Above the intermediate scale, the running of* c_Φ, c_χ, *and* $c_{\chi\Phi}$ *is shown using the matching conditions in* (7.5). *The free parameters are chosen as follows: At* $Q = m_t$, $\lambda_s = 0$ *and* $\lambda_{sH} = 0.46$ *(which corresponds to* $m_{\rm DM} \simeq 1.5$ *TeV); At* M_{int}, $\tilde{c}_\Phi = c'_\Delta = c_{\Phi\Delta} = c_{\chi\Delta} = c'_{\chi\Delta} = c'_{\chi\Phi} = 0$ *and* $c_\Delta = -c'_{\Phi\Delta} = -m_{\chi\Delta}/v_R = 0.05$. *The non-zero couplings are taken so that the low-energy mass spectrum we consider here is realized.*

Above the intermediate scale, it is necessary to include in addition to s, the right-handed doublet $\chi(\mathbf{1},\mathbf{1},\mathbf{2},1)$ which contains s, the Higgs triplet $\Delta(\mathbf{1},\mathbf{1},\mathbf{3},2)$ residing in the **126**, two heavy complex fields in addition to the SM Higgs doublet which all sit in a complex $\Phi(\mathbf{1},\mathbf{2},\mathbf{2},0)$, and finally the three right handed neutrinos sitting in the fermionic **16** matter representations. Above the intermediate scale, we write $\Phi = (\phi_1, \tilde{\phi}_2)$, $\tilde{\Phi} \equiv \sigma_2 \Phi^* \sigma_2$ (σ_a are the Pauli matrices), $\chi = (\chi^+, \chi^0)^T$, and

$$\Delta = \begin{pmatrix} \Delta^+/\sqrt{2} & \Delta^{++} \\ \Delta^0 & -\Delta^+/\sqrt{2} \end{pmatrix} , \tag{7.3}$$

where $\phi_i = (\phi_i^0, \phi_i^-)^T$ is an $\mathrm{SU}(2)_L$ doublet; $\tilde{\phi} \equiv i\sigma_2 \phi^*$. Then a quartic potential can be

written as

$$
\begin{aligned}
V^{(4)}_{\rm abv} = & \frac{c_\Delta}{2}\left(\mathbf{tr}(\Delta^\dagger\Delta)\right)^2 + \frac{c'_\Delta}{4}\mathbf{tr}\left(\Delta\Delta\right)\mathbf{tr}\left(\Delta^\dagger\Delta^\dagger\right) \\
& + \frac{c_\Phi}{2}\left(\mathbf{tr}(\Phi^\dagger\Phi)\right)^2 + \frac{\tilde{c}_\Phi}{4}\mathbf{tr}(\tilde{\Phi}^\dagger\Phi)\mathbf{tr}(\Phi^\dagger\tilde{\Phi}) \\
& + c_{\Phi\Delta}\mathbf{tr}(\Delta^\dagger\Delta)\mathbf{tr}(\Phi^\dagger\Phi) + \frac{c_\chi}{2}|\chi|^4 + c_{\chi\Phi}|\chi|^2\mathbf{tr}(\Phi^\dagger\Phi) \\
& + c_{\chi\Delta}|\chi|^2\mathbf{tr}(\Delta^\dagger\Delta) + c'_{\chi\Delta}\chi^\dagger[\Delta^\dagger,\Delta]\chi \\
& + c'_{\Phi\Delta}\mathbf{tr}\left(\Phi^\dagger\Phi[\Delta^\dagger,\Delta]\right) + c'_{\chi\Phi}\chi^\dagger\Phi^\dagger\Phi\chi + \dots \ . \qquad (7.4)
\end{aligned}
$$

Note that we have only included those quartic couplings which can be generated through RGE evolution, with the exception of the last two; $c'_{\Phi\Delta}$ is needed to split the masses of the two-Higgs doublet, Φ, while $c'_{\chi\Phi}$ is induced by the $c'_{\Phi\Delta}$ term via RGE effects.

The quartic terms that contain two powers of Δ, as well as the cubic coupling (see Eq. (7.6)) produce non-trivial tree-level threshold corrections at $M_{\rm int}$, after Δ acquires a vev and the heavy fields are integrated out:

$$
\begin{aligned}
\lambda &= c_\Phi - \frac{(c_{\Phi\Delta}+c'_{\Phi\Delta})^2}{c_\Delta} \ , \\
\lambda_{sH} &= c_{\chi\Phi} - \frac{(c_{\Phi\Delta}+c'_{\Phi\Delta})[m_{\chi\Delta}+(c_{\chi\Delta}-c'_{\chi\Delta})v_R]}{c_\Delta v_R} \ , \\
\lambda_s &= 3c_\chi - 3\frac{[m_{\chi\Delta}+v_R(c_{\chi\Delta}-c'_{\chi\Delta})]^2}{c_\Delta v_R^2} \ , \qquad (7.5)
\end{aligned}
$$

where $\langle\Delta\rangle = v_R T_-$ with $T_- \equiv (\sigma_1 - i\sigma_2)/2$. As is well known, these threshold effects always go in the direction of benefiting vacuum stability [86]. The evolution of the quartic couplings, c_Φ, c_χ, and $c_{\chi\Phi}$ above the intermediate scale are also shown in Fig. 7.1 using the matching conditions in (7.5). We use the one-loop RGEs for these quartic couplings. Although we do not explicitly display the running of all quartic terms above the intermediate scale, we have checked that although some run negative (notably c'_Δ), we have verified that the couplings satisfy sufficient conditions which guarantee stability of the vacuum up to the GUT scale.

The quadratic and cubic parts (which can lead to mass terms) of the potential can be written as

$$
\begin{aligned}
V^{(2,3)}_{\rm abv} = & \ m_\chi^2|\chi|^2 + m_\Phi^2\mathbf{tr}(\Phi^\dagger\Phi) + m_\Delta^2\mathbf{tr}(\Delta^\dagger\Delta) \\
& + m_{\chi\Delta}\left(\tilde{\chi}^\dagger\Delta^\dagger\chi\right) + \text{h.c.} \ , \qquad (7.6)
\end{aligned}
$$

where we take $m_{\chi\Delta}$ to be real for simplicity. The relevant matching conditions with the weak scale mass parameters are

$$\mu_s^2 = m_\chi^2 + \left(c_{\chi\Delta} - c'_{\chi\Delta}\right) v_R^2 + 2 m_{\chi\Delta} v_R \ ,$$
$$\mu^2 = m_\Phi^2 + \left(c_{\Phi\Delta} + c'_{\Phi\Delta}\right) v_R^2 \ , \tag{7.7}$$

where the low energy fields are related to the high energy fields as $\phi_1 = H$ and $\chi^0 = (s + ia)/\sqrt{2}$.

The running of λ_s receives a large contribution from λ_{sH}, $d\lambda_s/d\ln Q = 12\lambda_{sH}^2/(4\pi)^2 + \cdots$ and thus by demanding perturbativity of the couplings ($\lambda_i \lesssim 1/\beta_i$, where β_i is a relevant beta-function coefficient) up to the intermediate scale [2] , we can set an upper bound on $\lambda_{sH} \lesssim 1.3$. However, requiring perturbativity of the c_i's above the intermediate scale places a stronger bound on $\lambda_s(M_{\rm int}) \lesssim 2.4$ which requires $\lambda_{sH}(m_t) \lesssim 0.9$. Non-zero values for other couplings further push the upper limit to $\lambda_{sH}(m_t) \lesssim 0.6$ in order to avoid Landau poles up to the GUT scale. This is illustrated in Fig. 7.2, where we use β_i/c_i as an indicator of the relative size between one-loop and tree level contributions. Other choices of indicator such as c_i do not severely affect the result because c_i(GUT) rises drastically when $\lambda_{sH}(m_t) \sim 0.6$. Since λ_{sH} controls the annihilation cross section for s: $\sigma_{\rm ann} v_{\rm rel} \simeq \lambda_{sH}^2/16\pi m_{\rm DM}^2$, and the relic density is proportional to $1/\langle\sigma_{\rm ann} v_{\rm rel}\rangle$, the upper limit on λ_{sH} corresponds to an upper limit to the DM mass $m_{\rm DM} \lesssim 2$ TeV, similar to that in the minimal dark matter model [44] without an intermediate scale.

7.2 Renormalization group evolution of mass parameters

The Higgs mass parameter, μ^2, must be negative in order to break the electroweak symmetry, and in the SM, μ^2 remains negative as it is run up to high energies. The presence of the dark matter scalar however affects the running as $d\mu^2/d\ln Q = \lambda_{sH}\mu_s^2/(4\pi)^2 + \cdots$ and causes μ^2 to run positive at higher renormalization scales [8]. In other words, the dark matter candidate can induce radiative electroweak symmetry similar to the mechanism in supersymmetric models. As the running of μ depends on the combination $\lambda_{sH}\mu_s^2$ we can obtain a minimum value for μ_s (and hence $m_{\rm DM}$) which is independent of the relic

[2] we can also require that the Landau pole does not appear below $M_{\rm int}$, this only result in 6% difference from the bound obtained above.

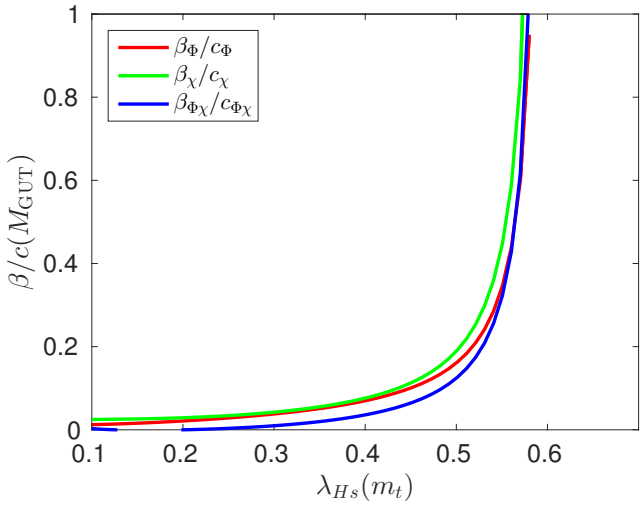

Figure 7.2: *β_i/c_i at the GUT scale as a funtion of $\lambda_{sH}(m_t)$, for the parameters correspond to Fig. 7.1.*

density constraint by maximizing λ_{sH}. In Fig. 7.3, we display the log of the mass scale M at which $\mu_s = 0$ as a function of $\mu_s(m_t)$, for $\lambda_{sH} = 0.6$. The red(yellow) horizontal line marks the intermediate scale and 1 TeV. We find that $\mu^2 > 0$ at the intermediate scale (at 1 TeV) when $\mu_s \gtrsim 360$ GeV (1150 GeV), corresponding to $m_{\rm DM} \gtrsim 380$ GeV (1160 GeV). Here, we set $\lambda_s(m_t) = 0$. Taking the limits on λ_{sH} from the perturbativity of λ_s and the limit on μ_s from the requirement of radiative electroweak symmetry breaking, we find that the dark matter mass must lie in a restricted range (when demanding symmetry breaking at 1 TeV) $m_{\rm DM} = 1.2$–2 TeV.

When one imposes the constraint from the relic density, we obtain somewhat stronger bounds on λ_{sH}. In Fig. 7.4, we show the value of $\mathrm{sgn}(\mu^2)|\mu|$ for $Q = M_{\rm int}$ and 1 TeV as a function of $\lambda_{sH}(m_t)$. Here again, we set $\lambda_s(m_t) = 0$. As one can see that when $Q = M_{\rm int}$, we have $\lambda_{sH}(m_t) > 0.2$ corresponding to $m_{\rm DM} > 670$ TeV and when $Q = 1$ TeV, we have $\lambda_{sH}(m_t) > 0.41$ corresponding to $m_{\rm DM} > 1.35$ TeV.

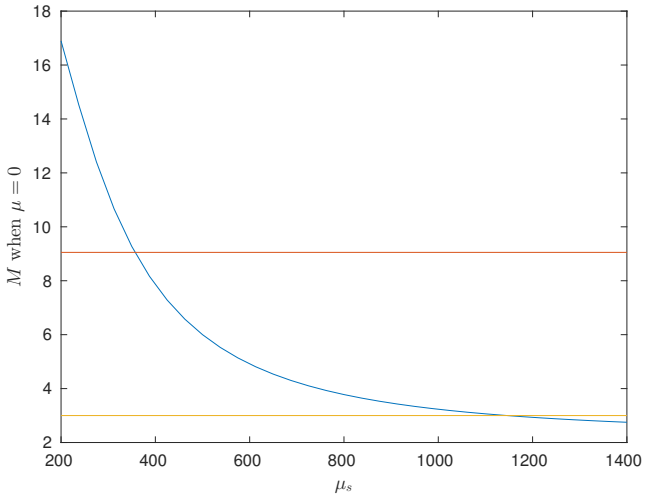

Figure 7.3: *the* log *of the mass scale* M *at which* $\mu_s = 0$ *as a function of* $\mu_s(m_t)$*, for* $\lambda_{sH} = 0.6$*. The red(yellow) horizontal line marks the intermediate scale and* 1 *TeV respectively.*

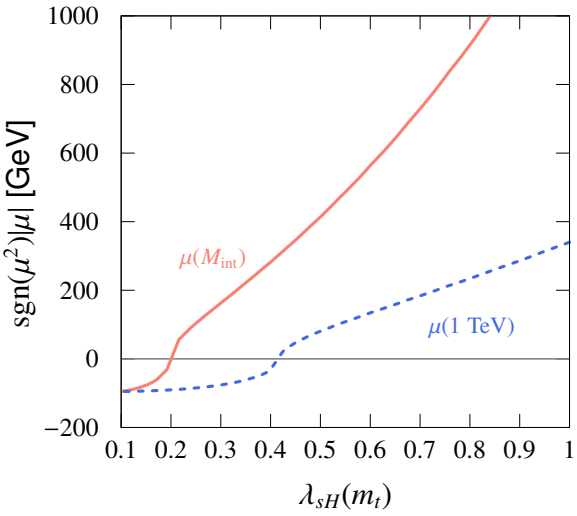

Figure 7.4: *The value of* $\mathrm{sgn}(\mu^2)|\mu|$ *for* $Q = M_{\rm int}$ *and* 1 *TeV as a function of* $\lambda_{sH}(m_t)$*.* m_s *at the weak scale is determined from the requirement for the thermal relic abundance.*

Chapter 8

Conclusion

Besides gauge coupling unification, SO(10) models contain several interesting features beyond the SM: The right-handed neutrinos are contained in the same fundamental representation as the Standard Model fermions; The seesaw mechanism that explains the smallness of the light neutrino mass can be induced by the breaking of the intermediate symmetry at a high scale; The generation of baryon-anti-baryon asymmetry in the universe can be realized by leptogenesis; Neutron oscillations and proton decay are generally predicted so that the models can be tested by corresponding experiments. The minimal SO(10) models does not contain a candidate of dark matter, and in this thesis we have combined the framework of non-supersymmetric SO(10) unification theories with several dark matter models, including NETDM, WIMP and ADM.

We have shown that the $\mathbb{Z}_2$ symmetry required for dark matter stability appears naturally as long as the Higgs that breaks SO(10) into the Standard Model gauge group is chosen appropriately. With this $\mathbb{Z}_2$ symmetry, scalar DM must have odd $B-L$, and may belong to a **16** or a **144** representation; the fermionic DM is $B-L$ even and is constained in a **10**, **45**, **54**, **120**, **126**, **210** or **210′** representation. Both the dark matter multiplet and the heavy Higgs multiplets affect the beta function of gauge coupling constants and are therefore the content of the model is strongly constrained by the requirement of gauge coupling unification and the proton decay lifetime. The number of models that survive such constrained is quite limited even if our start from a very long list of candidates, which combines different DM representations and different intermediate scale symmetry. In Chapter 4 there are only two viable models in the

NETDM scenario: one each based on $M_{\rm int} = {\rm SU}(4)_C \otimes {\rm SU}(2)_L \otimes {\rm SU}(2)_R$ and ${\rm SU}(4)_C \otimes {\rm SU}(2)_L \otimes {\rm SU}(2)_R \otimes D$ with DM contained in a $(\mathbf{1},\mathbf{1},\mathbf{3})_D \in \mathbf{45}_D$ and $(\mathbf{15},\mathbf{1},\mathbf{1})_W \in \mathbf{45}_W$ respectively.

There are more surviving models in the WIMP DM scenario considered in Chapter 5. Among the scalar WIMP candidates, the $Y = 0$ singlet and $Y = 1/2$ doublet are possible candidates for ${\rm SU}(4)_C \otimes {\rm SU}(2)_L \otimes {\rm SU}(2)_R$ and ${\rm SU}(3)_C \otimes {\rm SU}(2)_L \otimes {\rm SU}(2)_R \otimes {\rm U}(1)_{B-L}$ (with or without a left-right symmetry) intermediate gauge groups. These originate from either the **16** or **144** of SO(10). The latter group (without the left-right symmetry) is also consistent with a state originating from the **144** being a triplet under ${\rm SU}(2)_R$. The fermion candidates were even more restrictive. Models with $Y = 0$ must come from a ${\rm SU}(2)_L$ triplet (singlets are not WIMPs). In this case only one model was found using the ${\rm SU}(4)_C \otimes {\rm SU}(2)_L \otimes {\rm SU}(2)_R$ intermediate gauge group and requiring additional Higgses (already present in R_1) at the intermediate scale. Models with $Y = 1/2$ doublets were found for ${\rm SU}(4)_C \otimes {\rm SU}(2)_L \otimes {\rm U}(1)_R$ with a singlet fermion required for mixing, and ${\rm SU}(4)_C \otimes {\rm SU}(2)_L \otimes {\rm SU}(2)_R$ with a triplet fermion for mixing. In both cases, additional Higgses from R_1 are required at the intermediate scale. More possibilities can be found if the additional Higgs are taken outside R_1.

For ADM scenario in Chapter 6, the models are even more restricted, and the minimal models are all ruled out becuase the mass splitting required by direct detection bound usually lead to oscillation between dark matter and its anti-matter and wash out the asymmetry of the dark matter density generated in the early universe. This lead us to considering non-minimal models by introducing additional states that develope asymmetry by transfer from the top quark asymmetry. The mass of the DM in this model is severely constrained by depletion of symmetric density.

Finally in Chapter 7, we study the stability of the Higgs doublet scalar potentail in the $\mathtt{SA}_{3221}$ WIMP DM model. We showed that the vacuum can be made stable up to the GUT scale. Moreover, requiring radiative electroweak symmetry breaking and perturbativity up to the GUT scale constrained the DM mass in a narrow range of 1.35-2 TeV.

As discussed listed above, introducing dark matter representation to a minimal SO(10) model with intermediate scale solves several questions that are not addressed in the SM. This framework is strongly constrained by observations, especially from

proton decay detection and dark matter direct detection experiments. There are still many open questions in this framework. For example, our dark matter candidate is put in by hand and the only constraint on the choice of representation is its stability; Moreover, we rely on fine tuned parameters to split the multiplets into fields with very different energy scales. Is there any assumption that we can make to elegantly reduce such ambiguity and to set the scales for the fields? On the unification aspect, it is also interesting to see how Yukawa coupling unification can restrict the models. Some of our SO(10) models have particle content that is similar to those of a supersymmetric model, so it is tempting to see if we can construct a viable supersymmetric SO(10) model with an intermediate scale. More work needs to be done in order to understand the relation between the unification of fundamental forces and the origin of the dark matter.

References

[1] N. Nagata, K. A. Olive and J. Zheng, arXiv:1611.04693 [hep-ph]; Y. Mambrini, N. Nagata, K. A. Olive and J. Zheng, Phys. Rev. D **93**, no. 11, 111703 (2016) doi:10.1103/PhysRevD.93.111703 [arXiv:1602.05583 [hep-ph]]; N. Nagata, K. A. Olive and J. Zheng, JHEP **1510**, 193 (2015) [arXiv:1509.00809 [hep-ph]]; Y. Mambrini, N. Nagata, K. A. Olive, J. Quevillon and J. Zheng, Phys. Rev. D **91**, no. 9, 095010 (2015) [arXiv:1502.06929 [hep-ph]].

[2] H. Georgi and S. Glashow, Phys. Rev. Lett. **32**, 438 (1974)

[3] J. R. Ellis, S. Kelley and D. V. Nanopoulos, Phys. Lett. B **249** (1990) 441 and Phys. Lett. B **260** (1991) 131; U. Amaldi, W. de Boer and H. Furstenau, Phys. Lett. B **260** (1991) 447; C. Giunti, C. W. Kim and U. W. Lee, Mod. Phys. Lett. A **6** (1991) 1745; P. Langacker and M. x. Luo, Phys. Rev. D **44**, 817 (1991).

[4] G. Aad *et al.* [ATLAS and CMS Collaborations], Phys. Rev. Lett. **114**, 191803 (2015) [arXiv:1503.07589 [hep-ex]].

[5] S. Rajpoot, Phys. Rev. D **22**, 2244 (1980); M. Yasue, Prog. Theor. Phys. **65**, 708 (1981) [Erratum-ibid. **65**, 1480 (1981)]; J. M. Gipson and R. E. Marshak, Phys. Rev. D **31**, 1705 (1985); D. Chang, R. N. Mohapatra, J. Gipson, R. E. Marshak and M. K. Parida, Phys. Rev. D **31**, 1718 (1985); N. G. Deshpande, E. Keith and P. B. Pal, Phys. Rev. D **46**, 2261 (1993); N. G. Deshpande, E. Keith and P. B. Pal, Phys. Rev. D **47**, 2892 (1993) [hep-ph/9211232]; S. Bertolini, L. Di Luzio and M. Malinsky, Phys. Rev. D **81**, 035015 (2010) [arXiv:0912.1796 [hep-ph]].

[6] M. Fukugita and T. Yanagida, In *Fukugita, M. (ed.), Suzuki, A. (ed.): Physics and astrophysics of neutrinos* 1-248. and Kyoto Univ. - YITP-K-1050 (93/12,rec.Feb.94) 248 p. C;

[7] Y. Mambrini, K. A. Olive, J. Quevillon and B. Zaldivar, Phys. Rev. Lett. **110**, 241306 (2013) [arXiv:1302.4438 [hep-ph]].

[8] M. Kadastik, K. Kannike and M. Raidal, Phys. Rev. D **81**, 015002 (2010) [arXiv:0903.2475 [hep-ph]]; M. Kadastik, K. Kannike and M. Raidal, Phys. Rev. D **80**, 085020 (2009) [Erratum-ibid. D **81**, 029903 (2010)] [arXiv:0907.1894 [hep-ph]].

[9] M. Frigerio and T. Hambye, Phys. Rev. D **81**, 075002 (2010) [arXiv:0912.1545 [hep-ph]]; T. Hambye, PoS IDM **2010**, 098 (2011) [arXiv:1012.4587 [hep-ph]].

[10] V. A. Kuzmin and M. E. Shaposhnikov, Phys. Lett. B **92**, 115 (1980); T. W. B. Kibble, G. Lazarides and Q. Shafi, Phys. Rev. D **26**, 435 (1982); D. Chang, R. N. Mohapatra and M. K. Parida, Phys. Rev. Lett. **52**, 1072 (1984); D. Chang, R. N. Mohapatra and M. K. Parida, Phys. Rev. D **30**, 1052 (1984); D. Chang, R. N. Mohapatra, J. Gipson, R. E. Marshak and M. K. Parida, Phys. Rev. D **31**, 1718 (1985).

[11] F. del Aguila and L. E. Ibanez, Nucl. Phys. B **177**, 60 (1981).

[12] R. N. Mohapatra and G. Senjanovic, Phys. Rev. D **27**, 1601 (1983).

[13] J. C. Pati and A. Salam, Phys. Rev. D **10**, 275 (1974) [Erratum-ibid. D **11**, 703 (1975)].

[14] B. Bajc, A. Melfo, G. Senjanovic and F. Vissani, Phys. Rev. D **73**, 055001 (2006) [hep-ph/0510139].

[15] T. Fukuyama, A. Ilakovac, T. Kikuchi, S. Meljanac and N. Okada, Eur. Phys. J. C **42**, 191 (2005) [hep-ph/0401213].

[16] W. Siegel, Phys. Lett. B **84**, 193 (1979).

[17] S. Weinberg, Phys. Lett. B **91**, 51 (1980); L. J. Hall, Nucl. Phys. B **178** (1981) 75.

[18] S. A. R. Ellis and J. D. Wells, arXiv:1502.01362 [hep-ph].

[19] H. Goldberg, Phys. Rev. Lett. **50** (1983) 1419; J. Ellis, J.S. Hagelin, D.V. Nanopoulos, K.A. Olive and M. Srednicki, Nucl. Phys. **B238** (1984) 453.

[20] T. Appelquist, H. C. Cheng and B. A. Dobrescu, Phys. Rev. D **64**, 035002 (2001) [hep-ph/0012100]; H. C. Cheng, K. T. Matchev and M. Schmaltz, Phys. Rev. D **66**, 036005 (2002) [hep-ph/0204342]; G. Servant and T. M. P. Tait, Nucl. Phys. B **650**, 391 (2003) [hep-ph/0206071]; H. C. Cheng, J. L. Feng and K. T. Matchev, Phys. Rev. Lett. **89**, 211301 (2002) [hep-ph/0207125]; M. Kakizaki, S. Matsumoto and M. Senami, Phys. Rev. D **74**, 023504 (2006) [hep-ph/0605280]; G. Belanger, M. Kakizaki and A. Pukhov, JCAP **1102**, 009 (2011) [arXiv:1012.2577 [hep-ph]].

[21] N. Arkani-Hamed, A. G. Cohen and H. Georgi, Phys. Lett. B **513**, 232 (2001) [hep-ph/0105239]; N. Arkani-Hamed, A. G. Cohen, E. Katz, A. E. Nelson, T. Gregoire and J. G. Wacker, JHEP **0208**, 021 (2002) [hep-ph/0206020]; N. Arkani-Hamed, A. G. Cohen, E. Katz and A. E. Nelson, JHEP **0207**, 034 (2002) [hep-ph/0206021]; H. C. Cheng and I. Low, JHEP **0408**, 061 (2004) [hep-ph/0405243]; I. Low, JHEP **0410**, 067 (2004) [hep-ph/0409025]; J. Hubisz and P. Meade, Phys. Rev. D **71**, 035016 (2005) [hep-ph/0411264]; A. Birkedal, A. Noble, M. Perelstein and A. Spray, Phys. Rev. D **74**, 035002 (2006) [hep-ph/0603077].

[22] T. W. B. Kibble, G. Lazarides and Q. Shafi, Phys. Lett. B **113**, 237 (1982).

[23] R. N. Mohapatra, Phys. Rev. D **34**, 3457 (1986).

[24] L. M. Krauss and F. Wilczek, Phys. Rev. Lett. **62**, 1221 (1989).

[25] L. E. Ibanez and G. G. Ross, Phys. Lett. B **260**, 291 (1991); L. E. Ibanez and G. G. Ross, Nucl. Phys. B **368**, 3 (1992).

[26] S. P. Martin, Phys. Rev. D **46**, 2769 (1992) [hep-ph/9207218].

[27] M. De Montigny and M. Masip, Phys. Rev. D **49**, 3734 (1994) [hep-ph/9309312].

[28] R. Slansky, Phys. Rept. **79**, 1 (1981).

[29] Y. Mambrini, N. Nagata, K. A. Olive, J. Quevillon and J. Zheng, Phys. Rev. D **91**, 095010 (2015) [arXiv:1502.06929 [hep-ph]].

[30] P. F. Smith and J. R. J. Bennett, Nucl. Phys. B **149**, 525 (1979); P. F. Smith, J. R. J. Bennett, G. J. Homer, J. D. Lewin, H. E. Walford and W. A. Smith, Nucl. Phys. B **206**, 333 (1982); T. K. Hemmick, D. Elmore, T. Gentile, P. W. Kubik, S. L. Olsen, D. Ciampa, D. Nitz and H. Kagan *et al.*, Phys. Rev. D **41**, 2074 (1990); P. Verkerk, G. Grynberg, B. Pichard, M. Spiro, S. Zylberajch, M. E. Goldberg and P. Fayet, Phys. Rev. Lett. **68**, 1116 (1992); T. Yamagata, Y. Takamori and H. Utsunomiya, Phys. Rev. D **47**, 1231 (1993).

[31] M. Cirelli, N. Fornengo and A. Strumia, Nucl. Phys. B **753**, 178 (2006) [hep-ph/0512090]; M. Cirelli, A. Strumia and M. Tamburini, Nucl. Phys. B **787**, 152 (2007) [arXiv:0706.4071 [hep-ph]]; M. Cirelli and A. Strumia, New J. Phys. **11**, 105005 (2009) [arXiv:0903.3381 [hep-ph]].

[32] R. Essig, Phys. Rev. D **78**, 015004 (2008) [arXiv:0710.1668 [hep-ph]].

[33] T. Hambye, F.-S. Ling, L. Lopez Honorez and J. Rocher, JHEP **0907**, 090 (2009) [Erratum-ibid. **1005**, 066 (2010)].

[34] J. Hisano, D. Kobayashi, N. Mori and E. Senaha, Phys. Lett. B **742**, 80 (2015) [arXiv:1410.3569 [hep-ph]].

[35] J. Hisano, S. Matsumoto, M. Nagai, O. Saito and M. Senami, Phys. Lett. B **646**, 34 (2007) [hep-ph/0610249].

[36] N. Nagata and S. Shirai, JHEP **1501**, 029 (2015) [arXiv:1410.4549 [hep-ph]].

[37] N. Nagata and S. Shirai, Phys. Rev. D **91**, 055035 (2015) [arXiv:1411.0752 [hep-ph]].

[38] S. M. Boucenna, M. B. Krauss and E. Nardi, Phys. Lett. B **748**, 191 (2015) [arXiv:1503.01119 [hep-ph]].

[39] K. Harigaya, K. Ichikawa, A. Kundu, S. Matsumoto and S. Shirai, arXiv:1504.03402 [hep-ph].

[40] J. Heeck and S. Patra, arXiv:1507.01584 [hep-ph].

[41] M. Cirelli, T. Hambye, P. Panci, F. Sala and M. Taoso, arXiv:1507.05519 [hep-ph]; C. Garcia-Cely, A. Ibarra, A. S. Lamperstorfer and M. H. G. Tytgat, arXiv:1507.05536 [hep-ph].

[42] C. W. Chiang and E. Senaha, arXiv:1508.02891 [hep-ph].

[43] B. Feldstein, M. Ibe and T. T. Yanagida, Phys. Rev. Lett. **112**, 101301 (2014) [arXiv:1310.7495 [hep-ph]].

[44] V. Silveira and A. Zee, Phys. Lett. B **161**, 136 (1985); J. McDonald, Phys. Rev. D **50**, 3637 (1994) [hep-ph/0702143]; C. P. Burgess, M. Pospelov and T. ter Veldhuis, Nucl. Phys. B **619**, 709 (2001) [hep-ph/0011335]; H. Davoudiasl, R. Kitano, T. Li and H. Murayama, Phys. Lett. B **609**, 117 (2005) [hep-ph/0405097].

[45] P. A. R. Ade *et al.* [Planck Collaboration], arXiv:1502.01589 [astro-ph.CO].

[46] M. Farina, D. Pappadopulo and A. Strumia, JHEP **1308**, 022 (2013) [arXiv:1303.7244 [hep-ph]].

[47] J. Hisano, S. Matsumoto and M. M. Nojiri, Phys. Rev. Lett. **92**, 031303 (2004) [hep-ph/0307216]; J. Hisano, S. Matsumoto, M. M. Nojiri and O. Saito, Phys. Rev. D **71**, 063528 (2005) [hep-ph/0412403].

[48] A. Arhrib, Y. L. S. Tsai, Q. Yuan and T. C. Yuan, JCAP **1406**, 030 (2014) [arXiv:1310.0358 [hep-ph]]; A. Ilnicka, M. Krawczyk and T. Robens, arXiv:1508.01671 [hep-ph].

[49] T. Abe and R. Sato, JHEP **1503**, 109 (2015) [arXiv:1501.04161 [hep-ph]].

[50] G. Lazarides, Q. Shafi and C. Wetterich, Nucl. Phys. B **181**, 287 (1981); K. S. Babu and R. N. Mohapatra, Phys. Rev. Lett. **70**, 2845 (1993) [hep-ph/9209215]; K. Matsuda, Y. Koide and T. Fukuyama, Phys. Rev. D **64**, 053015 (2001) [hep-ph/0010026]; T. Fukuyama, K. Ichikawa and Y. Mimura, arXiv:1508.07078 [hep-ph].

[51] V. Khachatryan *et al.* [CMS Collaboration], JHEP **1504**, 025 (2015) [arXiv:1412.6302 [hep-ex]]; G. Aad *et al.* [ATLAS Collaboration], Phys. Rev. D **90**, no. 5, 052005 (2014) [arXiv:1405.4123 [hep-ex]].

[52] G. Aad *et al.* [ATLAS Collaboration], arXiv:1508.04735 [hep-ex]; CMS Collaboration [CMS Collaboration], CMS-PAS-EXO-12-041; [CMS Collaboration], CMS-PAS-EXO-12-042.

[53] T. Fukuyama, A. Ilakovac, T. Kikuchi, S. Meljanac and N. Okada, J. Math. Phys. **46**, 033505 (2005) [hep-ph/0405300].

[54] P. Minkowski, Phys. Lett. B **67**, 421 (1977); T. Yanagida, Conf. Proc. C **7902131**, 95 (1979); M. Gell-Mann, P. Ramond and R. Slansky, Conf. Proc. C **790927**, 315 (1979) [arXiv:1306.4669 [hep-th]]; S. L. Glashow, NATO Sci. Ser. B **59**, 687 (1980); R. N. Mohapatra and G. Senjanovic, Phys. Rev. Lett. **44**, 912 (1980).

[55] R. N. Mohapatra and G. Senjanovic, Phys. Rev. D **23**, 165 (1981).

[56] N. Sakai and T. Yanagida, Nucl. Phys. B **197**, 533 (1982); S. Weinberg, Phys. Rev. D **26**, 287 (1982).

[57] M. Shiozawa, talk presented at TAUP 2013, September 8–13, Asilomar, CA, USA.

[58] K. S. Babu, E. Kearns, U. Al-Binni, S. Banerjee, D. V. Baxter, Z. Berezhiani, M. Bergevin and S. Bhattacharya *et al.*, arXiv:1311.5285 [hep-ph].

[59] K. Abe, T. Abe, H. Aihara, Y. Fukuda, Y. Hayato, K. Huang, A. K. Ichikawa and M. Ikeda *et al.*, arXiv:1109.3262 [hep-ex].

[60] M. Fukugita and T. Yanagida, Phys. Lett. B **174**, 45 (1986).

[61] M. A. Luty, Phys. Rev. D **45**, 455 (1992).

[62] N. S. Manton, Phys. Rev. D **28**, 2019 (1983); F. R. Klinkhamer and N. S. Manton, Phys. Rev. D **30**, 2212 (1984); R. F. Dashen, B. Hasslacher and A. Neveu, Phys. Rev. D **10**, 4130 (1974).

[63] V. A. Kuzmin, V. A. Rubakov and M. E. Shaposhnikov, Phys. Lett. B **155**, 36 (1985).

[64] L. Covi, E. Roulet and F. Vissani, Phys. Lett. B **384**, 169 (1996) [hep-ph/9605319].

[65] A.D. Dolgov, and A.D. Linde, *Phys. Lett.* **B116** (1982) 329; D.V. Nanopoulos, K.A. Olive, and M. Srednicki, *Phys. Lett.* **B127** (1983) 30.

[66] M. Ibe, S. Matsumoto and T. T. Yanagida, Phys. Lett. B **708**, 112 (2012) [arXiv:1110.5452 [hep-ph]].

[67] J.A. Harvey and M.S. Turner, *Phys. Rev.* **D42** (1990) 3344.

[68] H. K. Dreiner and G. G. Ross, Nucl. Phys. B **410**, 188 (1993) [hep-ph/9207221].

[69] M. D'Onofrio, K. Rummukainen and A. Tranberg, Phys. Rev. Lett. **113**, no. 14, 141602 (2014) [arXiv:1404.3565 [hep-ph]].

[70] M. Fukugita and T. Yanagida, *Phys. Rev.* **D42** (1990) 1285.

[71] B. A. Campbell, S. Davidson, J. R. Ellis and K. A. Olive, Phys. Lett. B **256**, 484 (1991); B. A. Campbell, S. Davidson, J. R. Ellis and K. A. Olive, Astropart. Phys. **1**, 77 (1992) W. Fischler, G.F. Giudice, R.G. Leigh and S. Paban, *Phys. Lett.* **B258** (1991) 45; L.E. Ibanez and F. Quevedo, *Phys. Lett.* **B283** (1992) 261.

[72] B. A. Campbell, S. Davidson and K. A. Olive, Nucl. Phys. B **399**, 111 (1993) [hep-ph/9302223].

[73] K. Blum, A. Efrati, Y. Grossman, Y. Nir and A. Riotto, Phys. Rev. Lett. **109**, 051302 (2012) [arXiv:1201.2699 [hep-ph]].

[74] G. Servant and S. Tulin, Phys. Rev. Lett. **111**, no. 15, 151601 (2013) [arXiv:1304.3464 [hep-ph]].

[75] S. M. Boucenna, M. B. Krauss and E. Nardi, Phys. Lett. B **748**, 191 (2015) [arXiv:1503.01119 [hep-ph]].

[76] M. Dhen and T. Hambye, Phys. Rev. D **92**, no. 7, 075013 (2015) [arXiv:1503.03444 [hep-ph]].

[77] G. Aad *et al.* [ATLAS and CMS Collaborations], JHEP **1608**, 045 (2016) [arXiv:1606.02266 [hep-ex]].

[78] T. Falk, A. Ferstl and K. A. Olive, Phys. Rev. D **59**, 055009 (1999) [Phys. Rev. D **60**, 119904 (1999)] [hep-ph/9806413]; J. R. Ellis, A. Ferstl and K. A. Olive, Phys. Lett. B **481**, 304 (2000) [hep-ph/0001005]; J. R. Ellis, K. A. Olive, Y. Santoso and V. C. Spanos, Phys. Rev. D **71**, 095007 (2005) [hep-ph/0502001].

[79] V. Mandic, A. Pierce, P. Gondolo and H. Murayama, hep-ph/0008022; J. R. Ellis, J. L. Feng, A. Ferstl, K. T. Matchev and K. A. Olive, Eur. Phys. J. C **24**, 311 (2002) [astro-ph/0110225].

[80] C. Cheung, L. J. Hall, D. Pinner and J. T. Ruderman, JHEP **1305**, 100 (2013) [arXiv:1211.4873 [hep-ph]]; P. Huang and C.E. M. Wagner, Phys. Rev. D **90**, no. 1, 015018 (2014) [arXiv:1404.0392 [hep-ph]]; A. Crivellin, M. Hoferichter, M. Procura and L. C. Tunstall, JHEP **1507** (2015) 129 [arXiv:1503.03478 [hep-ph]].

[81] S. Banerjee, S. Matsumoto, K. Mukaida and Y. L. S. Tsai, JHEP **1611**, 070 (2016) [arXiv:1603.07387 [hep-ph]].

[82] R. H. Cyburt, J. Ellis, B. D. Fields, F. Luo, K. A. Olive and V. C. Spanos, JCAP **0910**, 021 (2009) [arXiv:0907.5003 [astro-ph.CO]].

[83] The ATLAS collaboration [ATLAS Collaboration], ATLAS-CONF-2016-050.

[84] CMS Collaboration [CMS Collaboration], CMS-PAS-SUS-16-028.

[85] D. Buttazzo, G. Degrassi, P. P. Giardino, G. F. Giudice, F. Sala, A. Salvio and A. Strumia, JHEP **1312**, 089 (2013) [arXiv:1307.3536 [hep-ph]]; G. Degrassi, S. Di Vita, J. Elias-Miro, J. R. Espinosa, G. F. Giudice, G. Isidori and A. Strumia, JHEP **1208**, 098 (2012) [arXiv:1205.6497 [hep-ph]].

[86] J. Elias-Miro, J. R. Espinosa, G. F. Giudice, H. M. Lee and A. Strumia, JHEP **1206** (2012) 031 [arXiv:1203.0237 [hep-ph]]; J. Elias-Miro, J. R. Espinosa, G. F. Giudice, G. Isidori, A. Riotto and A. Strumia, Phys. Lett. B **709** (2012) 222 [arXiv:1112.3022 [hep-ph]].

[87] K. A. Olive *et al.* [Particle Data Group Collaboration], Chin. Phys. C **38**, 090001 (2014).

[88] [ATLAS and CDF and CMS and D0 Collaborations], arXiv:1403.4427 [hep-ex].

[89] [CMS Collaboration], CMS-PAS-HIG-13-001; [ATLAS Collaboration], ATLAS-CONF-2013-012, ATLAS-COM-CONF-2013-015; G. Aad *et al.* [ATLAS Collaboration], Phys. Lett. B **726**, 88 (2013) [Erratum-ibid. B **734**, 406 (2014)] [arXiv:1307.1427 [hep-ex]]; P. P. Giardino, K. Kannike, I. Masina, M. Raidal and A. Strumia, JHEP **1405**, 046 (2014) [arXiv:1303.3570 [hep-ph]].

[90] Y. Yamada, Phys. Lett. B **316**, 109 (1993) [hep-ph/9307217].

[91] M. E. Machacek and M. T. Vaughn, Nucl. Phys. B **222**, 83 (1983).

[92] F. Lyonnet, I. Schienbein, F. Staub and A. Wingerter, Comput. Phys. Commun. **185** (2014) 1130 [arXiv:1309.7030 [hep-ph]].

[93] M. Machacek, Nucl. Phys. B **159**, 37 (1979).

[94] S. Weinberg, Phys. Rev. Lett. **43**, 1566 (1979).

[95] F. Wilczek and A. Zee, Phys. Rev. Lett. **43**, 1571 (1979).

[96] L. F. Abbott and M. B. Wise, Phys. Rev. D **22**, 2208 (1980).

[97] C. Munoz, Phys. Lett. B **177**, 55 (1986).

[98] W. E. Caswell, J. Milutinovic and G. Senjanovic, Phys. Rev. D **26**, 161 (1982).

[99] P. Nath and R. M. Syed, Nucl. Phys. B **618**, 138 (2001) [hep-th/0109116];

[100] T. Nihei and J. Arafune, Prog. Theor. Phys. **93**, 665 (1995) [hep-ph/9412325].

[101] Y. Aoki, E. Shintani and A. Soni, Phys. Rev. D **89**, 014505 (2014) [arXiv:1304.7424 [hep-lat]].

[102] J. M. Cline, K. Kainulainen, P. Scott and C. Weniger, Phys. Rev. D **88**, 055025 (2013) Erratum: [Phys. Rev. D **92**, no. 3, 039906 (2015)] doi:10.1103/PhysRevD.92.039906, 10.1103/PhysRevD.88.055025 [arXiv:1306.4710 [hep-ph]].

[103] J. Hisano, K. Ishiwata and N. Nagata, JHEP **1506**, 097 (2015) [arXiv:1504.00915 [hep-ph]].

Appendix A

Input parameters

The values for the input parameters we have used in this paper are summarized in Table A.1. They are taken from Ref. [87] except for the top-quark pole mass and the Higgs mass, for which we use the values given in Refs. [88] and [89], respectively. In this table, the gauge coupling constants are defined in the $\overline{\rm MS}$ scheme, and thus we convert them to the $\overline{\rm DR}$ scheme at the electroweak scale using the one-loop relation [90]:

$$g_a(m_Z)_{\overline{\rm DR}} = g_a(m_Z)_{\overline{\rm MS}}\left(1 + \frac{C(G_a)\alpha_a(m_Z)_{\overline{\rm MS}}}{24\pi}\right) , \tag{A.1}$$

where $C(G_a)$ the quadratic Casimir invariant. For the mass of top quark, we convert the pole mass to its $\overline{\rm MS}$ mass by using [87]

$$m_t^{\overline{\rm MS}}(m_t^{\overline{\rm MS}}) = m_t\left(1 - \frac{4\alpha_s(m_t^{\overline{\rm MS}})}{3\pi}\right) , \tag{A.2}$$

from which we obtain the $\overline{\rm MS}$ top Yukawa coupling. The $\overline{\rm DR}$ Yukawa coupling is then given by

$$y_t^{\overline{\rm DR}} = y_t^{\overline{\rm MS}}\left[1 + \frac{\alpha_1}{480\pi} + \frac{3\alpha_2}{32\pi} - \frac{\alpha_3}{3\pi}\right] . \tag{A.3}$$

Table A.1: *Input parameters [87–89].*

Strong coupling constant	$\alpha_s(m_Z)$	0.1185(6)
QED coupling constant	$\alpha(m_Z)$	1/127.944(14)
Fermi coupling constant	G_F	$1.1663787(6) \times 10^{-5}$ GeV^{-2}
Weak-mixing angle	$\sin^2\theta_W(m_Z)$	0.23126(5)
Z-boson mass	m_Z	91.1876(21) GeV
top pole mass	m_t	173.34(82) GeV
Higgs mass	m_h	125.15(24) GeV

Appendix B

Renormalization group equations

In this section, we summarize the RGEs and the matching conditions used in text. The two-loop RGEs [91] of the gauge coupling constants g_a are written as

$$\mu \frac{dg_a}{d\mu} = \frac{b_a^{(1)}}{16\pi^2} g_a^3 + \frac{g_a^3}{(16\pi^2)^2} \left[\sum_{b=1}^{3} b_{ab}^{(2)} g_b^2 - c_a y_t^2 \right] . \tag{B.1}$$

Below, we will give the coefficients in each theory discussed in this paper. For the contribution of Yukawa couplings, we include them only in the SM running, as unknown Yukawa couplings appear above the intermediate scale. Their effects should be taken into account as theoretical uncertainties. All of the 1-loop RGEs have been checked with the code PyR@TE [92] and more importantly the 2-loop RGEs have been computed with this code.

Appendix C

Standard Model

In the SM, we have

$$b_a^{(1)} = \begin{pmatrix} 41/10 \\ -19/6 \\ -7 \end{pmatrix}, \quad b_{ab}^{(2)} = \begin{pmatrix} 199/50 & 27/10 & 44/5 \\ 9/10 & 35/6 & 12 \\ 11/10 & 9/2 & -26 \end{pmatrix}, \quad c_a = \begin{pmatrix} 17/10 \\ 3/2 \\ 2 \end{pmatrix}. \tag{C.1}$$

Here, $a = 1, 2, 3$ correspond to U(1), $\mathrm{SU}(2)_L$, and $\mathrm{SU}(3)_C$, respectively, with the U(1) gauge coupling constant normalized as $g_1 \equiv \sqrt{5/3}g'$. Since the top Yukawa coupling contributes to the running of the gauge couplings at two-loop level, it is sufficient to consider the one-loop RGE for the top Yukawa coupling. Furthermore, we can safely neglect the contribution of the other Yukawa couplings. Thus, the relevant RGE is

$$\mu \frac{d}{d\mu} y_t = \frac{1}{16\pi^2} y_t \left[\frac{9}{2} y_t^2 - \frac{17}{20} g_1^2 - \frac{9}{4} g_2^2 - 8 g_3^2 \right]. \tag{C.2}$$

C.1 $\mathbf{SU}(4)_C \otimes \mathbf{SU}(2)_L \otimes \mathbf{SU}(2)_R$

As discussed in Sec. 2.2, above the intermediate mass scale, the theory contains the SM fermions, the gauge bosons, the $(\mathbf{10}, \mathbf{1}, \mathbf{3})_C$ field, and the $(\mathbf{1}, \mathbf{2}, \overline{\mathbf{2}})_C$ Higgs field. The beta-function coefficients in this case are given by

$$b_a^{(1)} = \begin{pmatrix} -3 \\ 11/3 \\ -23/3 \end{pmatrix}, \qquad b_{ab}^{(2)} = \begin{pmatrix} 8 & 3 & 45/2 \\ 3 & 584/3 & 765/2 \\ 9/2 & 153/2 & 643/6 \end{pmatrix}, \tag{C.3}$$

where $a = 2L, 2R, 4$ correspond to $\mathrm{SU}(2)_L$, $\mathrm{SU}(2)_R$, and $\mathrm{SU}(4)_C$, respectively. The matching conditions at the intermediate mass scale are

$$\begin{aligned} \frac{1}{g_1^2(M_{\rm int})} &= \frac{3}{5}\frac{1}{g_{2R}^2(M_{\rm int})} + \frac{2}{5}\frac{1}{g_4^2(M_{\rm int})} \ , \\ g_2(M_{\rm int}) &= g_{2L}(M_{\rm int}) \ , \\ g_3(M_{\rm int}) &= g_4(M_{\rm int}) \ . \end{aligned} \tag{C.4}$$

C.2 $\mathbf{SU}(4)_C \otimes \mathbf{SU}(2)_L \otimes \mathbf{SU}(2)_R \otimes D$

In this case, the $(\overline{\mathbf{10}}, \mathbf{3}, \mathbf{1})_C$ field is added to the previous theory. The beta-function coefficients then become

$$b_a^{(1)} = \begin{pmatrix} 11/3 \\ 11/3 \\ -14/3 \end{pmatrix}, \qquad b_{ab}^{(2)} = \begin{pmatrix} 584/3 & 3 & 765/2 \\ 3 & 584/3 & 765/2 \\ 153/2 & 153/2 & 1759/6 \end{pmatrix} \ , \tag{C.5}$$

where $a = 2L, 2R, 4$ correspond to $\mathrm{SU}(2)_L$, $\mathrm{SU}(2)_R$, and $\mathrm{SU}(4)_C$, respectively.

C.3 $\mathbf{SU}(4)_C \otimes \mathbf{SU}(2)_L \otimes \mathbf{U}(1)_R$

This theory contains the SM fermions, the gauge bosons, the $(\mathbf{10}, \mathbf{1}, 1)_C$ field, and the $(\mathbf{1}, \mathbf{2}, \frac{1}{2})$ Higgs field. The beta-function coefficients in this case are given by

$$b_a^{(1)} = \begin{pmatrix} -19/6 \\ 15/2 \\ -29/3 \end{pmatrix}, \qquad b_{ab}^{(2)} = \begin{pmatrix} 35/6 & 1/2 & 45/2 \\ 3/2 & 87/2 & 405/2 \\ 9/2 & 27/2 & -101/6 \end{pmatrix} \ , \tag{C.6}$$

where $a = 2L, 1R, 4$ correspond to $\mathrm{SU}(2)_L$, $\mathrm{U}(1)_R$, and $\mathrm{SU}(4)_C$, respectively. The matching conditions at the intermediate mass scale are

$$\begin{aligned} \frac{1}{g_1^2(M_{\rm int})} &= \frac{3}{5}\frac{1}{g_{1R}^2(M_{\rm int})} + \frac{2}{5}\frac{1}{g_4^2(M_{\rm int})} \ , \\ g_2(M_{\rm int}) &= g_{2L}(M_{\rm int}) \ , \\ g_3(M_{\rm int}) &= g_4(M_{\rm int}) \ . \end{aligned} \tag{C.7}$$

C.4 $\mathbf{SU}(3)_C \otimes \mathbf{SU}(2)_L \otimes \mathbf{SU}(2)_R \otimes \mathbf{U}(1)_{B-L}$

This theory contains the SM fermions, the gauge bosons, the $(\mathbf{1},\mathbf{1},\mathbf{3},-2)_C$ field, and the $(\mathbf{1},\mathbf{2},\mathbf{2},0)$ Higgs field. The beta-function coefficients in this case are given by

$$b_a^{(1)} = \begin{pmatrix} -3 \\ -7/3 \\ 11/2 \\ -7 \end{pmatrix}, \qquad b_{ab}^{(2)} = \begin{pmatrix} 8 & 3 & 3/2 & 12 \\ 3 & 80/3 & 27/2 & 12 \\ 9/2 & 81/2 & 61/2 & 4 \\ 9/2 & 9/2 & 1/2 & -26 \end{pmatrix}, \tag{C.8}$$

where $a = 2L, 2R, BL, 3$ correspond to $\mathrm{SU}(2)_L$, $\mathrm{SU}(2)_R$, $\mathrm{U}(1)_{B-L}$ and $\mathrm{SU}(3)_C$, respectively. The $\mathrm{U}(1)_{B-L}$ charge is normalized such that it satisfies the normalization condition of the SO(10) generators: $T_{B-L} = \sqrt{3/8}(B-L)$. The matching conditions at the intermediate mass scale are

$$\begin{aligned} \frac{1}{g_1^2(M_{\rm int})} &= \frac{3}{5}\frac{1}{g_{2R}^2(M_{\rm int})} + \frac{2}{5}\frac{1}{g_{BL}^2(M_{\rm int})} \ , \\ g_2(M_{\rm int}) &= g_{2L}(M_{\rm int}) \ , \\ g_3(M_{\rm int}) &= g_3(M_{\rm int}) \ . \end{aligned} \tag{C.9}$$

C.5 $\mathbf{SU}(3)_C \otimes \mathbf{SU}(2)_L \otimes \mathbf{SU}(2)_R \otimes \mathbf{U}(1)_{B-L} \otimes D$

For this left-right symmetric theory, the $(\mathbf{1},\mathbf{3},\mathbf{1},2)_C$ field is added to the previous case. The beta-function coefficients are then modified to

$$b_a^{(1)} = \begin{pmatrix} -7/3 \\ -7/3 \\ 7 \\ -7 \end{pmatrix}, \qquad b_{ab}^{(2)} = \begin{pmatrix} 80/3 & 3 & 27/2 & 12 \\ 3 & 80/3 & 27/2 & 12 \\ 81/2 & 81/2 & 115/2 & 4 \\ 9/2 & 9/2 & 1/2 & -26 \end{pmatrix}, \tag{C.10}$$

where $a = 2L, 2R, BL, 3$ correspond to $\mathrm{SU}(2)_L$, $\mathrm{SU}(2)_R$, $\mathrm{U}(1)_{B-L}$ and $\mathrm{SU}(3)_C$, respectively.

C.6 $\mathbf{SU}(3)_C \otimes \mathbf{SU}(2)_L \otimes \mathbf{U}(1)_R \otimes \mathbf{U}(1)_{B-L}$

This theory contains the SM fermions, the gauge bosons, the $(\mathbf{1},\mathbf{1},\mathbf{1},-2)_C$ field, and the $(\mathbf{1},\mathbf{2},1/2,0)$ Higgs field. The beta-function coefficients in this case are given by

$$b_a^{(1)} = \begin{pmatrix} -19/6 \\ 9/2 \\ 9/2 \\ -7 \end{pmatrix}, \qquad b_{ab}^{(2)} = \begin{pmatrix} 35/6 & 1/2 & 3/2 & 12 \\ 3/2 & 15/2 & 15/2 & 12 \\ 9/2 & 15/2 & 25/2 & 4 \\ 9/2 & 3/2 & 1/2 & -26 \end{pmatrix}, \tag{C.11}$$

where $a = 2L, 1R, BL, 3$ correspond to $\mathrm{SU}(2)_L$, $\mathrm{U}(1)_R$, $\mathrm{U}(1)_{B-L}$ and $\mathrm{SU}(3)_C$, respectively. The matching conditions at the intermediate mass scale are

$$\begin{aligned} \frac{1}{g_1^2(M_{\rm int})} &= \frac{3}{5}\frac{1}{g_{1R}^2(M_{\rm int})} + \frac{2}{5}\frac{1}{g_{BL}^2(M_{\rm int})} \ , \\ g_2(M_{\rm int}) &= g_{2L}(M_{\rm int}) \ , \\ g_3(M_{\rm int}) &= g_3(M_{\rm int}) \ . \end{aligned} \tag{C.12}$$

C.7 Model I

For DM model I, a $(\mathbf{1},\mathbf{1},\mathbf{3})_D$ Dirac fermion and a $(\mathbf{1},\mathbf{1},\mathbf{3})_R$ real scalar field are added to the theory described in Appendix C.1. The beta-function coefficients are then computed as

$$b_a^{(1)} = \begin{pmatrix} -3 \\ 20/3 \\ -23/3 \end{pmatrix}, \qquad b_{ab}^{(2)} = \begin{pmatrix} 8 & 3 & 45/2 \\ 3 & 740/3 & 765/2 \\ 9/2 & 153/2 & 643/6 \end{pmatrix}, \tag{C.13}$$

where $a = 2L, 2R, 4$ correspond to $\mathrm{SU}(2)_L$, $\mathrm{SU}(2)_R$, and $\mathrm{SU}(4)_C$, respectively.

C.8 Model II

For DM model II, a $(\mathbf{15},\mathbf{1},\mathbf{1})_W$ Weyl fermion and a $(\mathbf{15},\mathbf{1},\mathbf{1})_R$ real scalar field are added to the theory described in Appendix C.2. The beta-function coefficients are then

computed as

$$b_a^{(1)} = \begin{pmatrix} 11/3 \\ 11/3 \\ -4/3 \end{pmatrix}, \qquad b_{ab}^{(2)} = \begin{pmatrix} 584/3 & 3 & 765/2 \\ 3 & 584/3 & 765/2 \\ 153/2 & 153/2 & 2495/6 \end{pmatrix}, \tag{C.14}$$

where $a = 2L, 2R, 4$ correspond to $\mathrm{SU}(2)_L$, $\mathrm{SU}(2)_R$, and $\mathrm{SU}(4)_C$, respectively.

Appendix D

One-loop formulae for gauge coupling unification

At the one-loop level, the gauge coupling RGEs are easily solved analytically. By using the solutions, we can obtain analytic expressions for $M_{\rm int}$, $M_{\rm GUT}$, and $\alpha_{\rm GUT}$ as follows:

$$M_{\rm int} = m_Z \exp\left[\frac{2\pi(\tilde{\boldsymbol{b}} \times \boldsymbol{n}) \cdot \boldsymbol{\alpha_{-1}}}{(\tilde{\boldsymbol{b}} \times \boldsymbol{n}) \cdot \boldsymbol{b}}\right] , \tag{D.1}$$

$$M_{\rm GUT} = m_Z \exp\left[\frac{2\pi(\Delta\boldsymbol{b} \times \boldsymbol{n}) \cdot \boldsymbol{\alpha_{-1}}}{(\tilde{\boldsymbol{b}} \times \boldsymbol{n}) \cdot \boldsymbol{b}}\right] , \tag{D.2}$$

$$\alpha_{\rm GUT}^{-1} = \frac{(\tilde{\boldsymbol{b}} \times \boldsymbol{\alpha_{-1}}) \cdot \boldsymbol{b}}{(\tilde{\boldsymbol{b}} \times \boldsymbol{n}) \cdot \boldsymbol{b}} , \tag{D.3}$$

with

$$\boldsymbol{\alpha_{-1}} \equiv \begin{pmatrix} \alpha_1^{-1}(m_Z) \\ \alpha_2^{-1}(m_Z) \\ \alpha_3^{-1}(m_Z) \end{pmatrix} , \qquad \boldsymbol{b} \equiv \begin{pmatrix} b_1 \\ b_2 \\ b_3 \end{pmatrix} , \qquad \tilde{\boldsymbol{b}} \equiv \begin{pmatrix} \tilde{b}_1 \\ \tilde{b}_2 \\ \tilde{b}_3 \end{pmatrix} , \qquad \boldsymbol{n} \equiv \begin{pmatrix} 1 \\ 1 \\ 1 \end{pmatrix} , \tag{D.4}$$

where $\Delta\boldsymbol{b} \equiv \tilde{\boldsymbol{b}} - \boldsymbol{b}$, and b_a and $\tilde{b}_a$ denote the beta-function coefficients below and above the intermediate scale, respectively. The U(1) beta function above the intermediate scale is given by a linear combination of the beta functions of the intermediate gauge group. For instance, in the case of $\mathrm{SU}(4)_C \otimes \mathrm{SU}(2)_L \otimes \mathrm{SU}(2)_R$, we have

$$\tilde{b}_1 = \frac{2}{5} b_4 + \frac{3}{5} b_{2R} . \tag{D.5}$$

Similar expressions are obtained for other intermediate groups. Notice that the components of the beta-function coefficients which are proportional to $\boldsymbol{n}$ do not affect $M_{\rm GUT}$ and $M_{\rm int}$, as one can see from the formulae. Therefore, if one adds a multiplet to, *e.g.*, the $\mathrm{SU}(4)_C \otimes \mathrm{SU}(2)_L \otimes \mathrm{SU}(2)_R$ theory whose contribution to the beta-function coefficients is $\Delta b_4 = \Delta b_{2L} = \Delta b_{2R}$, then the multiplet does not alter $M_{\rm GUT}$ and $M_{\rm int}$ at one-loop level.

We also note that physics above the intermediate scale gives negligible effects on the determination of $M_{\rm int}$ in the presence of the left-right symmetry. We can see this feature by using Eq. (D.1). Let us consider the case of $\mathrm{SU}(4)_C \otimes \mathrm{SU}(2)_L \otimes \mathrm{SU}(2)_R \otimes D$. In the left-right symmetric theories, the beta functions of the $\mathrm{SU}(2)_L$ and $\mathrm{SU}(2)_R$ gauge couplings should be the same. Therefore, we have $b_{2L} = b_{2R}$, and

$$\tilde{\boldsymbol{b}} \times \boldsymbol{n} = (b_{2L} - b_4)\boldsymbol{c} \ , \tag{D.6}$$

with

$$\boldsymbol{c} = \begin{pmatrix} 1 \\ -\frac{3}{5} \\ -\frac{2}{5} \end{pmatrix} \ . \tag{D.7}$$

Therefore, Eq. (D.1) reads

$$M_{\rm int} = m_Z \exp\left[\frac{2\pi \boldsymbol{c} \cdot \boldsymbol{\alpha_{-1}}}{\boldsymbol{c} \cdot \boldsymbol{b}}\right] \ , \tag{D.8}$$

and thus, the intermediate scale does not depend on the beta function above $M_{\rm int}$. One can also see this feature by noting that above the intermediate scale $g_{2L} = g_{2R}$ holds at any scale. Hence, the intermediate scale corresponds to a point at which g_{2L} becomes equivalent to g_{2R}, which is determined only by the running below $M_{\rm int}$. A similar argument holds in the case of $\mathrm{SU}(3)_C \otimes \mathrm{SU}(2)_L \otimes \mathrm{SU}(2)_R \otimes \mathrm{U}(1)_{B-L} \otimes D$.

Appendix E

Proton decay calculation

In this section, we describe how we calculate proton decay lifetimes in the intermediate-scale scenarios. In these scenarios, proton decay is induced by the exchange of the GUT-scale gauge bosons [93]. The relevant part of the SO(10) gauge interaction is given by

$$\mathcal{L}_{\rm int} = \frac{g_{\rm GUT}}{\sqrt{2}}\left[(\overline{Q})_{ar}\not{X}^{air}P_R(L^{\mathcal{C}})_i + (\overline{Q})_{ai}\not{X}^{air}P_L(L^{\mathcal{C}})_r + \epsilon_{ij}\epsilon_{rs}\epsilon_{abc}(\overline{Q^{\mathcal{C}}})^{ar}\not{X}^{bis}P_L Q^{cj} + \text{h.c.}\right] , \tag{E.1}$$

where

$$Q = \begin{pmatrix} u \\ d \end{pmatrix} , \qquad L = \begin{pmatrix} \nu \\ e^- \end{pmatrix} , \tag{E.2}$$

X represents the GUT gauge bosons which induce proton decay, $g_{\rm GUT}$ is the unified gauge coupling constant, a, b, c are $\mathrm{SU}(3)_C$ indices, i, j are $\mathrm{SU}(2)_L$ indices, r, s are $\mathrm{SU}(2)_R$ indices, and $P_{R/L} \equiv (1 \pm \gamma_5)/2$ are the chirality projection operators. The exchange of the X fields generates dimension-six proton decay operators. These operators are expressed in a form that respects the intermediate gauge symmetries. Between the GUT and intermediate scales, the renormalization factors for the effective operators are in general different among the choices of $G_{\rm int}$. Below the intermediate scale, the low-energy effective theory is described by the $\mathrm{SU}(3)_C \otimes \mathrm{SU}(2)_L \otimes \mathrm{U}(1)_Y$ gauge theory, and thus after matching the theories above and below the intermediate scale, the prescription for the calculation is common to all of the cases. For this reason, we first describe the calculation below the intermediate scale. After that, we discuss each intermediate

gauge theory showing the matching conditions at the GUT and intermediate scales as well as the RGEs between them.

In the $\mathrm{SU}(3)_C \otimes \mathrm{SU}(2)_L \otimes \mathrm{U}(1)_Y$ gauge theory, the effective Lagrangian for proton decay is generically written as

$$\mathcal{L}_{\rm eff} = \sum_{I=1}^{4} C_I \mathcal{O}_I + \text{h.c.} \ , \tag{E.3}$$

with the effective operators given by [94–96]

$$\begin{aligned}
\mathcal{O}_1 &= \epsilon_{abc}\epsilon_{ij}(u_R^a d_R^b)(Q_L^{ci} L_L^j) \ , \\
\mathcal{O}_2 &= \epsilon_{abc}\epsilon_{ij}(Q_L^{ai} Q_L^{bj})(u_R^c e_R) \ , \\
\mathcal{O}_3 &= \epsilon_{abc}\epsilon_{ij}\epsilon_{kl}(Q_L^{ai} Q_L^{bk})(Q_L^{cl} L_L^j) \ , \\
\mathcal{O}_4 &= \epsilon_{abc}(u_R^a d_R^b)(u_R^c e_R) \ ,
\end{aligned} \tag{E.4}$$

up to dimension six. We then run down the coefficients to the electroweak scale. We will see below that the coefficients C_3 and C_4 vanish in all of the cases we consider in this paper, and thus we focus on C_1 and C_2. Their renormalization factors are [96]

$$C_1(\mu) = \left[\frac{\alpha_3(\mu)}{\alpha_3(M_{\rm int})}\right]^{-\frac{2}{b_3}} \left[\frac{\alpha_2(\mu)}{\alpha_2(M_{\rm int})}\right]^{-\frac{9}{4b_2}} \left[\frac{\alpha_1(\mu)}{\alpha_1(M_{\rm int})}\right]^{-\frac{11}{20b_1}} C_1(M_{\rm int}) \ , \tag{E.5}$$

$$C_2(\mu) = \left[\frac{\alpha_3(\mu)}{\alpha_3(M_{\rm int})}\right]^{-\frac{2}{b_3}} \left[\frac{\alpha_2(\mu)}{\alpha_2(M_{\rm int})}\right]^{-\frac{9}{4b_2}} \left[\frac{\alpha_1(\mu)}{\alpha_1(M_{\rm int})}\right]^{-\frac{23}{20b_1}} C_2(M_{\rm int}) \ , \tag{E.6}$$

where b_a denote the one-loop beta-function coefficients for the gauge couplings g_a and μ is an arbitrary scale. We need to change the beta-function coefficients appropriately when we across the DM mass threshold. Below the electroweak scale, the QCD corrections are the dominant contribution. By using the two-loop RGE given in Ref. [100], we compute the Wilson coefficients at the hadronic scale $\mu_{\rm had}$ as

$$C_i(\mu_{\rm had}) = \left[\frac{\alpha_s(\mu_{\rm had})}{\alpha_s(m_b)}\right]^{\frac{6}{25}} \left[\frac{\alpha_s(m_b)}{\alpha_s(m_Z)}\right]^{\frac{6}{23}} \left[\frac{\alpha_s(\mu_{\rm had}) + \frac{50\pi}{77}}{\alpha_s(m_b) + \frac{50\pi}{77}}\right]^{-\frac{173}{825}} \left[\frac{\alpha_s(m_b) + \frac{23\pi}{29}}{\alpha_s(m_Z) + \frac{23\pi}{29}}\right]^{-\frac{430}{2001}} C_i(m_Z) \ , \tag{E.7}$$

with $i = 1, 2$.

In non-SUSY GUTs, the dominant decay mode of proton is $p \to \pi^0 e^+$. The partial decay width of the mode is computed as

$$\Gamma(p \to \pi^0 e^+) = \frac{m_p}{32\pi}\left(1 - \frac{m_\pi^2}{m_p^2}\right)^2 \left[|\mathcal{A}_L|^2 + |\mathcal{A}_R|^2\right] \ , \tag{E.8}$$

where m_p and m_π are the masses of the proton and the neutral pion, respectively, and

$$\begin{aligned}\mathcal{A}_L &= C_1(\mu_{\rm had})\langle\pi^0|(ud)_R u_L|p\rangle \ , \\ \mathcal{A}_R &= 2C_2(\mu_{\rm had})\langle\pi^0|(ud)_L u_R|p\rangle \ . \end{aligned} \tag{E.9}$$

The hadron matrix elements are evaluated with the lattice QCD simulations in Ref. [101]. We have

$$\langle\pi^0|(ud)_R u_L|p\rangle = \langle\pi^0|(ud)_L u_R|p\rangle = -0.103(23)(34)\ {\rm GeV}^2 \ , \tag{E.10}$$

with $\mu_{\rm had} = 2$ GeV. Here, the first and second parentheses indicate statistical and systematic errors, respectively.

E.1 $G_{\rm int} = \mathbf{SU}(4)_C \otimes \mathbf{SU}(2)_L \otimes \mathbf{SU}(2)_R(\otimes D)$

For $G_{\rm int} = {\rm SU}(4)_C \otimes {\rm SU}(2)_L \otimes {\rm SU}(2)_R(\otimes D)$, the dimension-six effective operator is given by[1]

$$\mathcal{L}_{\rm eff} = C_{422} \cdot \epsilon_{ij}\epsilon_{rs}\epsilon_{\alpha\beta\gamma\delta}(\overline{\Psi^{\mathcal{C}}})^{\alpha i} P_L \Psi^{\beta j} (\overline{\Psi^{\mathcal{C}}})^{\gamma r} P_R \Psi^{\delta s} + {\rm h.c.} \ , \tag{E.12}$$

where $\alpha, \beta, \ldots$ denote the SU(4) indices, and the Dirac field $\Psi = (\Psi_L, \Psi_R)$ is defined by

$$\Psi_L = \begin{pmatrix} u_L^1 & u_L^2 & u_L^3 & \nu_L \\ d_L^1 & d_L^2 & d_L^3 & e_L \end{pmatrix} \ , \qquad \Psi_R^{\mathcal{C}} = \begin{pmatrix} d_{R1}^{\mathcal{C}} & d_{R2}^{\mathcal{C}} & d_{R3}^{\mathcal{C}} & e_R^{\mathcal{C}} \\ -u_{R1}^{\mathcal{C}} & -u_{R2}^{\mathcal{C}} & -u_{R3}^{\mathcal{C}} & -\nu_R^{\mathcal{C}} \end{pmatrix} \ . \tag{E.13}$$

Here, the indices represent the $\mathrm{SU}(3)_C$ color and $\mathcal{C}$ indicates charge conjugation. At tree level, the coefficient of the effective operator is evaluated as[2]

$$C_{422}(M_{\rm GUT}) = -\frac{g_{\rm GUT}^2}{2M_X^2} \ , \tag{E.14}$$

with M_X the mass of the heavy gauge field X. In this paper, we neglect fermion flavor mixings for simplicity.

---

[1] Note that

$$\epsilon_{ij}\epsilon_{kl}\epsilon_{\alpha\beta\gamma\delta}(\overline{\Psi^{\mathcal{C}}})^{\alpha i} P_L \Psi^{\beta j} (\overline{\Psi^{\mathcal{C}}})^{\gamma k} P_L \Psi^{\delta l} = \epsilon_{rs}\epsilon_{tu}\epsilon_{\alpha\beta\gamma\delta}(\overline{\Psi^{\mathcal{C}}})^{\alpha r} P_R \Psi^{\beta s} (\overline{\Psi^{\mathcal{C}}})^{\gamma t} P_R \Psi^{\delta u} = 0 \ , \tag{E.11}$$

and thus the operator in Eq. (E.12) is the unique choice.

[2] We have found that the sign of this equation is opposite to that given in Ref. [29].

The Wilson coefficient is evolved down to the intermediate scale using the RGE. The renormalization factor is computed to be [97]

$$C_{422}(M_{\rm int}) = \left[\frac{\alpha_4(M_{\rm int})}{\alpha_{\rm GUT}}\right]^{-\frac{15}{4b_4}} \left[\frac{\alpha_{2L}(M_{\rm int})}{\alpha_{\rm GUT}}\right]^{-\frac{9}{4b_{2L}}} \left[\frac{\alpha_{2R}(M_{\rm int})}{\alpha_{\rm GUT}}\right]^{-\frac{9}{4b_{2R}}} C_{422}(M_{\rm GUT}) \ . \tag{E.15}$$

Then, the effective operator is matched onto the operators in Eq. (E.4). The Wilson coefficients C_I are given by[3]

$$\begin{aligned} C_1(M_{\rm int}) &= 4C_{422}(M_{\rm int}) \ , \\ C_2(M_{\rm int}) &= 2C_{422}(M_{\rm int}) \ , \\ C_3(M_{\rm int}) &= C_4(M_{\rm int}) = 0 \ . \end{aligned} \tag{E.16}$$

E.2 $G_{\rm int} = \mathbf{SU}(4)_C \otimes \mathbf{SU}(2)_L \otimes \mathbf{U}(1)_R$

In the case of $G_{\rm int} = {\rm SU}(4)_C \otimes {\rm SU}(2)_L \otimes {\rm U}(1)_R$, the effective Lagrangian is written as

$$\mathcal{L}_{\rm eff} = C_{421} \cdot 2\epsilon_{ij}\epsilon_{\alpha\beta\gamma\delta}(\overline{\Psi^{\mathcal{C}}})^{\alpha i} P_L \Psi^{\beta j} (\overline{\mathcal{U}^{\mathcal{C}}})^{\gamma} P_R \mathcal{D}^{\delta} + {\rm h.c.} \ , \tag{E.17}$$

with

$$\mathcal{U} \equiv (u^1,\ u^2,\ u^3,\ \nu) \ , \qquad \mathcal{D} \equiv (d^1,\ d^2,\ d^3,\ e) \ . \tag{E.18}$$

The GUT-scale matching condition for the operator is

$$C_{421}(M_{\rm GUT}) = -\frac{g_{\rm GUT}^2}{2M_X^2} \ , \tag{E.19}$$

and the renormalization factor is given by [97]

$$C_{421}(M_{\rm int}) = \left[\frac{\alpha_4(M_{\rm int})}{\alpha_{\rm GUT}}\right]^{-\frac{15}{4b_4}} \left[\frac{\alpha_{2L}(M_{\rm int})}{\alpha_{\rm GUT}}\right]^{-\frac{9}{4b_{2L}}} \left[\frac{\alpha_{R}(M_{\rm int})}{\alpha_{\rm GUT}}\right]^{-\frac{3}{4b_{R}}} C_{421}(M_{\rm GUT}) \ . \tag{E.20}$$

For the intermediate-scale matching conditions, we have

$$\begin{aligned} C_1(M_{\rm int}) &= 4C_{421}(M_{\rm int}) \ , \\ C_2(M_{\rm int}) &= 2C_{421}(M_{\rm int}) \ , \\ C_3(M_{\rm int}) &= C_4(M_{\rm int}) = 0 \ . \end{aligned} \tag{E.21}$$

[3] We have fixed an error in the matching conditions given in Ref. [29].

E.3 $G_{\rm int} = \mathbf{SU}(3)_C \otimes \mathbf{SU}(2)_L \otimes \mathbf{SU}(2)_R \otimes \mathbf{U}(1)_{B-L}(\otimes D)$

When $G_{\rm int} = {\rm SU}(3)_C \otimes {\rm SU}(2)_L \otimes {\rm SU}(2)_R \otimes {\rm U}(1)_{B-L}(\otimes D)$, there are four independent effective operators [98],

$$\begin{aligned}
\mathcal{Q}_1 &= 2\epsilon_{ij}\epsilon_{rs}\epsilon_{abc}(\overline{Q^{\mathcal{C}}})^{ai} P_L Q^{bj} (\overline{Q^{\mathcal{C}}})^{cr} P_R L^s \ , \\
\mathcal{Q}_2 &= 2\epsilon_{ij}\epsilon_{rs}\epsilon_{abc}(\overline{Q^{\mathcal{C}}})^{ai} P_L L^j (\overline{Q^{\mathcal{C}}})^{br} P_R Q^{cs} \ , \\
\mathcal{Q}_3 &= 2\epsilon_{il}\epsilon_{jk}\epsilon_{abc}(\overline{Q^{\mathcal{C}}})^{ai} P_L Q^{bj} (\overline{Q^{\mathcal{C}}})^{ck} P_L L^l \ , \\
\mathcal{Q}_4 &= 2\epsilon_{ps}\epsilon_{qr}\epsilon_{abc}(\overline{Q^{\mathcal{C}}})^{ap} P_R Q^{bq} (\overline{Q^{\mathcal{C}}})^{cr} P_R L^s \ ,
\end{aligned} \tag{E.22}$$

and thus the effective Lagrangian is expressed as

$$\mathcal{L}_{\rm eff} = \sum_{I=1}^{4} C_{3221}^{(I)} \mathcal{Q}_I + {\rm h.c.} \tag{E.23}$$

For the GUT-scale matching condition, we have

$$\begin{aligned}
C_{3221}^{(1)}(M_{\rm GUT}) &= C_{3221}^{(2)}(M_{\rm GUT}) = -\frac{g_{\rm GUT}^2}{2M_X^2} \ , \\
C_{3221}^{(3)}(M_{\rm GUT}) &= C_{3221}^{(4)}(M_{\rm GUT}) = 0 \ .
\end{aligned} \tag{E.24}$$

The renormalization factors for the coefficients $C_{3221}^{(1)}$ and $C_{3221}^{(2)}$ are given in Refs. [97,98]:

$$\frac{C(M_{\rm int})}{C(M_{\rm GUT})} = \left[\frac{\alpha_3(M_{\rm int})}{\alpha_{\rm GUT}}\right]^{-\frac{2}{b_3}} \left[\frac{\alpha_{2L}(M_{\rm int})}{\alpha_{\rm GUT}}\right]^{-\frac{9}{4b_{2L}}} \left[\frac{\alpha_{2R}(M_{\rm int})}{\alpha_{\rm GUT}}\right]^{-\frac{9}{4b_{2R}}} \left[\frac{\alpha_{B-L}(M_{\rm int})}{\alpha_{\rm GUT}}\right]^{-\frac{1}{4b_{B-L}}} , \tag{E.25}$$

for $C = C_{3221}^{(1)}$ and $C_{3221}^{(2)}$. Then the Wilson coefficients at the electroweak scale are matched onto those of the operators (E.4) as

$$\begin{aligned}
C_1(M_{\rm int}) &= 4C_{3221}^{(2)}(M_{\rm int}) \ , \\
C_2(M_{\rm int}) &= 2C_{3221}^{(1)}(M_{\rm int}) \ , \\
C_3(M_{\rm int}) &= C_4(M_{\rm int}) = 0 \ .
\end{aligned} \tag{E.26}$$

Appendix F

Example of fine-tuning for a scalar WIMP model

To show the process of mass fine-tuning explicitly, in this section, we consider the case of $R_{\rm DM} = \mathbf{16}$ with $G_{\rm int} = {\rm SU}(3)_C \otimes {\rm SU}(2)_L \otimes {\rm SU}(2)_R \otimes {\rm U}(1)_{B-L}$ as an example. We take $R_1 = \mathbf{45}$, which contains two independent SM singlet components that might develop VEVs; one is in a $(\mathbf{1}, \mathbf{1}, \mathbf{3})$ while the other is in a $(\mathbf{15}, \mathbf{1}, \mathbf{1})$ under ${\rm SU}(4)_C \otimes {\rm SU}(2)_L \otimes {\rm SU}(2)_R$. We refer to these VEVs as A_1 and A_2, respectively, and other notation is taken from Eq. (3.7). Since the components of a scalar **16** have the same quantum numbers as those of a generation of the SM fermions, we denote them by the same symbol as for the corresponding SM fermions with a tilde, just like the notation for sfermions in supersymmetric models.

Let us first study the $R^*_{\rm DM} R_{\rm DM} R_1$ coupling. Since R_1 is the adjoint representation of SO(10), the decomposition of this coupling in terms of the component fields has a similar form to the gauge interaction for a **16** spinor representation. We have

$$\kappa_1 R^*_{\rm DM} R_{\rm DM} \langle R_1 \rangle = \kappa_1 \Bigg[\left(-\sqrt{2} A_1 - \sqrt{3} A_2 \right) \widetilde{\nu}^*_R \widetilde{\nu}_R + \left(\sqrt{2} A_1 - \sqrt{3} A_2 \right) \widetilde{e}^*_R \widetilde{e}_R + \sqrt{3} A_2 \widetilde{L}^*_L \widetilde{L}_L + \left(\sqrt{2} A_1 + \frac{1}{\sqrt{3}} A_2 \right) \widetilde{d}^*_R \widetilde{d}_R + \left(-\sqrt{2} A_1 + \frac{1}{\sqrt{3}} A_2 \right) \widetilde{u}^*_R \widetilde{u}_R - \frac{1}{\sqrt{3}} A_2 \widetilde{Q}^*_L \widetilde{Q}_L \Bigg] , \tag{F.1}$$

where the contraction of the ${\rm SU}(3)_C$ and ${\rm SU}(2)_L$ indices is implicit. When $A_1 \neq 0$ and $A_2 = 0$, the mass spectrum preserves the ${\rm SU}(4)_C \otimes {\rm SU}(2)_L \otimes {\rm U}(1)_R$ symmetry, while

when $A_2 \neq 0$ and $A_1 = 0$, then it is $\mathrm{SU}(3)_C \otimes \mathrm{SU}(2)_L \otimes \mathrm{SU}(2)_R \otimes \mathrm{U}(1)_{B-L}$ symmetric. If both of the VEVs have non-zero values, then the low-energy theory is invariant under the $\mathrm{SU}(3)_C \otimes \mathrm{SU}(2)_L \otimes \mathrm{U}(1)_R \otimes \mathrm{U}(1)_{B-L}$ symmetry. The coefficients of A_2 for left and right doublets have different signs, which indicates the breaking of left-right symmetry. Here, we choose $A_1 = 0$ and $A_2 = v_{\mathbf{45}}$ to obtain $G_{\rm int} = \mathrm{SU}(3)_C \otimes \mathrm{SU}(2)_L \otimes \mathrm{SU}(2)_R \otimes \mathrm{U}(1)_{B-L}$.

Next we consider the mass terms generated by $\lambda_2^{\mathbf{45}}(R_{\rm DM}^* R_{\rm DM})_{\mathbf{45}}(R_2^* R_2)_{\mathbf{45}}$. The SM singlet in $R_2 = \mathbf{126}$ transforms as $(\mathbf{10}, \mathbf{1}, \mathbf{3})$ under $\mathrm{SU}(4)_C \otimes \mathrm{SU}(2)_L \otimes \mathrm{SU}(2)_R$, which acquires a VEV $v_{\mathbf{126}}$ to break $G_{\rm int}$ into the SM gauge group. According to the result in Ref. [53, 99], the resultant mass terms are[1]

$$\lambda_2^{\mathbf{45}} (R_{\rm DM}^* R_{\rm DM})_{\mathbf{45}} \langle (R_2^* R_2)_{\mathbf{45}} \rangle = \lambda_2^{\mathbf{45}} v_{\mathbf{126}}^2 \Big[-\widetilde{\nu}_R^* \widetilde{\nu}_R + \frac{3}{5} \left(\widetilde{L}_L^* \widetilde{L}_L + \widetilde{d}_R^* \widetilde{d}_R \right) - \frac{1}{5} \left(\widetilde{e}_R^* \widetilde{e}_R + \widetilde{u}_R^* \widetilde{u}_R + \widetilde{Q}_L^* \widetilde{Q}_L \right) \Big] . \tag{F.2}$$

Notice that the right-hand side of the expression can be grouped in terms of SU(5) multiplets. This is expected since $v_{\mathbf{126}}$ is invariant under the SU(5) transformation. From the above equations, it is found that we can ensure that only the DM component has a mass around TeV scale by fine-tuning the parameters M^2, κ_1 and $\lambda_2^{\mathbf{45}}$. For example, to obtain the model $\mathtt{SA}_{\mathtt{3221}}$, we can take

$$\begin{aligned} M^2 - \sqrt{3}\kappa_1 v_{\mathbf{45}} &\sim \mathcal{O}(M_{\rm int}^2) , \\ M^2 - \sqrt{3}\kappa_1 v_{\mathbf{45}} - \lambda_2^{\mathbf{45}} v_{\mathbf{126}}^2 &\sim \mathcal{O}(\mathrm{TeV}^2) . \end{aligned} \tag{F.3}$$

Then, $\widetilde{\nu}_R$ acquires a TeV-scale mass, while the mass of $\widetilde{e}_R$ is $\mathcal{O}(M_{\rm int})$. The rest of the components lie around the GUT scale. On the other hand, if we take

$$\begin{aligned} M^2 + \sqrt{3}\kappa_1 v_{\mathbf{45}} &\sim \mathcal{O}(M_{\rm int}^2) , \\ M^2 + \sqrt{3}\kappa_1 v_{\mathbf{45}} + \frac{3}{5}\lambda_2^{\mathbf{45}} v_{\mathbf{126}}^2 &\sim \mathcal{O}(\mathrm{TeV}^2) , \end{aligned} \tag{F.4}$$

then we can make only the $\widetilde{L}_L$ component have a TeV-scale mass and the other components have GUT-scale masses. Thus we obtain the $\mathtt{SB}_{\mathtt{3221}}$ model.

[1] Note that since $(R_2^* R_2)_{\mathbf{45}}$ contains a $\mathbf{45}$, there is a contribution to the mass corresponding to Eq. (F.1) at the intermediate scale proportional to $\lambda_2^{\mathbf{45}}$ with independent coefficients $\tilde{A}_1$ and $\tilde{A}_2$. The result shown is obtained from Eq. (F.1) by taking $\tilde{A}_1 = \frac{\sqrt{2}}{5} v_{\mathbf{126}}^2$ and $\tilde{A}_2 = \frac{\sqrt{3}}{5} v_{\mathbf{126}}^2$, up to an overall factor.

To simplify our argument, in the above discussion, we have taken into account only the contribution of the M^2, κ_1, and $\lambda_2^{\mathbf{45}}$ terms, and neglected that of the other terms in Eq. (3.7). Even in the presence of the other contributions, we can always perform a similar fine-tuning among the parameters to realize desired mass spectrum for our DM models.